



National Library  
of Canada

Bibliothèque nationale  
du Canada

Canadian Theses Service

Service des thèses canadiennes

Ottawa, Canada  
K1A 0N4

## NOTICE

The quality of this microform is heavily dependent upon the quality of the original thesis submitted for microfilming. Every effort has been made to ensure the highest quality of reproduction possible.

If pages are missing, contact the university which granted the degree.

Some pages may have indistinct print especially if the original pages were typed with a poor typewriter ribbon or if the university sent us an inferior photocopy.

Previously copyrighted materials (journal articles, published tests, etc.) are not filmed.

Reproduction in full or in part of this microform is governed by the Canadian Copyright Act, R.S.C. 1970, c. C-30.

## AVIS

La qualité de cette microforme dépend grandement de la qualité de la thèse soumise au microfilmage. Nous avons tout fait pour assurer une qualité supérieure de reproduction.

S'il manque des pages, veuillez communiquer avec l'université qui a conféré le grade.

La qualité d'impression de certaines pages peut varier à désirer, surtout si les pages originales ont été dactylographiées à l'aide d'un ruban usé ou si l'université nous a fait parvenir une photocopie de qualité inférieure.

Les documents qui font déjà l'objet d'un droit d'auteur (articles de revue, tests publiés, etc.) ne sont pas microfilmés.

La reproduction, même partielle, de cette microforme est soumise à la Loi canadienne sur le droit d'auteur, SRC 1970, c. C-30.

THE UNIVERSITY OF ALBERTA

Oriental Effects in a Buoyant Cavity Flow

by

Jianchiu Han

A THESIS

SUBMITTED TO THE FACULTY OF GRADUATE STUDIES AND RESEARCH  
IN PARTIAL FULFILMENT OF THE REQUIREMENTS FOR THE DEGREE  
OF Master of Science

Department of Mechanical Engineering

EDMONTON, ALBERTA

Fall, 1988

Permission has been granted to the National Library of Canada to microfilm this thesis and to lend or sell copies of the film.

The author (copyright owner) has reserved other publication rights, and neither the thesis nor extensive extracts from it may be printed or otherwise reproduced without his/her written permission.

L'autorisation a été accordée à la Bibliothèque nationale du Canada de microfilmer cette thèse et de prêter ou de vendre des exemplaires du film.

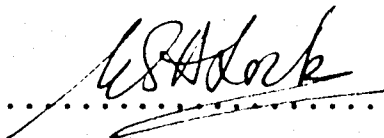
L'auteur (titulaire du droit d'auteur) se réserve les autres droits de publication; ni la thèse ni de longs extraits de celle-ci ne doivent être imprimés ou autrement reproduits sans son autorisation écrite.

ISBN 0-315-45598-5


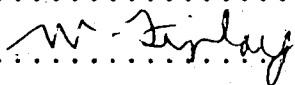


THE UNIVERSITY OF ALBERTA  
FACULTY OF GRADUATE STUDIES AND RESEARCH

The undersigned certify that they have read, and recommend to the Faculty of Graduate Studies and Research, for acceptance, a thesis entitled Orientational Effects in a Buoyant Cavity Flow submitted by Jianchiu Han in partial fulfilment of the requirements for the degree of Master of Science.

.....  


Supervisor

.....  
  
.....  
  
.....

Date..... July 22nd 1988.....

To My Wife

Chian

2

## ABSTRACT

In this study, three-dimensional natural convection in a rectangular cavity was investigated using a numerical method called SIMPLE-C. Situations of two cavity geometries were studied.

In the situation of  $A_x=A_z=0.2$  cavity, effect of Rayleigh number for the horizontal cavity and effect of tilt angle for fixed Rayleigh number were examined. For the horizontal cavity the flow pattern is a S-shaped parallel shear flow in the primary plane, superimposed with two pairs of counter-rotating vortices in the lateral secondary plane. For the Rayleigh number of range 50 to  $10^4$ , no fundamental change in flow pattern was found. When the cavity was tilted from  $-90^\circ$  to  $90^\circ$ , three flow regimes, horizontal, modified and filament pattern, took over sequentially. Skewing the cavity and the way to impose the temperature gradient on the system had no fundamental effect on the flow pattern.

For the  $A_x=5$  and  $A_z=1$  cavity, different paths were followed in changing the orientation of the cavity while the Rayleigh number was fixed at  $10^4$ . When the cavity was skewed from  $A$  to  $D$ , gradual transition from a transverse cell to a longitudinal roll was observed and no bifurcation was found along path  $AD$ . In the situation of rolling, a region of about  $10^\circ$  near  $B$  where the solution was branched was found. In the situation of tilting, the bifurcation region was as large as  $45^\circ$  from  $B$ . In the bifurcation region, the flow pattern can be either a longitudinal roll or a series of

transverse rolls depending upon the initial input.



## ACKNOWLEDGEMENT

The author wishes to express his sincere appreciation to Dr. L. S. H. Lock, who supervised the research project, for his guidance and encouragement throughout the course of preparation of this thesis.

Financial aid in the form of Teaching/Research Assistantship was provided by the Department of Mechanical Engineering. Partial funding of the project was also supplied by Alberta Municipal Affairs. They are greatly appreciated.

The computing time allotted on the Array Processor by the Computing Services is acknowledged.

Finally, the author is most grateful to his wife for her encouragement and immeasurable emotional support during his study at the University of Alberta.

## Table of Contents

Chapter	Page
I. INTRODUCTION .....	1
A. PRELIMINARY .....	1
B. GEOMETRY OF THE SYSTEM .....	5
C. REVIEW OF EXISTING WORK .....	9
Vertical Cavity: two-dimensional .....	10
Three-dimensional Flow .....	12
Benard-Rayleigh Convection .....	14
II. FORMULATION OF THE PROBLEM .....	17
A. FORMULATION .....	17
Conservation Laws .....	17
Boussinesq Approximation .....	18
Boundary Conditions .....	22
B. NORMALIZATION .....	23
C. SOME QUALITATIVE CONSIDERATIONS OF THE GOVERNING EQUATIONS .....	26
Symmetry .....	26
Circulation, Primary and Secondary Planes .....	28
III. METHOD OF SOLUTION .....	32
A. INTRODUCTION .....	32
B. DISCRETIZATION .....	34
C. ALGORITHM .....	39
D. CONTROL AND ACCURACY OF THE PROGRAM .....	40
E. METHOD OF PRESENTATION .....	42
IV. LONGITUDINAL TEMPERATURE GRADIENT $A_x=0.2$ , $A_z=0.2$ CAVITY .....	47
A. CONFIGURATION A: THE EFFECT OF RAYLEIGH NUMBER .....	48
B. THE EFFECT OF TILT .....	60

Horizontal Pattern .....	64
Modified Horizontal Pattern .....	64
Filament Pattern .....	68
C. THE EFFECT OF SKEW .....	74
D. CONCLUSIONS .....	74
V. TRANSVERSE TEMPERATURE GRADIENT $A_x=5$ , $A_z=1$ CAVITY	78
A. THE EFFECT OF SKEW .....	79
Configuration A .....	79
Path <i>AD</i> .....	81
B. THE EFFECT OF ROLL .....	91
Path <i>DB</i> .....	92
<i>B</i> Obtained by Uniform Input .....	97
Path <i>BD</i> .....	101
C. THE EFFECT OF TILT .....	106
Path <i>AB</i> .....	106
Path <i>B(6TR)→A</i> .....	108
Path <i>B(LR)→A</i> .....	113
D. OTHER SITUATIONS .....	116
E. SOME THOUGHTS ON BENARD CONVECTION .....	118
Uniqueness Versus Bifurcation .....	118
Formation of a Flow Pattern .....	120
Validity of Numerical Methods .....	122
F. CONCLUSIONS .....	122
REFERENCES .....	125
APPENDIX .....	128

## List of Figures

Figure	Page
I.1 Geometry of the system .....	6
II.1 Working principle to predict circulation direction .....	30
III.1 Discretization of the computational domain .....	35
III.2 A sample finite volume .....	37
III.3 Consistency check for the program: variable Ra .....	43
III.4 Consistency check for the program: Variable $\alpha$ .....	44
IV.1 xy plane velocity, $z=0.5$ , $Ra=50$ .....	49
IV.2 xy plane velocity, $z=0.5$ , $Ra=2.5 \times 10^4$ .....	50
IV.3 xy plane velocity, $z=0.5$ , $Ra=10^6$ .....	51
IV.4 v velocity at different y, $Ra=2.5 \times 10^4$ .....	53
IV.5 Temperature distribution along y, $Ra=2.5 \times 10^4$ .....	55
IV.6 xz plane velocity along y, $Ra=2.5 \times 10^4$ .....	57
IV.7 Nu contribution from each wall, $Ra=2.5 \times 10^4$ .....	58
IV.8 Heat transfer rates for different Ra .....	61
IV.9 xy plane velocity, $z=0.5$ , $Ra=2.5 \times 10^4$ , BC3 .....	62
IV.10 Nusselt number for different tilt angle .....	63
IV.11 xy plane velocity, $z=0.5$ , $\alpha=30^\circ$ .....	66
IV.12 xz plane velocity, $y=0.714$ , several $\alpha$ .....	67
IV.13 Sketch of filament model .....	69
IV.14 xy plane velocity, $z=0.5$ , $\alpha=85^\circ$ .....	71
IV.15 v velocity along y, $\alpha=60^\circ$ .....	72
IV.16 xz plane velocity along y, $\alpha=45^\circ$ .....	73
IV.17 xz plane velocity, $y=2.5$ , several $\theta$ .....	75

Figure	Page
V.1	xy plane velocity, $z=0.5$ , at A .....80
V.2	yz plane velocity, $x=4.95$ , at A .....82
V.3	u velocity along x, at A .....83
V.4	yz plane velocity, $x=2.45$ , several $\theta$ .....85
V.5	yz plane velocity, $x=0.05$ , several $\theta$ .....87
V.6	xz plane velocity, $y=0.958$ , several $\theta$ .....88
V.7	xy plane velocity, $z=0.958$ , several $\theta$ .....89
V.8	Nusselt number for different skew angles .....90
V.9	Nusselt number for different roll angles .....93
V.10	yz plane velocity, $x=2.45$ , several $\gamma$ .....94
V.11	xy plane velocity, $z=0.208$ , at B .....95
V.12	xz plane velocity, $y=0.208$ , at B .....96
V.13	xy plane velocity, $z=0.5$ , at B, 0 input .....98
V.14	xy plane velocity, $z=0.5$ , at B, -0.5 input .....100
V.15	xz plane velocity, $y=0.917$ , at B(6TR) .....102
V.16	yz plane velocity along x, at B(6TR) .....103
V.17	yz plane velocity, $x=3.75$ , path BD .....105
V.18	Nusselt number along path AB .....107
V.19	xy plane velocity, $z=0.5$ , $\alpha=80^\circ$ , path AB .....109
V.20	xy plane velocity, $z=0.5$ , $\alpha=90^\circ$ , path AB .....110
V.21	Nusselt number along path B(6TR)A .....111
V.22	xy plane velocity, $z=0.5$ , $\alpha=70^\circ$ , path B(6TR)A .....112
V.23	Nusselt number along path B(LR)A .....114
V.24	xy plane velocity, $z=0.5$ , $\alpha=80^\circ$ , path B(LR)A .....115
V.25	Nusselt numbers for various cell structures .....117

## NOMENCLATURE

A	power-law interpolation function; surface area
A <sub>x</sub>	H/W, aspect ratio in X-direction
A <sub>z</sub>	S/W, aspect ratio in Z-direction
A	reference configuration name
a	coefficient of discretized algebraic equation
B	reference configuration name
C <sub>p</sub>	specific heat for isobaric process
C	reference configuration name
D	flux due to diffusion
D	reference configuration name
F	flux due to convection
g	gravitational acceleration constant
g	gravitational acceleration vector
H	height of the cavity
k	thermal conductivity
Nu	Nusselt number
P	pressure; cell Peclet number
p	normalized pressure
Pr	Prandtl number
Q	total heat flux through the system
Ra	Rayleigh number
S	span of the cavity; source term in the model equation
T	temperature
T <sub>ijk</sub>	trial function
U	velocity component
u	normalized velocity component

V	velocity component
Vijk	control volume
V	velocity
W	velocity component
w	normalized velocity component
X	coordinate
x	normalized coordinate
Y	coordinate
y	normalized coordinate
Z	coordinate
z	normalized coordinate

#### Greek Letters

$\alpha$	tilt angle
$\beta$	thermal expansion coefficient
$\gamma$	roll angle
$\mu$	kinematic viscosity
$\nu$	dynamic viscosity
$\kappa$	thermal diffusivity
$\rho$	density
$\theta$	skew angle
$\phi$	normalized temperature
$\Phi$	angle between temperature gradient and gravity
$\Gamma$	diffusivity for madel equation

#### Subscripts

0	reference state
---	-----------------

B bottom neighboring point  
b bottom interpolation point  
c cooled wall  
d dynamic  
E east neighboring point  
e east interpolation point  
h heated wall  
max maximum  
N north neighboring point  
n north interpolation point  
P calculated point  
p isobaric process  
S south neighboring point  
s south interpolation point  
T top neighboring point  
t top interpolation point  
W west neighboring point  
w west interpolation point



## I. INTRODUCTION

### A. PRELIMINARY

All fluid flows occurring on the earth are subject to gravitational force. When the temperature is not uniformly distributed in the fluid, this temperature nonuniformity will generally cause density nonuniformity. If the temperature gradient is parallel and opposite to the gravity vector, the fluid will remain stationary, thus creating the situation of stable stratification. If the temperature gradient has the same direction as the gravity vector, convection will set in if the magnitude of the temperature gradient exceeds a certain threshold value. In the instance when the temperature gradient in the fluid is not parallel to the gravity vector, convection sets in however small the magnitude of the temperature gradient. This kind of convection, caused by the nonuniformity of the temperature (thus density) in the fluid under the action of gravity, is called natural convection, or free convection in contrast to forced convection caused by mechanical means.

Once natural convection happens, the energy and mass transport fluxes in the fluid are changed. Natural convection may either play a dominant role (pure natural convection) or alter the transport process significantly (mixed convection).

Natural convection is one of the most common phenomena in nature. It ranges from the motion of the mantle of the

earth to the formation of the ozone layer resulting in a very wide spectrum of people from different fields studying the phenomena. They include geophysicists and astrophysicists, meteorologists, oceanographers, applied mathematicians and engineers; with each group of people emphasis is placed on a different aspect of the problem. The engineer's main interests are on the problems of everyday life and his major task is to predict the behavior of a physical system (idealized or not) under various conditions so as to provide guidelines for industrial designs. The economic and technological developments in the past two decades have shifted the engineering emphasis more and more on energy conservation and ecological considerations. This shift has stimulated activities in research aimed at an understanding of natural convection in many natural and technological situations: this understanding, for instance, is essential to designs of energy-efficient devices and the development of possible new energy sources; and it is also essential to the monitoring and controlling of environmental pollution. Technological demands and the development of computing techniques in recent decades have greatly increased investigations in this area. It is believed that this trend will persist through the 1990's.[1,2]

Natural convection can be classified into external flow and internal flow. When the mass of fluid is completely confined in a cavity made of rigid walls and the temperature gradient in the fluid is caused by the nonuniformity of

temperature on the walls, the resultant natural convection is an internal flow. If the fluid is not completely contained by a cavity of rigid walls and the temperature gradient in the fluid is caused by either a surface, line or a point energy source, the natural convection is an external flow. Examples of the latter case are: natural convection along a vertical plane with a higher temperature than that of the fluid (surface source); the plume of a candle in the air (can be idealized as point source).

Examples of internal natural convection are abundant. Among these, two of technological interest are convection in building elements (cavity walls, double-glaze windows) and convection in a thermosyphon. These two instances actually represent the two opposite directions in application of natural convection. We know that natural convection will increase energy transport ability (heat transfer rate) of the fluid in the cavity substantially. In some situations this increase is desirable while in others the increase is a nuisance. In the situation of building elements, what we want is to get better insulation to prevent heat loss through the elements. So the main task is how to suppress natural convection. In the situation of thermosyphon, on the other hand, the task is to enhance the natural convection, and thus increase the energy transport ability of the thermosyphon. In history, both applications have been the motivation for research in natural convection.

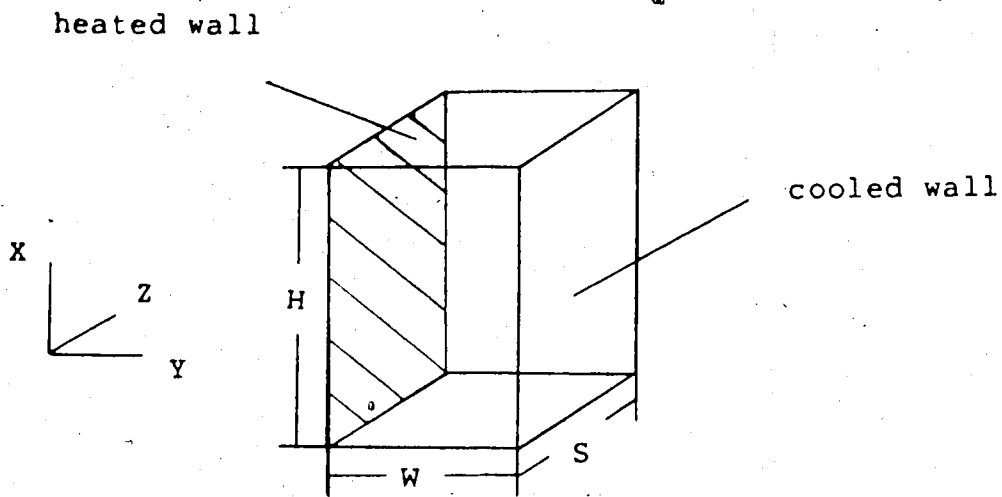
Whatever the application, an understanding of basic physics of natural convection is essential. In many applications, the rectangular cavity is the common geometry because it is geometrically relatively simple. Yet natural convection in it has all the characteristics of natural convection in an enclosure. So in this study, we will use the rectangular cavity as the fluid container. This rectangular box (we will use cavity, enclosure and box interchangeably to refer to the same thing) can have one wall kept uniformly at a high temperature and the opposite wall at a low temperature; four other walls can have perfectly conducting or perfectly insulating surfaces.

The behavior of the system is generally determined by five geometric and physical factors. They are the size of the box, the orientation of the box with respect to the gravity, the magnitude and direction of the temperature gradient imposed on the system and the fluid contained in the box. In this study air is used as the fluid in the box and the direction of the temperature gradient is always fixed relative to the box axes. This reduces the determining factors to three: the size and orientation of the box and the magnitude of the temperature gradient. All of these factors can be properly specified by dimensionless parameters which will be discussed in due course. In the next section, the method to describe the geometry of the box will be introduced. The parameter to describe the magnitude of the temperature gradient will be given in next chapter.

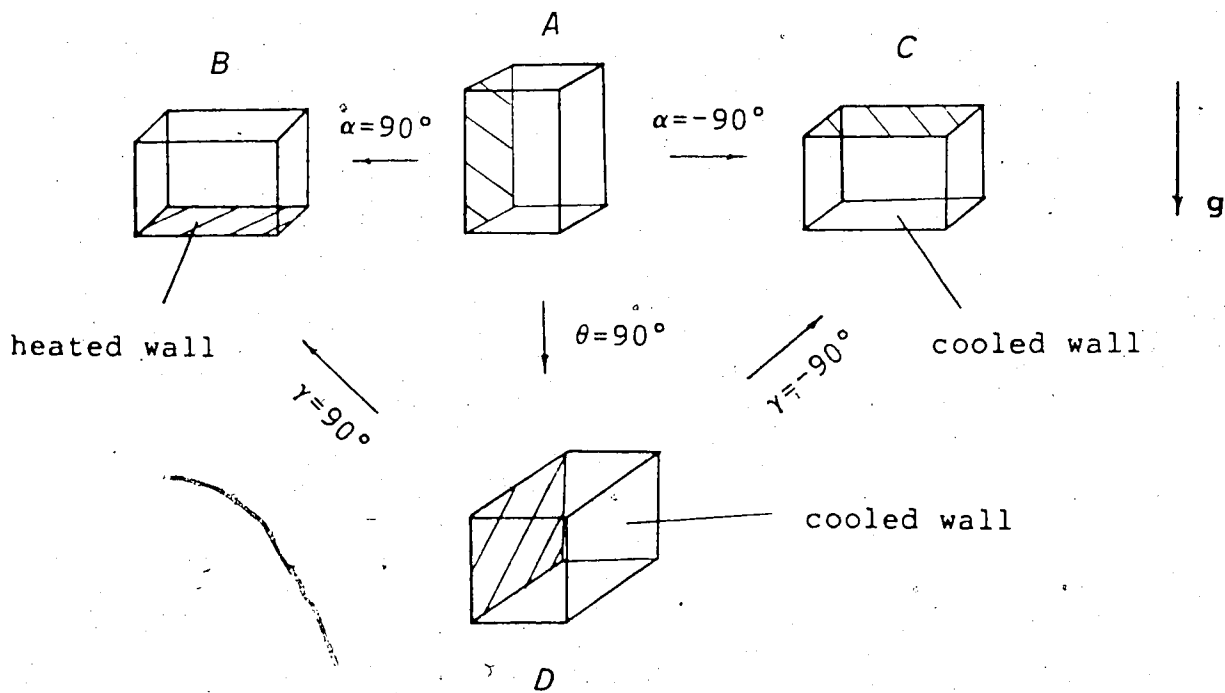
## B. GEOMETRY OF THE SYSTEM

The size of the box is specified by three lengths:  $W$ ,  $H$  and  $S$ , as shown in Fig.I-1.  $W$  is the width of the gap between the heated and the cooled walls.  $H$  (height) denotes the longer dimension of the remaining two leaving  $S$  (span) for the last dimension. We can alternatively define two dimensionless parameters, called aspect ratios, to describe the geometry of the box.  $A_x = H/W$  and  $A_z = S/W$  are aspect ratios in the  $X$ - and  $Z$ -directions respectively. The coordinates are indicated on the figure.

The coordinate system is fixed to the box in the following way. Choose one of the four corners on the heated surface of the box as the origin of the system, and three radiating edges from this point as three axes of  $X$ ,  $Y$  and  $Z$ . The direction of  $Y$ -axis points to the negative temperature gradient direction, i.e. points from the heated wall to the cooled wall. The  $X$ -axis lies along the longer one of the two remaining edges, and the  $Z$ -axis lies along the shorter one, with their directions such that the  $(X, Y, Z)$  system will form a right-handed coordinate system. When the two edges, other than that of the temperature direction, are of equal length, the  $X$ -axis can be arranged along any one of the two edges with the  $Z$ -axis along the other to make the  $(X, Y, Z)$  system a right-handed system. It can be seen that not all the four possible choices of coordinate systems are equally good. Two of them will locate the box in the region of  $Z < 0$ . The other two are equivalent and locate the box in the region of  $Z > 0$ .



a) Coordinates system



b) Reference configurations

Figure 1.1 Geometry of the system

In due course, we will fix the coordinate system in this way. Having fixed the coordinate system on the box, we can now develop the method to describe the orientation of the box with respect to gravity.

The orientation of the box with respect to gravity can be generally described by three orientation angles which could be any set of three independent space angles. To select the appropriate angles, it is desirable to first distinguish reference configurations to which an arbitrary orientation of the box can be referred. A classical configuration called the vertical cavity in the literature can serve as a reference. This is the case in which the X-axis is parallel but opposite to the gravity vector. In this study this is called configuration A (A for brevity). We define configuration B as the orientation of the box in which the Y-axis is parallel and opposite to the gravity vector. This corresponds to the classical Benard-Rayleigh convection situation (heated from below). C is the B configuration inverted, that is, when the box is heated from above, and the Y-axis is parallel to, and has the same sense as, the gravity vector. When the Z-axis is parallel and opposite to the gravity, we say the system is in configuration D. These four configurations are illustrated in fig.I-1.

It is can be easily seen that starting from one reference configuration, and rotating the box about any axis by  $90^\circ$ , we can get another one. Three angles are defined to

describe these processes. When we are viewing the box from  $Z=-\infty$ , rotating the box counter-clock-wisely, the angle traveled is called the tilt angle  $\alpha$ . Similarly, viewing from  $Y=+\infty$ , rotating the box counter-clock-wisely, we define a skew angle  $\theta$ . Viewing from  $X=+\infty$ , rotating the box counter-clock-wisely, defines the roll angle  $\gamma$ . With the above definitions, we can see that  $B$  can be obtained from  $A$  by a rotation of  $\alpha=90^\circ$ , or from  $D$  by a rotation of  $\gamma=90^\circ$ . Similarly,  $C$  can be obtained either from  $A$  with  $\alpha=-90^\circ$  or from  $D$  with  $\gamma=-90^\circ$  and  $D$  from  $A$  ( $\theta=90^\circ$ ) or from  $B$  ( $\gamma=-90^\circ$ ).

Two observations about the orientation of the box with respect to gravity are:

1. Any arbitrary orientation of the box can be uniquely specified knowing a reference configuration and the three angles defined above.
2. Taking  $A$  as the reference, the domain of  $-90^\circ < \alpha < 90^\circ$ ,  $0 < \theta < 90^\circ$ ,  $-90^\circ < \gamma < 90^\circ$  would cover all possible physically independent configurations.

It should be noted here that the behavior of the system is rather complicated, especially around the configuration  $B$  where bifurcation of the solution may be expected, and thus implying hysteresis behavior. The final state of the system is then not only dependent on the temperature difference imposed, box size and orientation, but also on the initial condition of the system or the path through which the final orientation is obtained. So it is important to distinguish different paths by which a final state is obtained. To make



the description clear and concise, for arbitrary configurations  $a$  and  $b$  say, we use  $ab$  to denote the process in which  $b$  is obtained by starting from  $a$  and rotating the appropriate angle through  $90^\circ$ . Thus path  $AB$  is the process that starts from  $A$ , rotates  $\alpha$  through  $90^\circ$  to get  $B$ .  $AB$  could be different from  $DB$ , say.

Having stated the problem we are solving and defined the geometrical parameters to describe the system (more parameters will be introduced later), we will examine the work that has been done to date in this area in the remainder of this chapter.

### C. REVIEW OF EXISTING WORK

The literature of natural convection in a rectangular cavity is huge. In this review we can only briefly examine a small part of it which is the most pertinent to this study.

Because of the many possibilities of changing the parameters describing the system, the number of special cases is numerous. However, two cases regarding the orientation of the cavity are the most studied and serve as a point of departure: the vertical cavity convection and Benard convection, corresponding to configuration  $A$  and  $B$  in our notation. These two cases will be the subject of this review too. We will first look at what has been done in the two-dimensional vertical cavity. Then the three-dimensional and the Benard convection problems will be briefly reviewed.

### Vertical Cavity: two-dimensional

Although there are two or three pieces of earlier experimental work, it is generally considered that the paper of G. W. Batchelor [3], 1954, was the first one of this kind addressed to the problem of natural convection in a vertical cavity. This work, motivated by the double-glaze window problem, was a theoretical one in which two extreme cases were examined: the case of low Rayleigh number or large aspect ratio and the case of very high Rayleigh number. ( $Ra = \beta g (T_h - T_c) W^3 / \mu \kappa$  is called the Rayleigh number which characterizes the relative magnitude of buoyancy and viscous force. More detailed discussion will be given later in the next chapter). In the first case, he concluded, in regions not too near the top and bottom walls, the flow had a parallel, S-shaped velocity profile with the fluid rising along the heated wall and descending along the cooled wall. The temperature profile was found to be linear across the gap between the two walls of different temperature. Heat transfer was by conduction. For the case of high Rayleigh number, boundary layers would be formed along the walls. An isothermal, constant-vorticity core existed in the interior of the cavity between the two boundary layers. He derived equations of boundary layers without solving them. G. Poots [4] later solved these boundary layer equations using the isothermal constant-vorticity core conditions and compared his predictions with experimental results then available. It is surprising that they agreed quite well considering the

fact that the assumed core condition was incorrect, as revealed later.

Eckert & Carlson [5] measured the temperature distribution in an air layer contained by two vertical plates of different temperatures. Their results clearly showed that, contrary to Batchelor's assumption, the core region was not isothermal but rather stratified in the vertical direction. This also implied that the core region could not have a rigid-body like rotation but stayed stationary. This resolved the question of whether the core is an isothermal constant-vorticity one or a stratified stationary one; both are mathematically possible from the governing equations.

Around 1965, Elder [6,7] showed both experimentally and numerically the existence of secondary flow in the interior of the cavity when the Rayleigh number is sufficiently high. The discovery of secondary flow stimulated further interest in the study of instability and the occurrence of secondary and tertiary flow. Later studies either confirmed or discovered new aspects of instability of the system: experimentally, theoretically and numerically. Papers on this subject area are a great many. Several ones of importance are listed in the references [8,9,10,11,12].

Paralleling the above effort, much work has been done in developing heat transfer correlations in order to provide guidelines for engineering design. Several excellent accurate correlations are available and can be found in

reference [13].

After more than thirty years of research, natural convection in a vertical cavity is quite well understood as long as it is taken as a two-dimensional problem. The major conclusions can be summarized as following:

1.  $0 < Ra < 10^3$ , Conduction regime: Cubic velocity profile, linear temperature profile.
2.  $10^3 < Ra < 5 \times 10^4$ , Transition Regime.
3.  $Ra > 5 \times 10^4$ , Boundary layer regime characterized by:
  - a. Boundary layers along two walls like wall jets.
  - b. Stationary thermal stratified core.
  - c.  $1/4$  power heat transfer correlation.
4.  $Ra > 10^5$ : Secondary flow in form of multi-cellular 'cats-eye' structure sets in.
5.  $Ra > 8 \times 10^5$ : Tertiary flow caused by secondary shear sets in.
6.  $Ra > 10^7$ : Flow becomes unsteady. Travelling waves were observed.
7.  $Ra 10^8 - 10^9$ : Turbulence prevails.

### Three-dimensional Flow

The aforementioned work is primarily modeled two-dimensionally. This is valid when either the third dimension is very large or extremely small. Three-dimensional features of natural convection in enclosures were not seriously considered until the mid-70's when the development of computing techniques, hard and

software, reached a point that made the study of three-dimensional flow possible.

The paper by Ozoe et. al. [14] is probably the first attempt to solve the three-dimensional problem numerically. At about the same time, Mallinson & de Vahl Davis [15] made a more complete study of the three-dimensional effect on natural convection in the vertical cavity. Highlights of the conclusions from this paper are:

1. The flow is not two-dimensional if the third dimension of the cavity is comparable with the other dimensions ( $Az=O(Ax)=O(1)$ ).
2. There is a weak flow in the third dimension which is caused by: a) the interaction between the primary circulation and the side wall; and b) the temperature gradient in that direction.
3. The Nusselt number (Nu) for the three-dimensional model is lower than that for the corresponding two-dimensional model.

Several papers have appeared in the past decade on three-dimensional natural convection. Besides the most general conclusions mentioned above, there were many specific properties noted. The three-dimensional flow structure and the associated heat transfer property are usually quite complicated and problem dependent. Case study is perhaps more appropriate than trying to state general conclusions. Two examples of case studies are given in references [11] and [12]. Three-dimensional natural

convection is still an area of fast growth and discovery.

### Benard-Rayleigh Convection

When the system is in configuration  $B$ , certain fascinating flow features will show up due to the coincidence of the temperature gradient imposed on the system and the gravitational acceleration vector. Actually, the study of the system in configuration  $B$  has been a debating ground for physicists and applied mathematicians, and the flow in this case was given a classical name - Benard-Rayleigh Convection, after the names of two pioneers of this field. Accumulated for about 90 years, publications in this area are simply too numerous to cover in this review. So we will only mention some of the most important contributions in order to lay a background for our future study.

At the turn of the century, H. Benard discovered the regular hexagonal flow pattern in a molten spermaceti layer (about 1mm thick) heated from below [18]. This experimental discovery opened up a new research area. Lord Rayleigh, in 1916, first theoretically predicted the onset of convection in an infinite horizontal fluid layer heated from below and confined between two free boundaries by solving a set of linearized governing equations [19]. The book by S. Chandrasekhar summarized all the linear theory results to date and is still the best source book on this subject today [20]. S. H. Davis [21] and I. Catton [22], by applying the

Galerkin method to the linearized governing equations, predicted the onset of convection and the preferred mode of motion in boxes of different aspect ratio. Their prediction was confirmed experimentally by Stork and Müller [23]. K. H. Winters and T. W. Brown recently found that for Rayleigh number slightly higher than the critical Rayleigh number, rolls parallel to both long and short sides of the box are possible flow patterns [35].

While the linear theory predicted the onset of convection, the non-linear theory achieved little in explaining various phenomena observed in experiments. Two excellent review articles on this problem, with emphasis on non-linear theory, are given in references [24] and [25]. Without going further into details, we list below the major conclusions for the Benard-Rayleigh convection.

Linear theory has been very successful in predicting the onset of convection in both two-dimensional and three-dimensional geometries:

1.  $Ra < Ra_c$ , there is no motion.
2.  $Ra > Ra_c$ , convection sets in and the heat transfer rate increases substantially.
3.  $Ra_c = 1707$  for an infinite fluid layer (two-dimensional).
4. In three-dimensional situations:  $Ra_c = Ra_c(Ax, Az)$  exist, and a series of rolls with axes parallel to the shorter side wall is usually considered to be the flow pattern.

Non-linear theory is unable to answer questions such as:

1. What is the planform: rolls, rings or polygons ?
2. What is the role of initial conditions in determining the flow pattern ?
3. What is the correlation between the wave number and Rayleigh number:
  - a. theory: wave number increases as Ra increases.
  - b. experiment: wave number decreases as Ra increases.
4. Is there nonlinear subcritical convection ?



## II. FORMULATION OF THE PROBLEM

In the previous chapter, the model system was described and five geometrical parameters describing the configuration of the system were defined. Two of the parameters have regard to the size of the box:  $A_x$  and  $A_z$ ; three of them describe the orientation:  $\alpha$ ,  $\theta$  and  $\gamma$ . We are now in a position to study the fluid and its motion under the actions of gravitational force and temperature gradient. First, in section A, the governing equations will be introduced. Then, by normalizing this set of equations in section B, two dimensionless parameters, known as the Rayleigh number,  $Ra$ , and the Prandtl number,  $Pr$ , will be identified. In section C, several qualitative properties of the governing equations and the boundary conditions are explored.

### A. FORMULATION

#### Conservation Laws

The governing equations for this system are the mathematical statements of the conservation laws. If the viscous dissipation of energy in the fluid is neglected, the equations for conservation of mass, momentum and energy can be written as:

$$\frac{D\rho}{Dt} + \rho \nabla \cdot \mathbf{V} = 0 \quad (II.1)$$

$$\rho \frac{D\mathbf{V}}{Dt} = -\nabla \cdot \mathbf{P} + \mu \nabla^2 \mathbf{V} + \rho \mathbf{g} \quad (II.2)$$

$$\rho C_p \frac{DT}{Dt} = k \nabla^2 T \quad (\text{II.3})$$

The  $D/Dt$  is the material derivative which consists of contributions from both the local and advective time rate of change. It should be noted here that the density of the fluid is variable and connected with the temperature and pressure through the equation of state. So, in general, this equation must be supplemented to close the set of equation.

#### **Boussinesq Approximation**

Two difficulties may arise here. First, the equation of state of a fluid may not be known accurately. Second, greater difficulties would be encountered in developing the method for solving compressible flow. So it is extremely difficult, if not impossible, to solve the problem without making some assumptions to simplify the situation. The common practice in simplifying the situation is to introduce the so-called Boussinesq approximation, invented by J. Boussinesq in 1903 [26]. This assumption is valid if:

1. The temperature of the fluid is not too high, as variable physical properties of the fluid may result.
2. The temperature difference between the heated and cooled walls is not too great and therefore the quadratic and higher terms of this difference may be neglected when the density is expanded as a Taylor series in temperature difference.

The scope of validity of this approximation is another topic

of interest, and a recent discussion on this problem is given in reference [27]. In all the situations considered here, the parameter range is well within the boundary of validity. So this approximation will be employed throughout this study without further notice.

From now on, we will restrict ourselves to Newtonian, Boussinesqian air. More specifically, the following assumptions about the air are made:

1. Air has constant physical properties (viscosity, thermal diffusivity, etc.).
2. There is no viscous dissipation.
3. Density variations are negligible except when buoyancy is concerned.
4. The density change in the buoyancy term is so small that it does not depend on the pressure and can be linearized in terms of temperature change.

Considerations are also restricted to situations of steady motion, i.e., the local time derivative is zero.

Now the Boussinesq approximation will be used to simplify eq. (II.1-3). First let us choose a reference state at which the fluid has density  $\rho_0$  and temperature  $T_0$ . The choice of this reference state is quite arbitrary but a natural choice is

$$T_0 = 0.5(T_h + T_c)$$

where  $T_h$  and  $T_c$  refer to temperatures of the heated and

cooled walls, respectively. We have assumed that

$$\rho = \rho_0 - \beta(T-T_0)$$

where  $\beta = -(1/\rho)(\partial\rho/\partial T)_p$  is the thermal expansion coefficient. Finally the buoyancy term becomes,

$$\rho g - \beta(T-T_0)g$$

Now split the pressure into two (static and dynamic) parts.

$$P = P_0 + P_d$$

The static pressure,  $P_0$ , is to balance the hydrostatic head of the fluid, i.e., the first part of the buoyancy. This static pressure has no effect on the flow pattern. It only serves as an arbitrary datum and obviously depends on the choice of the reference state. So,

$$-\nabla P_0 + \rho_0 g = 0$$

The dynamic pressure is the difference of the total pressure and the static pressure. It is this part of the pressure which is responsible for the details of the flow patterns. It is interesting to see that there is no separate equation to determine the pressure; nor is it prescribed. The dynamic

pressure is determined in the sense that the flow pattern calculated from the equation of motion must satisfy the continuity equation. From a different angle, we may view the continuity equation as an implicit equation which determines the pressure by demanding the result of the pressure. This viewpoint is very helpful when later the continuity equation is transformed into an equation for pressure to solve the governing equation numerically.

Finally, the simplified governing equations can be written down as:

$$\nabla \cdot \mathbf{V} = 0 \quad (\text{II.4})$$

$$\rho(\mathbf{V} \cdot \nabla)\mathbf{V} = -\nabla P + \mu \nabla^2 \mathbf{V} - \rho \beta g(T - T_0) \quad (\text{II.5})$$

$$\rho C_p \mathbf{V} \cdot \nabla T = k \nabla^2 T \quad (\text{II.6})$$

The above governing equations in vector form can be written in component form. Using the coordinate arrangement of the last chapter and referring the orientation angles to the configuration *A*, the component form equations are:

$$\frac{\partial U}{\partial X} + \frac{\partial V}{\partial Y} + \frac{\partial W}{\partial Z} = 0 \quad (\text{II.7})$$

$$U \frac{\partial U}{\partial X} + V \frac{\partial U}{\partial Y} + W \frac{\partial U}{\partial Z} = -\frac{1}{\rho} \frac{\partial P}{\partial X} + \nu \left( \frac{\partial^2 U}{\partial X^2} + \frac{\partial^2 U}{\partial Y^2} + \frac{\partial^2 U}{\partial Z^2} \right) + \beta g(T - T_0) \cdot \cos \alpha \cdot \cos \theta \quad (\text{II.8})$$

$$U \frac{\partial V}{\partial X} + V \frac{\partial V}{\partial Y} + W \frac{\partial V}{\partial Z} = -\frac{1}{\rho} \frac{\partial P}{\partial Y} + \nu \left( \frac{\partial^2 V}{\partial X^2} + \frac{\partial^2 V}{\partial Y^2} + \frac{\partial^2 V}{\partial Z^2} \right) + \beta g (T - T_0) \cdot \sin \alpha \cdot \cos \theta \quad (\text{II.9})$$

$$U \frac{\partial W}{\partial X} + V \frac{\partial W}{\partial Y} + W \frac{\partial W}{\partial Z} = -\frac{1}{\rho} \frac{\partial P}{\partial Z} + \nu \left( \frac{\partial^2 W}{\partial X^2} + \frac{\partial^2 W}{\partial Y^2} + \frac{\partial^2 W}{\partial Z^2} \right) + \beta g (T - T_0) \cdot \sin \theta \quad (\text{II.10})$$

$$U \frac{\partial T}{\partial X} + V \frac{\partial T}{\partial Y} + W \frac{\partial T}{\partial Z} = \kappa \left( \frac{\partial^2 T}{\partial X^2} + \frac{\partial^2 T}{\partial Y^2} + \frac{\partial^2 T}{\partial Z^2} \right) \quad (\text{II.11})$$

### Boundary Conditions

The boundary conditions of no-slip on the walls are adopted for the three components of the velocity, i.e.,

$$U = V = W = 0 \text{ on all six walls.}$$

Three kinds of temperature boundary condition will be used in this study. They are

1. BC1: Isothermal heated and cooled opposite walls of temperatures  $T_h$  and  $T_c$ , respectively, with four perfectly conducting connecting walls of linear temperature distribution along Y, i.e.:

$$T = T_h \text{ for } Y = 0$$

$$T = T_c \text{ for } Y = W$$

$$T = T_h - (T_h - T_c) Y/W \text{ for } X = 0, X = H, Z = 0, Z = S.$$

2. BC2: Isothermal heated and cooled opposite walls with four perfectly insulated connecting walls:

$$T = T_h \text{ for } Y = 0$$

$$T = T_c \text{ for } Y = W$$

$$\partial T / \partial X = 0 \text{ for } X = 0 \text{ and } X = H$$

$$\partial T / \partial Z = 0 \text{ for } Z=0 \text{ and } Z=S$$

3. BC3: Perfectly insulated heated and cooled walls with four perfectly conducting walls of linear temperature distribution in the Y-direction, i.e.,

$$\partial T / \partial Y = 0 \text{ for } Y=0 \text{ and } Y=W$$

$$T = T_h - (T_h - T_c) Y/W \text{ for } X=0, X=H, Z=0, Z=S.$$

## B. NORMALIZATION

Normalization will now be employed to transform the governing equations into a more appropriate form. Proper normalization of the governing equations would bring us at least three benefits.

1. A group of non-dimensional similarity parameters (which can completely define the physical process of the system) can be identified.
2. By scaling each term in the normalized equations, the relative importance of each term for a given set of parameters can be determined, and thus reasonable approximations can be made, or some qualitative (order of magnitude) estimate of the behavior of the system can be obtained. This kind of estimate is very useful in having some idea of what result we should anticipate.
3. By choosing proper scales, we can make the normalized field variables (V and T) of order unity. This provides better control over the numerical procedure employed to solve the equations.

It is obvious that there cannot be a universally valid set of scales which enables us to get all the aforementioned three benefits. Since our concerns are primarily control over the numerical procedure, the third criterion will be emphasized with some compromise to others.

The scales (characteristic quantities) for each variables in this study are chosen to be:

Variable	Scale
X	H
Y	W
Z	S
U	$Ax\sqrt{(\beta g[T_h - T_o]W)}$
V	$\sqrt{(\beta g[T_h - T_o]W)}$
W	$Az\sqrt{(\beta g[T_h - T_o]W)}$
T	$T_h - T_o$
P	$\beta g(T_h - T_o)W$

Substituting the above scales into eqs.(II.7-11), and using lower case letters to represent the normalized variables, we can write the normalized equations as follows:

$$\frac{\partial u}{\partial x} + \frac{\partial v}{\partial y} + \frac{\partial w}{\partial z} = 0 \quad (\text{II.12})$$

$$\text{DOCV}(u) = -\frac{1}{Ax^2} \cdot \frac{\partial p}{\partial x} + \text{DOCD}(u) + \frac{1}{Ax} \cdot \phi \cdot \cos\alpha \cdot \cos\theta \quad (\text{II.13})$$



$$\text{DOCV}(v) = -\frac{\partial p}{\partial y} + \text{DOCD}(v) + \phi \cdot \sin\alpha \cdot \cos\theta \quad (\text{II.14})$$

$$\text{DOCV}(w) = -\frac{1}{Az^2} \cdot \frac{\partial p}{\partial z} + \text{DOCD}(w) + \frac{1}{Az} \cdot \phi \cdot \sin\theta \quad (\text{II.15})$$

$$\text{DOCV}(\phi) = \frac{1}{Pr} \cdot \text{DOCD}(\phi) \quad (\text{II.16})$$

where

$$\text{DOCV} = u \frac{\partial}{\partial x} + v \frac{\partial}{\partial y} + w \frac{\partial}{\partial z}$$

and

$$\text{DOCD} = \sqrt{(2Pr/Ra)} \cdot \left( \frac{1}{Ax^2} \cdot \frac{\partial^2}{\partial x^2} + \frac{\partial^2}{\partial y^2} + \frac{1}{Az^2} \cdot \frac{\partial^2}{\partial z^2} \right)$$

are Differential Operators for Convection and Conduction, respectively;

$\phi = (T-T_0)/(T_h-T_0)$  is the normalized temperature;

$Ra = \beta g (T_h - T_c) W^3 / \nu \kappa$  is the Rayleigh number;

$Pr = \nu / \kappa$  is the Prandtl number.

As a result of normalization, two more parameters, Ra and Pr, describing the system appear. The Rayleigh number characterizes the relative magnitude of the buoyancy and the viscous force. Ra is determined by the magnitude of the temperature gradient, the geometry and the fluid used. On the other hand, the Prandtl number is a property of the fluid and characterizes the relative ability of the fluid to transport momentum versus heat. In this study, Pr is fixed

at 0.71.

The normalized boundary conditions follow automatically.

Taking the BC1 as an example:

$u=v=w=0$  on all walls.

$\phi=1$  for  $y=0$

$\phi=-1$  for  $y=1$

$\phi=1-2y$  for  $x=1, x=1, z=0, z=1$ .

### C. SOME QUALITATIVE CONSIDERATIONS OF THE GOVERNING EQUATIONS

#### Symmetry

For the set of equations (II.12-16) (and BC1, BC2 and BC3, some sorts of symmetry exist. This can be seen clearer by moving the origin of the coordinate system to the center of the cavity such that the 'normalized' domain is  $-0.5 < x, y, z < 0.5$ .

1. Centro-symmetry. Transforming the variable  $(x, y, z, u, v, w, \phi)$  to  $(-x, -y, -z, -u, -v, -w, -\phi)$ , we find that the governing equations (II.12-16) and the three boundary condition sets are left unchanged. Invariance under the above transformation means that if  $(x, y, z, u, v, w, \phi)$  is a solution to the problem,  $(-x, -y, -z, -u, -v, -w, -\phi)$  is also a solution to the problem. This is equivalent to stating that the solution of the problem is anti-symmetric about the center of the cavity. This property is general, regardless of the

orientation of the cavity. When the orientation of the cavity is more restricted, more symmetry properties which are very useful from a computational point of view exist.

2. XY plane centro-symmetry. For situations of  $\theta = 0$ , the equations and boundary conditions are invariant if we make the transformation  $(x, y, u, v, \phi) \rightarrow (-x, -y, -u, -v, -\phi)$ . This implies that at each z-section the xy-plane solution is anti-symmetric about the center of the plane.
3. z central-plane symmetry. Again when  $\theta = 0$ , transformation of  $(z, w) \rightarrow (-z, -w)$  will not change the forms of both governing equations and boundary conditions. This is equivalent to stating that the z-central plane is like a mirror. The solution on one side of the z-middle plane is exactly the mirror image of the other side of this plane, i.e.  $u$ ,  $v$  and  $\phi$  are symmetric and  $w$  is anti-symmetric about the  $z=0.5$  plane.

The symmetric properties of the solution just revealed are very useful. The first two symmetric properties of the solution can serve as a check on the validity of the solution. Taking advantage of the third one, we can model only half of the domain to save computing effort and to obtain higher accuracy of the solution by placing a given number of nodes in a smaller space.

An important point to be emphasized here is that the symmetric solution discussed is not a necessary requirement.

In other words, the equations and boundary conditions do admit to non-symmetric solutions and in many cases they do occur. This kind of non-symmetric solution is observed when the system is at or near configuration B. More about this will be discussed later.

### Circulation, Primary and Secondary Planes

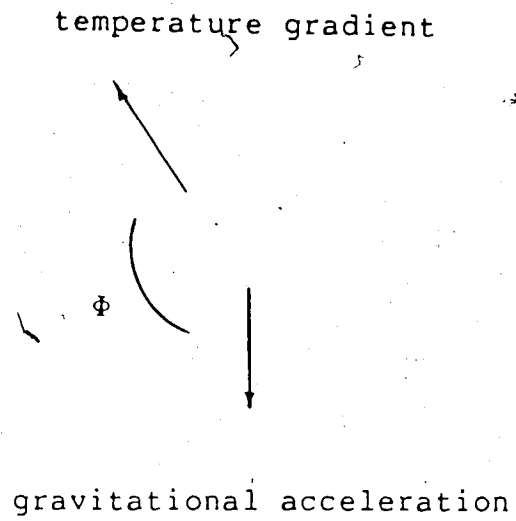
Two vectors play the determining role in a natural convection system: the Gravitational Acceleration (GA) vector and the Temperature Gradient (TG) vector. The direction of the gravity vector is fixed downward while the direction of the temperature gradient at each point within the fluid is variable. Although the TG is important in determining the behavior of the system, it does not appear explicitly in the governing equations; nor does the angle between the two vectors. Actually, the TG is imposed on the system by the boundary conditions. In this study, the TG thus imposed will be referred to as the Global Temperature Gradient (GTG) which will, together with other conditions, determine the velocity and temperature distributions in the fluid. As the result of fluid motion, the TG at each point is different from the GTG and will be called the Local Temperature Gradient (LTG).

It can be proven, using the governing equations, that it is the angle  $\Phi$  between GA and TG which determines whether convection will set in (see [28], for example). Three situations are possible:

1.  $\phi=180^\circ$ , the fluid is stably stratified and no motion will occur.
2.  $\phi=0^\circ$ , no motion will occur until the magnitude of the temperature gradient exceeds a certain threshold.
3. In all other situations the fluid motion occurs immediately.

In this last situation, the primary feature of the flow pattern around the point concerned can be predicted qualitatively in the following way. The vectors GA and TG, when not parallel to each other, will determine a unique plane in which both vectors lie. The primary feature of the flow pattern near a point will be a circulation in this plane. The direction of the vorticity is given by the vector product of GA and TG (fig.II-1). The plane in which the circulation occurs at a point will be called the Circulation Plane (CP) at this point. It should be noted here that when  $\phi=0^\circ$  there is an infinite number of possible circulation planes, thus causing indefiniteness in the flow pattern.

The CP just introduced is a local property determined by LTG and GA. For the whole system, the circulation plane of the GTG will be called the Primary Plane. Major events of the fluid motion occur in the primary plane. Planes perpendicular to the primary plane and to one of the axes of the coordinate system are Secondary Planes in which three-dimensional effects of the flow pattern are best exhibited. Once again, for configuration B the primary plane is indefinite implying ambiguity of the flow pattern at this



circulation direction

The diagram shows a circular path with arrows indicating a counter-clockwise direction of circulation.

Figure II.1 Working principle to predict circulation direction

configuration.

5

✓

### III. METHOD OF SOLUTION

#### A. INTRODUCTION

The governing equations (II.12-16) form a set of coupled nonlinear partial differential equations. They can not be solved analytically in a closed form. The only possible way to solve them is to resort to a numerical technique.

The Navier-Stokes equations (II.13-15) and energy equation (II.16) are examples of a general type of convection-diffusion equation which has convection terms, diffusion terms and source terms. The difficulty in solving this type of equation numerically lies in how to treat the convection term. The second order accurate central difference scheme, which is suitable for solutions of the conduction equation, would lead to instability or divergence of the solution for most practical cell Peclet number (or Reynolds number). On the other hand, the up-wind scheme guarantees a converged solution by introducing an artificial diffusion term which will make the cell Peclet number always small enough to ensure stability. But this artificial diffusion term may cause intolerable errors for small to moderate cell Peclet numbers; hence a dilemma which has no general resolution. A successful scheme is always a compromise between accuracy and numerical stability.

Besides the numerical stability problem, the Navier-Stokes equation has a problem of its own. The source



terms contain the pressure gradient. The difficulty comes out of the fact that the pressure is neither prescribed nor given explicitly by an equation. Hence any attempt to solve the Navier-Stokes equation must first answer the question: how should the pressure term be treated. There are mainly two ways of doing this. One is to cross-differentiate the equations to eliminate the pressure terms at the cost of increasing the order of the equations and the number of variables. In this method, one has to produce supplementary higher order boundary conditions required by the equations. This approach is often called the streamline-vorticity method since the dependent variables are the stream function and vorticity. An alternative way to overcome the difficulty is to transform the continuity equation into an equation for pressure with the understanding that the pressure is but an agent to enforce the continuity requirement. This approach leads to the SIMPLE-type algorithm. This approach is going to be followed in this study.

Any numerical method is necessarily an approximation procedure applied to the governing equations. There are quite a few well-developed approximation procedures to solve partial differential equations nowadays. Two major classes of procedures are the Finite Difference Method (FDM) and the Finite Element Method (FEM). As many authors have pointed out (e.g. [29,30]), these two classes of procedures can be unified under the name of the Weighted Residual Method. In this sense, the difference between different approximation

procedures is but a matter of choice of different weighting (trial) functions in approximating the 'real' functions. Among many possibilities, FDM and FEM utilize piece-wise trial functions to make the to-be-determined constants in front of the trial functions to be the actual field values at a set of discretized nodal points. In calculating the values at these points, an approximation of the field variables is obtained.

In the next section, a brief description of the discretization procedure is given. In section C, an algorithm called SIMPLE-C will be described. In section D, some problems concerning coding of the algorithm, control of the program and accuracy will be discussed. In the last section of this chapter, the various ways of presenting three-dimensional flows will be briefly discussed.

## B. DISCRETIZATION

To illustrate the method, consider the energy equation:

$$\rho V \cdot \nabla \phi = \nabla \cdot (\Gamma \nabla \phi) + S \quad (\text{III.1})$$

As mentioned before, the trial (base) function in our method is piece-wise unit function on a series of 'finite volumes'. First, the whole domain is divided into  $N \times M \times L$  small rectangular volumes as illustrated in fig.III-1.  $N$  is the number of divisions in the x-direction and  $M$  and  $L$  are those for the y and z-direction respectively. Each small volume

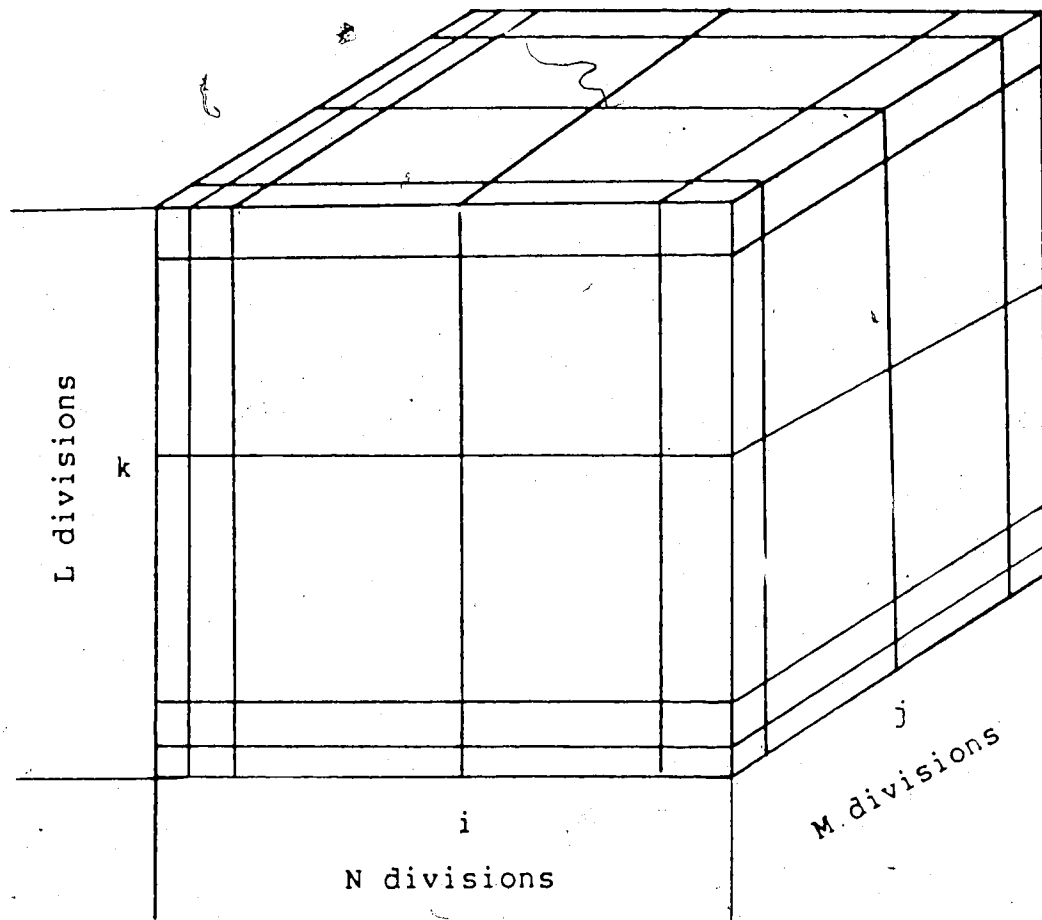


Figure III.1 Discretization of the computational domain

thus obtained is called a finite volume and  $V_{ijk}$  is used to denote the finite volume of the  $i$ th in the  $x$ -direction,  $j$ th in the  $y$ -direction and  $k$ th in the  $z$ -direction.

The trial function we are going to use is defined as:

$$\begin{aligned} T_{ijk}(x,y,z) &= 1 \text{ if } (x,y,z) \in V_{ijk} \\ T_{ijk}(x,y,z) &= 0 \text{ otherwise.} \end{aligned} \quad (\text{III.2})$$

Multiplying the trial function  $T_{ijk}$  with the equation to be discretized and integrating over the whole domain, we get the discretized equation of No.  $(i,j,k)$ :

$$\int T_{ijk} \rho \mathbf{v} \cdot \nabla \phi \, dV = \int T_{ijk} \nabla \cdot (\Gamma \nabla \phi) \, dV + \int T_{ijk} S \, dV$$

or

$$\int \rho \mathbf{v} \cdot \nabla \phi \, dV = \int \nabla \cdot (\Gamma \nabla \phi) \, dV + \int S \, dV \quad (\text{III.3})$$

To evaluate the integral in (III.3), we focus our attention on the sample finite volume depicted in fig.III-2. The center point of the finite volume, the calculated point, is designated as  $P$  and the neighboring points as  $E, W, N, S, T$  and  $B$ . Points on the six surfaces are called  $e, w, n, s, t$  and  $b$ . The result of the integration can be written in the form of an algebraic equation relating the variable value at  $P$  with neighboring points:

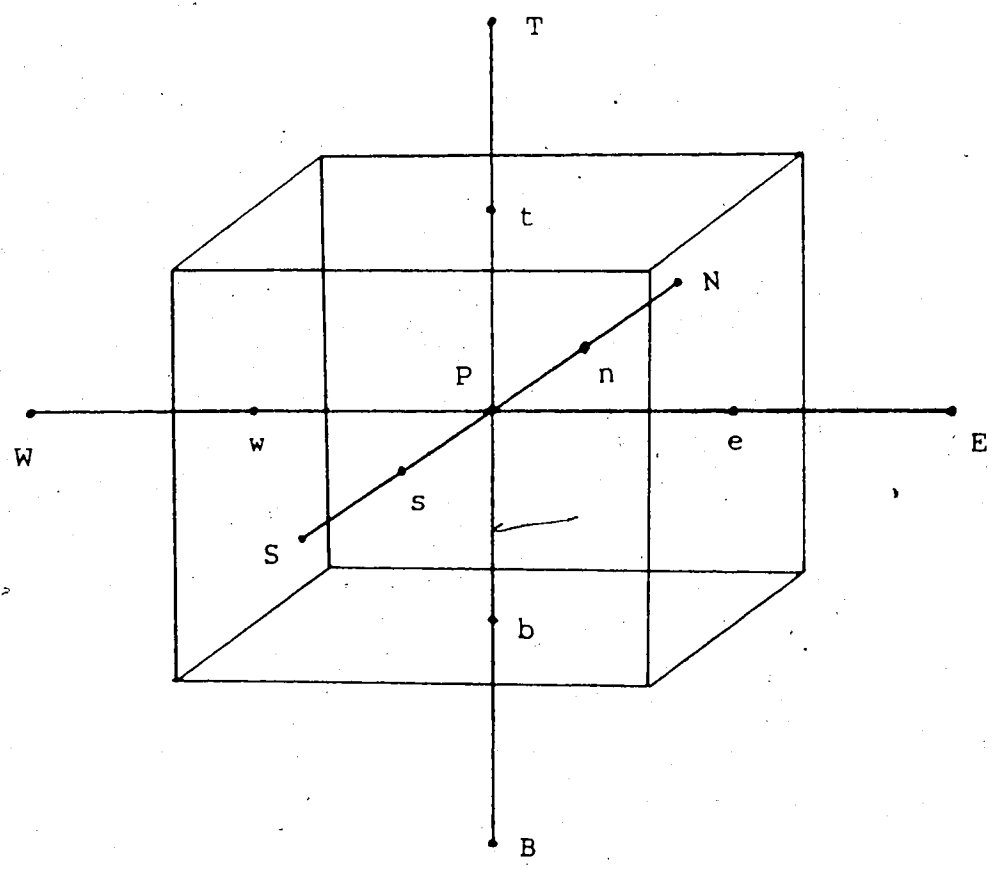


Figure III.2 A sample finite volume

$$a_P \phi_P = a_E \phi_E + a_W \phi_W + a_N \phi_N + a_S \phi_S + a_T \phi_T + a_B \phi_B + b \quad (\text{III.4})$$

The coefficients  $a$  incorporate the influence of the neighboring points on the calculated point. To calculate these coefficients an interpolation function between neighboring points must be chosen. It is the choice of these interpolation functions that characterize the scheme (upwinding, hybrid, etc.). We adopt here the so-called power-law interpolation recommended by Patankar [31]. This is basically a hybrid scheme which reduces to the upwind scheme when the cell Peclet number is greater than 10 and otherwise is a 5th power curve to approximate the exact profile in between the nodal points. After manipulations, the coefficients can be shown to be:

$$a_E = D_e A(|P_e|) + \text{MAX}(-F_e, 0)$$

$$a_W = D_w A(|P_w|) + \text{MAX}(F_w, 0)$$

$$a_N = D_n A(|P_n|) + \text{MAX}(-F_n, 0)$$

$$a_S = D_s A(|P_s|) + \text{MAX}(F_s, 0)$$

$$a_T = D_t A(|P_t|) + \text{MAX}(-F_t, 0)$$

$$a_B = D_b A(|P_b|) + \text{MAX}(F_b, 0)$$

$$b = S \Delta x \Delta y \Delta z$$

$$a_P = a_E + a_W + a_N + a_S + a_T + a_B$$

where

$$F_e = (\rho u)_e \Delta y \Delta z \quad D_e = \Gamma_e \Delta y \Delta z / (\delta x)_e$$

$$F_w = (\rho u)_w \Delta y \Delta z \quad D_w = \Gamma_w \Delta y \Delta z / (\delta x)_w$$

$$F_n = (\rho v)_n \Delta z \Delta x \quad D_n = \Gamma_n \Delta z \Delta x / (\delta y)_n$$

$$\begin{aligned}
 F_s &= (\rho v)_s \Delta z \Delta x & D_s &= \Gamma_s \Delta z \Delta x / (\delta y)_s \\
 F_t &= (\rho w)_t \Delta x \Delta y & D_t &= \Gamma_t \Delta x \Delta y / (\delta z)_t \\
 F_b &= (\rho w)_b \Delta x \Delta y & D_b &= \Gamma_b \Delta x \Delta y / (\delta z)_b
 \end{aligned}$$

and

$$P = F/D$$

$$A(|P|) = \text{MAX}(0, (1 - 0.1|P|)^3)$$

The MAX is the function to pick up the larger one of the two arguments.

Knowing the coefficients, eq.(III.4) is a linear algebraic equation which can be solved, together with the boundary conditions, using the TDMA algorithm. For details, see [31].

### C. ALGORITHM

It has been noted that the major difficulty in solving the Navier-Stokes equations numerically resides in the pressure. To overcome this difficulty, in the SIMPLE algorithm, the continuity equation is transformed into an equation for pressure. The mathematical details of this algorithm can be found in [31] and will not be repeated here. The procedure consists basically of the following steps:

1. Integrate the Navier-Stokes equation throughout the cell to get a relationship between the velocity and the pressure.
2. Make approximations to this relation.

3. Demand that the velocity satisfy continuity identically. Determine the velocity correction necessary to satisfy this demand.
4. Use the velocity-pressure relation to determine the pressure correction necessary to give the velocity correction in step 3.
5. Update both pressure and velocity by adding their corrections.
6. Repeat the above steps until the solution is converged to some specified accuracy.

Various features can be added to make the algorithm more usable. An example is the SIMPLE-R, a revised version of SIMPLE. What we will use in this study is another modified version of SIMPLE, the SIMPLE-C, which follows exactly the procedure described above except that it incorporates an improved approximation at step 2 which is believed to make the algorithm more consistent (thus the 'C'). See [32] for details.

#### D. CONTROL AND ACCURACY OF THE PROGRAM

The SIMPLE-C algorithm is realized in FORTRAN-77 language. The program has five subroutines and about six hundred lines of code. It can adapt to a non-uniform grid system in any prescribed form as long as the control volume is rectangular and can handle boundary conditions of Dirichlet, Neumann and mixed types. The complete code is listed in the Appendix.



In this program, two levels of accuracy control are implemented. The first level is control over the constant coefficient algebraic equations. This control is in the SOLVER in the form of a residual criterion. The second level of control is exercised over the relative errors in the dependent variables for two consecutive iterations. This is done by subroutine ERR. While the values for the first level control are variable, that for the second level is 1%.

As a test of the validity of the program, the same problem treated by Mallinson & de Vahl Davis was re-calculated. Listed below is a comparison for  $Ax=1$ ,  $Az=2$  and  $Ra=10^4$  with a  $15 \times 15 \times 29$  mesh:

Comparison with Reference [15]

Nu in [15]	Our Nu	$\Delta Nu/Nu$
2.20	2.24	1.79%
$W_{max}$ in [15]	Our $W_{max}$	$\Delta W/W$
2.286	2.256	1.31%

It is seen that the agreement is excellent considering the fact that in this program the staggered grid system is employed while it was not in [15].

A consistency study was undertaken using several mesh networks for  $Ax=Az=0.2$ . The three mesh system tested were  $11 \times 51 \times 11$ ,  $13 \times 61 \times 13$  and  $15 \times 71 \times 15$  resulting in cubic finite

volumes of 0.1, 0.0833 and 0.0714. It is found that even the most coarse grid system can still catch all the features of the flow structure. In terms of revealing qualitative features of the flow pattern, all three grid systems tested were equally good. Comparisons of representative Nu obtained from different grid systems are shown in figs. III-3 and 4 for the  $A_x=A_z=0.2$  cavity at  $A$  for several Ra; and at  $Ra=2.5 \times 10^4$  for several tilt angle  $\alpha$ . As the grid system changes from 0.1 to 0.0833, the difference in Nu compared with that obtained using the 0.0714 grid system goes from about 10-15% to 3-5%. So it is reasonable to believe that the accuracy in Nusselt number obtained using the  $15 \times 71 \times 15$  grid system is reliable within about 5-10%. The flow pattern, on the other hand, is qualitatively unchanged for the three different mesh systems.

#### E. METHOD OF PRESENTATION

Of special interest in this study is the three-dimensional structure of the flow pattern. It is obviously not an easy task to present three-dimensional reality on two-dimensional paper. There seems to be no single best way to do the job. Mallinson & de Vahl Davis ([15]) showed the flow structure by tracing a particle for a certain length of time. This method, good for a certain purposes, is also employed by several other authors, but it has at least two drawbacks: a) It does not give clearly an overall picture of the whole flow field since only one

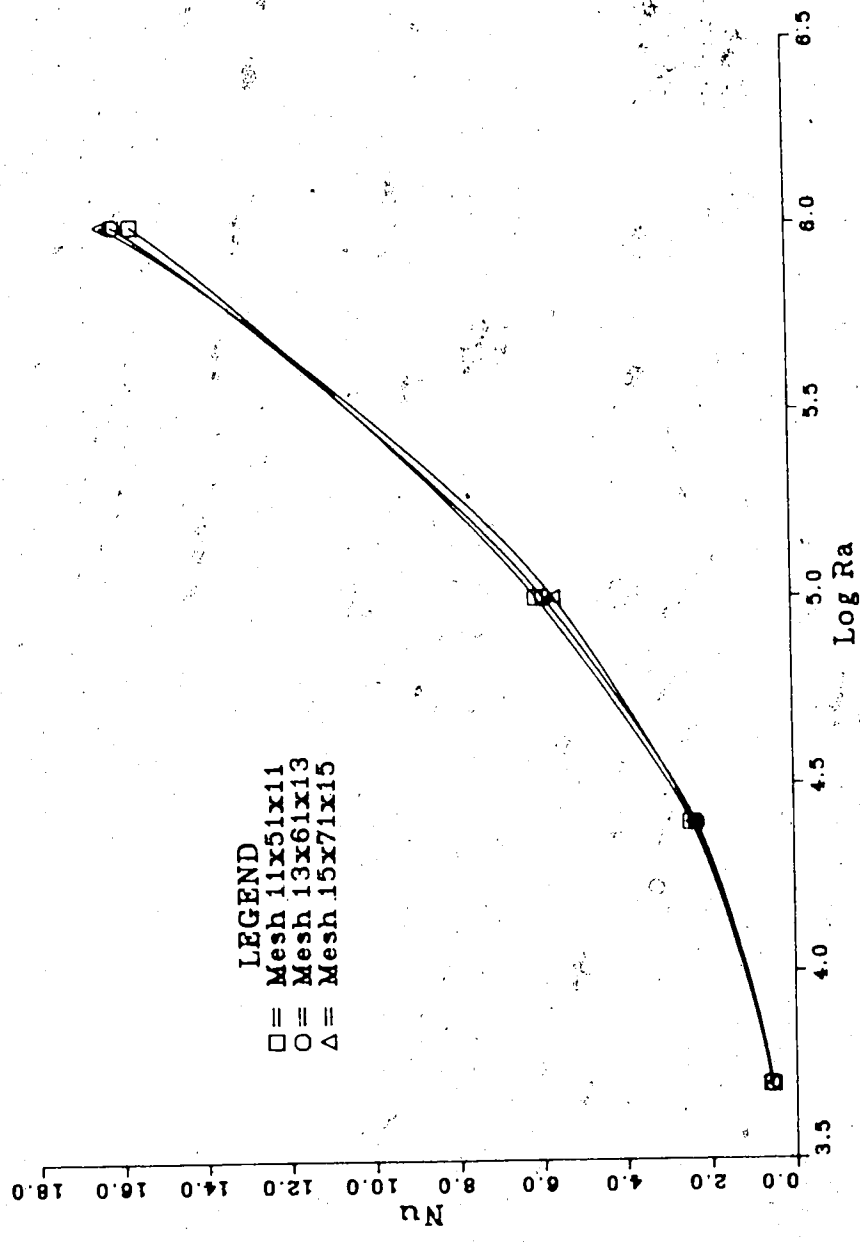


Figure III.3 Consistency check for the program: variable Ra

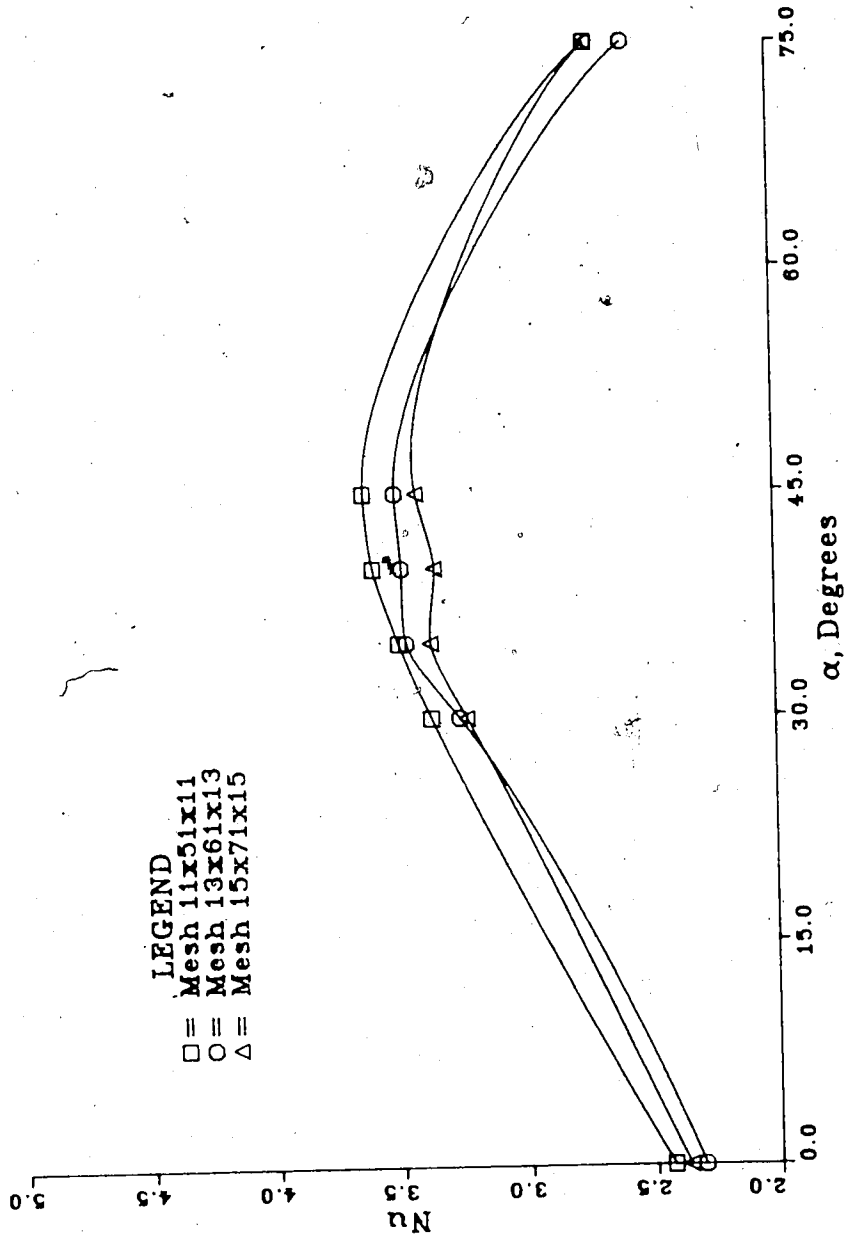


Figure III.4 Consistency check for the program: Variable  $\alpha$

particle is traced. By following only a small part of the fluid, some important features might be missed; b) It is very expensive and time-consuming to integrate the velocity to get a particle path. We will not use this method but instead show the velocity at different cross sections of the cavity.

There are three normal planes for a three-dimensional object. Each plane can be specified by the names of the axes which lie in this plane together with the distance from the origin in the direction normal to the plane. For example, it is clear what is meant by "the xy plane at  $z=0.3$ ". By plotting out velocities at selected planes, the whole flow structure can be constructed.

The velocity at a plane may be described using three-dimensional arrows representing the velocities at nodal points in the plane. But the three-dimensional arrows will be distorted and overlapping in a two-dimensional plane thus making the picture difficult to read. Therefore an alternative is pursued. The velocity will be broken into tangential and normal components to the plane. The tangential components are represented by two-dimensional arrows in the plane and the normal component by a three-dimensional surface over the plane, the distance from the surface to the plane representing the magnitude of the normal velocity. By showing both tangential and normal velocity at various planes, a vivid picture of the three-dimensional flow can be portrayed.

For temperature, we will demonstrate its distribution not by plotting the isothermal contours in a plane but rather by the three-dimensional surfaces similar to those used for normal velocity, since they are more vivid.

#### IV. LONGITUDINAL TEMPERATURE GRADIENT $Ax=0.2$ , $Az=0.2$ CAVITY

In this chapter, natural convection in a slender box will be studied. The longest dimension, in the direction of the GTG, is five times longer than the other two dimensions which are equal. In section A, the effect of increasing the Rayleigh number for configuration A is examined. In section B,  $Ra$  is kept constant at  $2.5 \times 10^4$  while the effect of tilt from A is examined. In section C, the effect of skew from configuration A is studied.

For section A and B, the mid-z plane symmetry exists as explained in chapter II. Taking advantage of this symmetry, calculations in the first two sections are carried out using a  $15 \times 71 \times 8$  mesh network covering half the computational domain. In the absence of this symmetry, the results of the third section are obtained using a  $13 \times 51 \times 13$  mesh network covering the whole computational domain.

The Rayleigh number used in this section is based on the shortest length,  $H$ , i.e.,  $Ra = \beta g \Delta T H^3 / \nu \kappa$ . The Nusselt number is based on the heat transfer rate through all the walls of the box not only the heated wall, the conventional way. So,  $Nu = QH / A \kappa \Delta T$ , where  $Q$  is the total heat flux through all the walls of the box and  $A = H^2 + 2HW$  is half the total wall area of the box.

When  $Ax \geq 1$ , the behavior of the system is determined by the  $u$  velocity component which may therefore be used in a classification of regimes. If  $Ax = 0.2$ , on the other hand, the longer dimension is the  $y$ -direction and the important

features of the system are reflected in the profile of the  $v$  velocity. So we will try in due course to compare the profile of the  $v$  velocity in this cavity with the  $u$  velocity in the  $Ax \geq 1$  cavity and thereby make an appropriate classification of flow regimes.

#### A. CONFIGURATION A: THE EFFECT OF RAYLEIGH NUMBER

In this configuration, the primary plane is the  $xy$  plane. The  $xy$  plane velocities, especially the  $v$  velocity, play the determining role for this system. The mid- $z$   $xy$  plane velocities are plotted in fig.IV-1,2,3 for  $Ra=50$ ,  $2.5 \times 10^4$  and  $10^6$ . Boundary conditions BC1 have been used.

Fig.IV-1 shows a weak circulation in the direction predicted by the working principle of section II-C-2 (WP II-C-2). For  $Ra=50$ , the flow is so weak that it has no effect on temperature distribution in the fluid. The LTG at every point of the system is the same as the GTG and lies parallel to the  $y$ -axis. Correspondingly, the circulation plane at each point is coincident with the primary plane. No secondary flow appears. Heat is only transported through the system at the heated and cooled walls by conduction. The whole system behaves like a solid under a temperature gradient, and is thus in the conduction regime.

Fig.IV-2 and 3 are at Rayleigh numbers for transition and boundary layer flows, respectively, with  $Ax \geq 1$  cavity. Things are different for the  $Ax=0.2$  cavity. It has been mentioned that for  $Ax \geq 1$  cavity the most important velocity



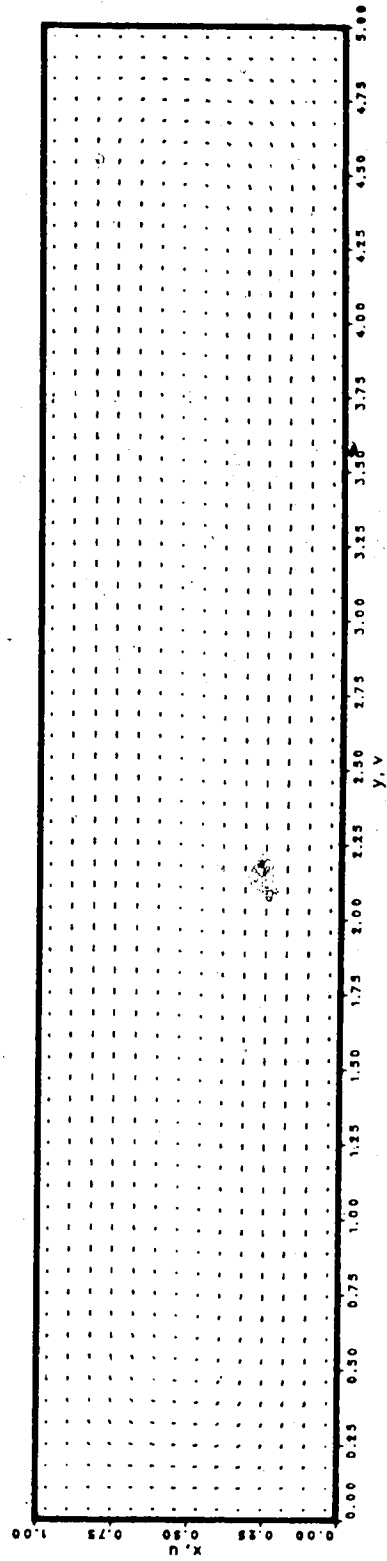


Figure IV.1 xy plane velocity,  $z=0.5$ ,  $Ra=50$

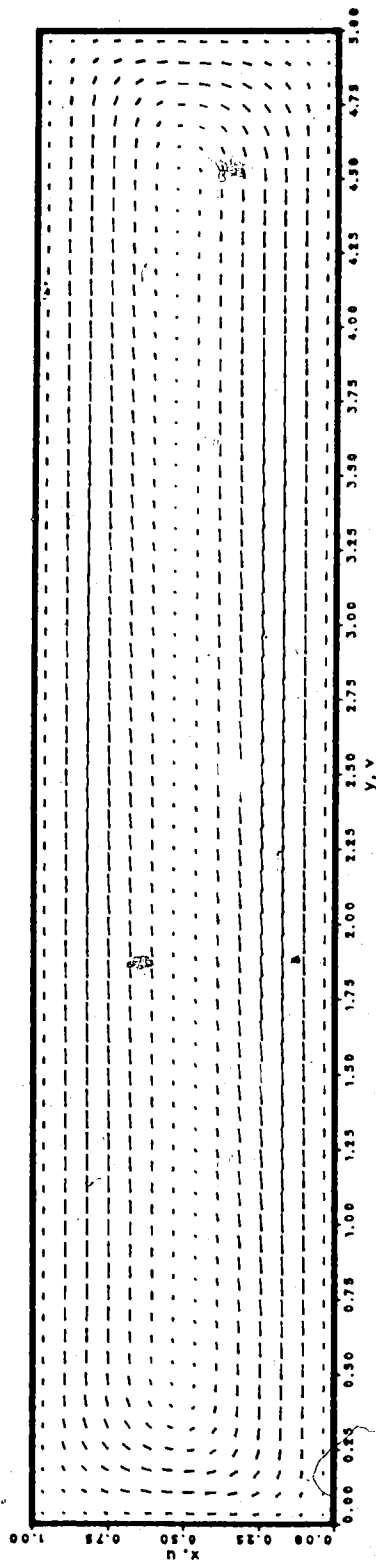


Figure IV.2 xy plane velocity,  $z=0.5$ ,  $Ra=2.5 \times 10^4$

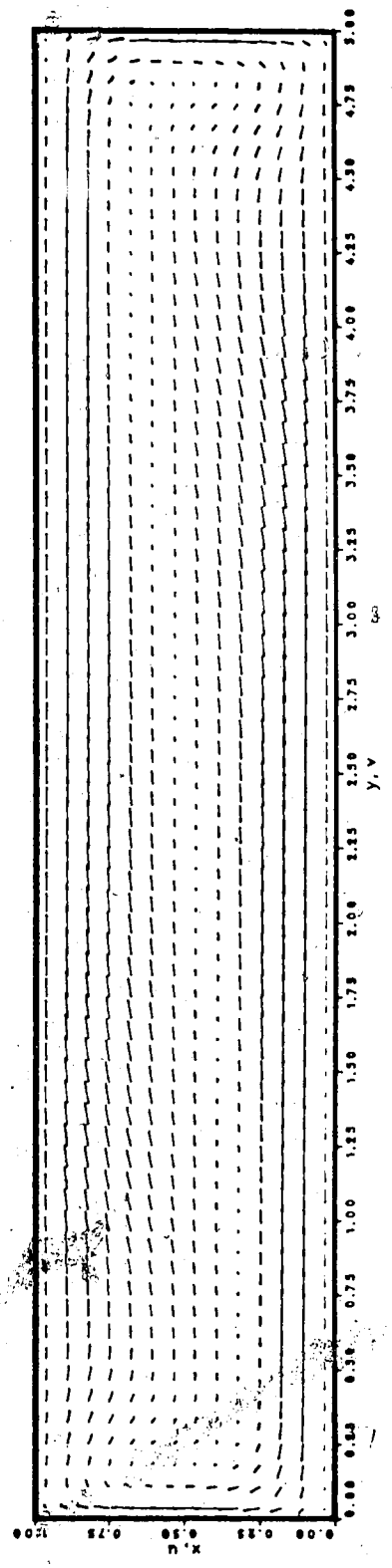


Figure IV.3 xy plane velocity,  $z=0.5$ ,  $Ra=10^4$

component is  $u$ , in contrast to  $v$  for the  $Ax=0.2$  cavity. Classification of regimes made for the  $Ax \geq 1$  cavity is based on the behavior of  $u$  velocity. For the  $Ax=0.2$  cavity, however, the criteria of classification of regimes must be based on the behavior of the  $v$  velocity. It is noted that, at  $A$ , the driving force for  $u$  is buoyancy, while that for the  $v$  is pressure gradient. The difference in the nature of the driving force for  $u$  and  $v$  results in the difference in  $u$  and  $v$  for the same nominal condition (same  $Ra$ ). This difference in behavior of the most important velocity components for the  $Ax \geq 1$  and  $Ax < 1$  cavities determines that the classification of regimes in one case does not necessarily hold true in the other case. Indeed, from fig.IV-3 we can hardly find the evidence required for us to consider the system being in a boundary layer regime in the sense that two thin fluid layers move in opposite directions along the top and bottom walls without interfering with each other and a large (compared with boundary layers) stationary core exists in between these two layers (see Section I-C-1). Actually, the  $v$  velocity, having a S-shaped profile, is more or less a parallel shear flow as illustrated in fig.IV-4. The basic shape of the profile does not change with increasing Rayleigh number although the strength of the flow does increase. In summary, for configuration  $A$ , the primary circulation increases its strength as  $Ra$  increases. The  $v$  velocity profile remains an S-shaped parallel shear flow and no boundary layer regime in the conventional sense exists

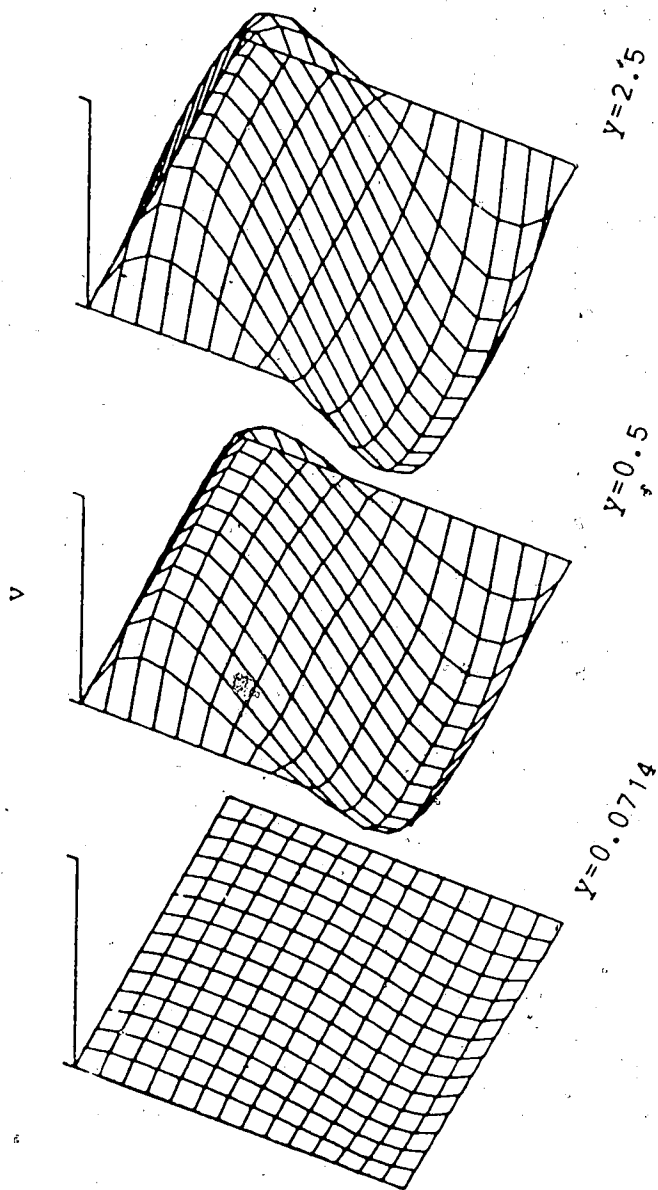


Figure IV.4 v velocity at different  $y$ ,  $Ra=2.5 \times 10^4$

for  $Ra=50$  to  $10^4$ .

Having looked at the flow in primary plane, the flow pattern in the secondary planes will now be examined. As soon as  $Ra=O(10^2)$ , the flow in the cavity is strong enough to make the temperature distribution deviate from a linear distribution along  $y$ -direction. The LTG at each point in the box is no longer coincident with the GTG and correspondingly the circulation plane at each point is different from the primary plane. Motion occurs in the secondary planes. Fig.IV-5 gives an example of the temperature distribution for  $xz$  planes at several  $y$  positions.

To predict the flow pattern in the secondary  $xz$  plane we can resolve the LTG in the three axis directions. The  $y$ -component of LTG will maintain the primary circulation. The  $x$ -component is parallel to  $GA$ , and thus plays no role in determining the flow pattern. So it is the  $z$ -component of LTG which is responsible for the formation of the flow pattern in the  $xz$  secondary plane. From fig.IV-5, it can be seen that the temperature gradient points towards the mid- $z$  plane for the upper part of the fluid and towards the side  $z$ -walls for the lower portion of the box. According to the principle for the prediction of circulation direction (WP II-C-2), there should be two pairs of counter-rotating vortices extending throughout the cavity. The directions of the vortices are such that the upper-right vortex (viewed from  $y=-\infty$ ) has the direction of the positive  $y$ -direction and those of the others are arranged accordingly. However,

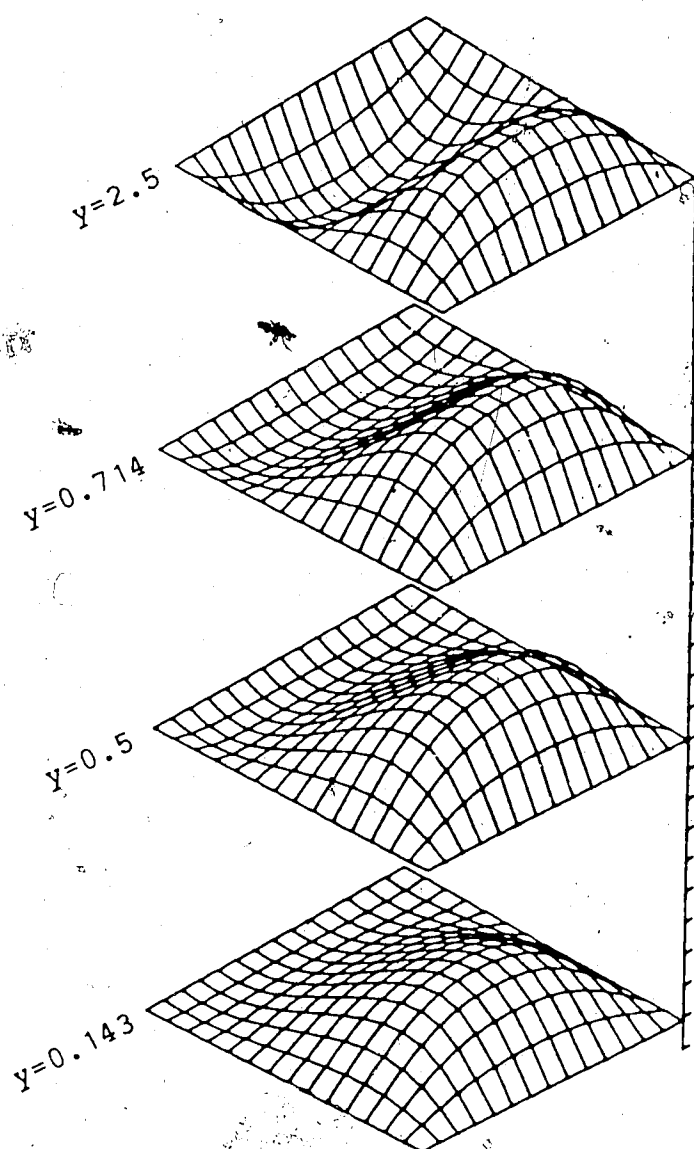


Figure IV.5 Temperature distribution along  $y$ ,  $Ra=2.5 \times 10^4$

because of the strong convection of the primary flow, the up-stream condition has a determining effect on the down-stream pattern. In another words, the flow pattern is not completely determined locally by the LTG but has to take the strong influence of upstream conditions into account. Near the heated wall (the same is true for the cooled wall except all the velocities have an opposite direction), under the action of the strong buoyancy, the fluid rises with a large  $u$  velocity. In this region there is no apparent vorticity in the  $xz$  plane. Because of the strong upstream influence, this kind of pattern prevails until about  $y=0.7$ . After about  $y=0.7$ , the lower pair of vortices forms and an embryo of an upper pair of vortices appears. As we go further down the  $y$ -direction, the upper pair develops and the lower pair adjusts accordingly. At the mid- $y$   $xz$  plane, two fully-developed pairs of counter-rotating vortices are established as shown in fig.IV-6.

The occurrence of this secondary flow caused by the  $z$ -component of the LTG is expected to increase the heat transfer rate through the side, top and bottom walls since it continuously turns the inner fluid out and outer fluid in, thus making a continuous interchange of hot and cold fluid. The contributions of heat transfer through each wall is plotted in fig.IV-7 from which it is evident that the major contributions to heat transfer come from the bottom and side walls. The contribution from the heated end wall is minor (only 10-20%). It is believed that the magnitude of



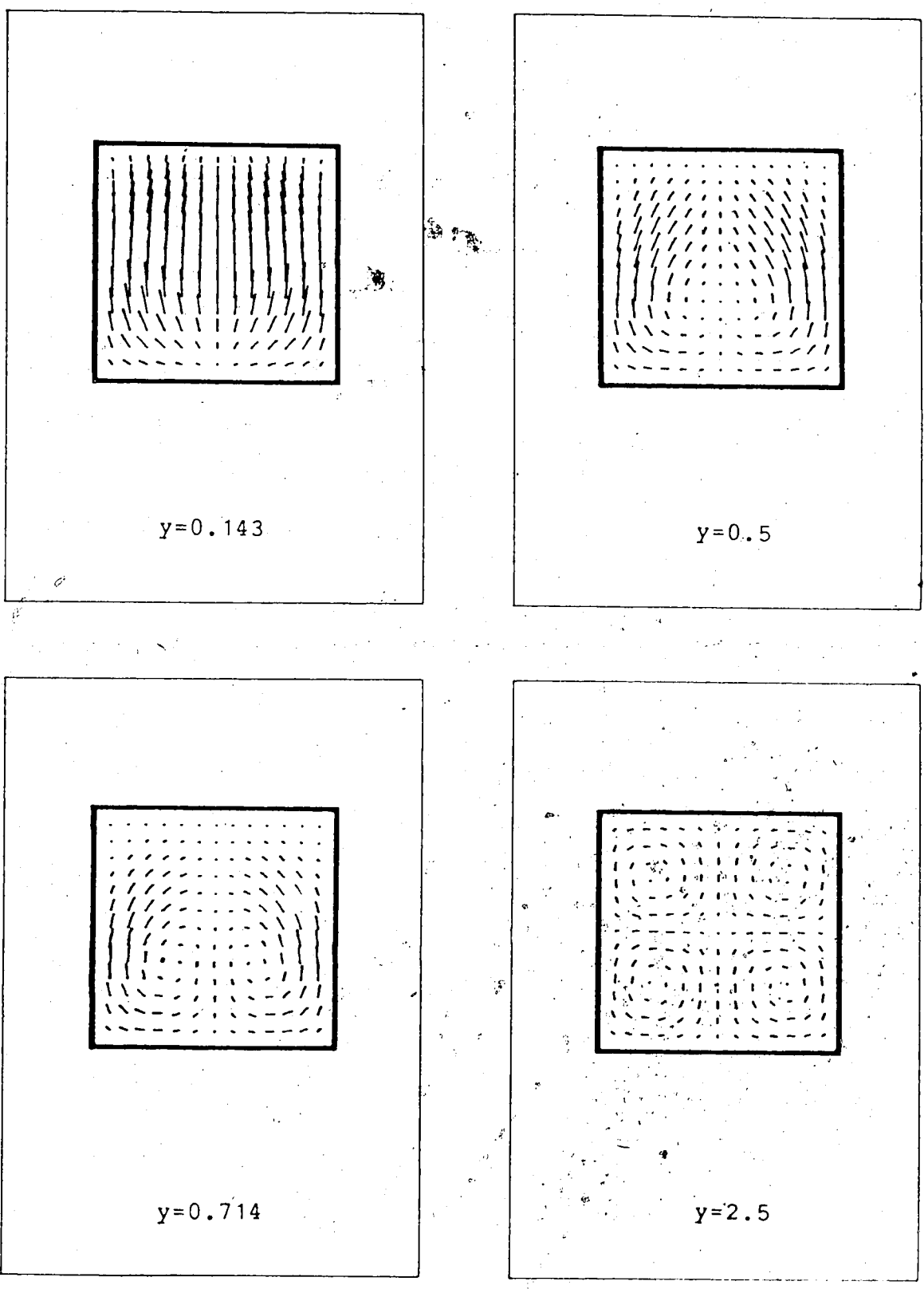


Figure IV.6 xz plane velocity along y, Ra=2.5x10<sup>4</sup>

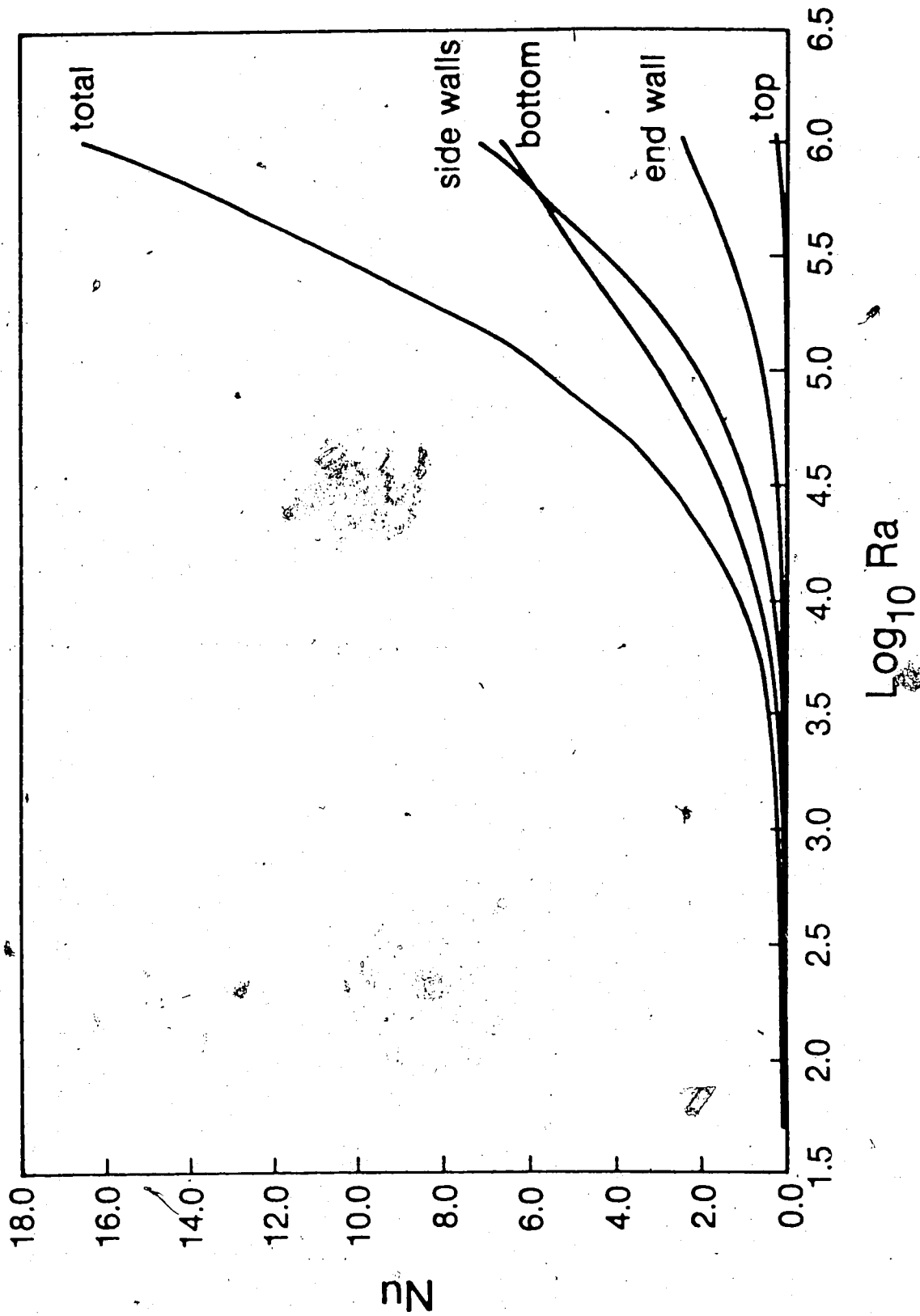


Figure IV.7 Nu contribution from each wall

the heat flux through the bottom and side walls is due to the mixing action of the secondary vortices. As an analogy, the occurrence of secondary vortices in developing pipe flow would enhance the heat transfer rate by a factor of 5 to 8. How much heat transfer enhancement is due to the secondary vortices in this case is still to be determined quantitatively.

It is interesting to note that the secondary flow is intrinsically a three-dimensional property of the system. In a two-dimensional model, there is no opportunity for secondary vortices to exist. Thus the comparison of two-dimensional and three-dimensional results is likely to provide a quantitative evaluation of how important the secondary vortices are in enhancing the heat transfer. However, caution should be employed when such a comparison is made because the presence of the z-walls not only introduces secondary vortices but also slows the primary circulation down. This slowing down effect would offset the enhancement induced by the secondary vortices and could complicate the comparison.

Thus far, the GTG has been imposed on the system by maintaining two end walls isothermally at different temperatures. There are other possible ways of achieving the same GTG on the system. BC3 is the boundary condition in which the side, top and bottom walls have a temperature gradient of desired magnitude but the two end walls are

adiabatic. The Rayleigh number is still based on the GTG of the system. Solutions were obtained using BC3 for  $Ra=10^4$ ,  $2.5 \times 10^4$  and  $10^5$ . The solid curve in fig.IV-8 is the solution using BC1 and the discrete circles are for BC3. Fig.IV-9 shows the mid-z xy plane velocity for  $Ra=2.5 \times 10^4$  using BC3, and may be compared with fig.IV-2. It is concluded that the ways by which the GTG is imposed is unimportant. Two different ways of imposing GTG make no significant difference in the solution as long as the resultant GTG is the same.

#### B. THE EFFECT OF TILT

In configuration A it was found that the flow pattern remained essentially the same for the range of Rayleigh number 50 to  $10^4$ . The flow pattern is mainly two opposite filaments on which two pairs of lateral vortices were superimposed. This flow pattern will be referred to as the horizontal pattern. In this section, the Rayleigh number will be kept at  $2.5 \times 10^4$ , while the effect of tilt on the flow patterns and heat transfer rates will be examined. Throughout this section BC1 will be used. It will be shown that as  $\alpha$  goes from  $-90^\circ$  to  $85^\circ$ , the flow pattern undergoes 2 transitions which are reflected in the heat transfer rates.

The values of Nu versus tilt angle  $\alpha$  measured from A is plotted in fig.IV-10. From this figure, three regimes can be identified. For  $\alpha=-90^\circ$  to  $5^\circ$ , Nu increases monotonically;

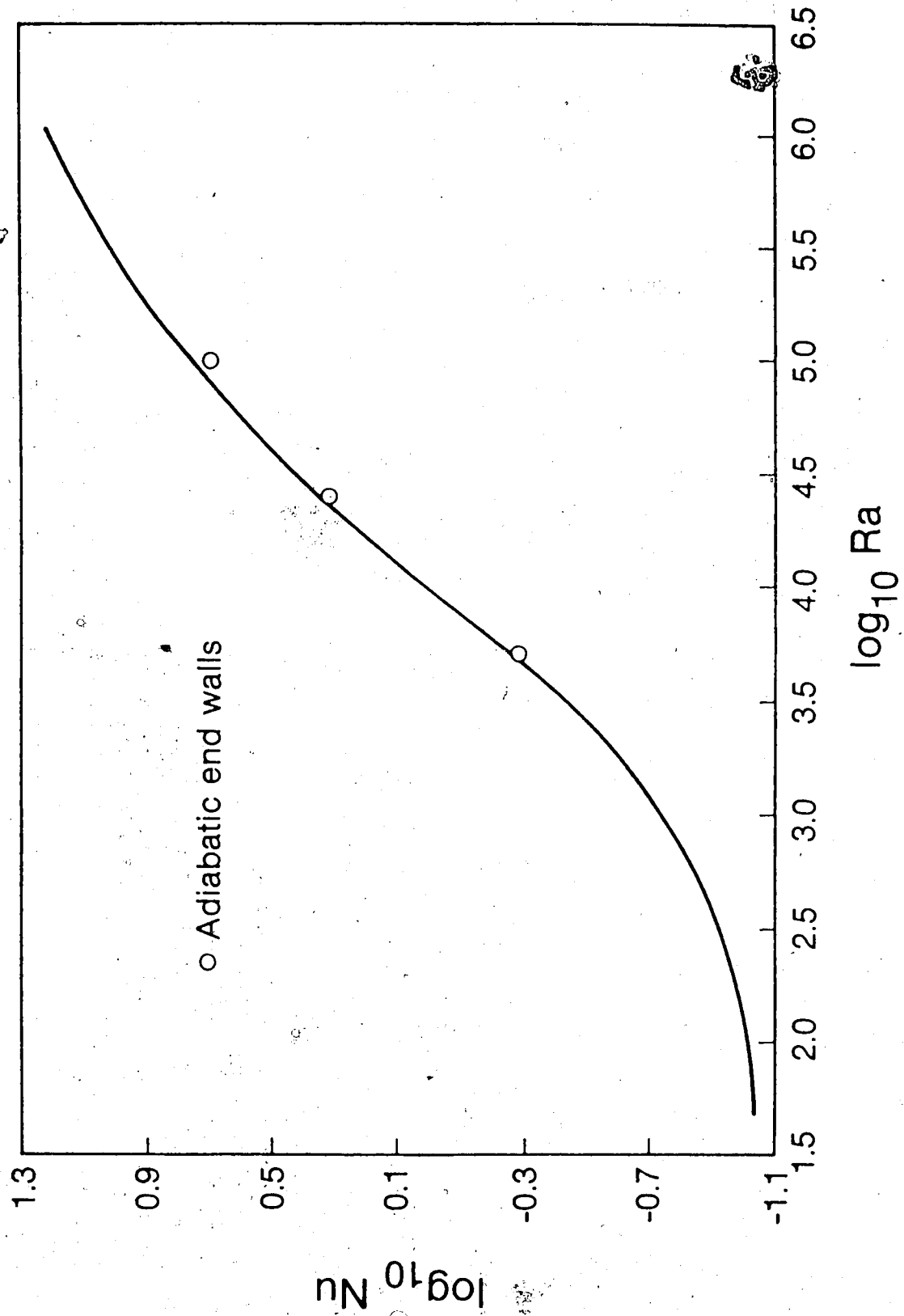


Figure IV.8 Heat transfer rates for different Ra

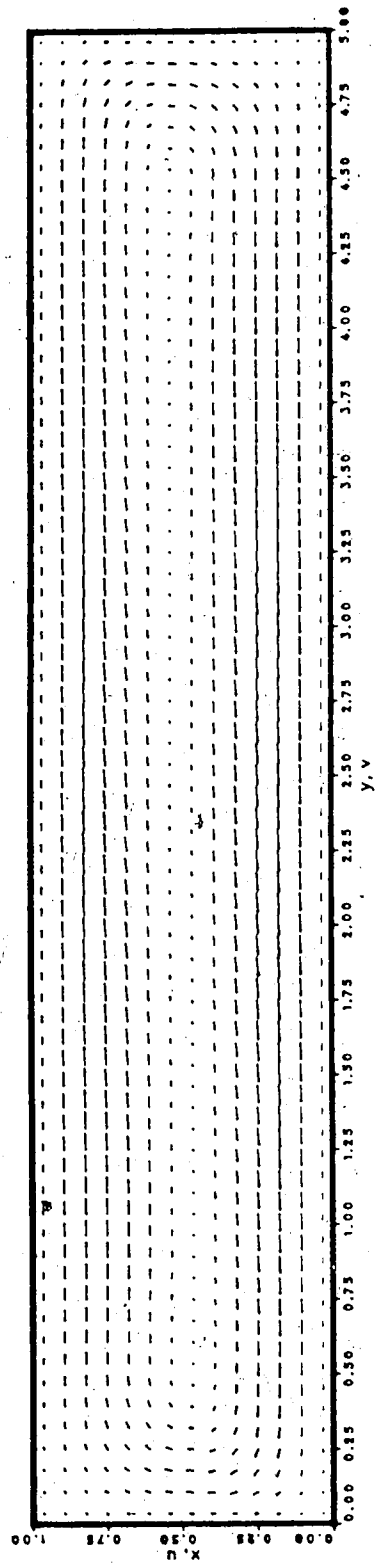


Figure IV.9 xy plane velocity,  $z=0.5$ ,  $Ra=2.5 \times 10^4$ , BC3

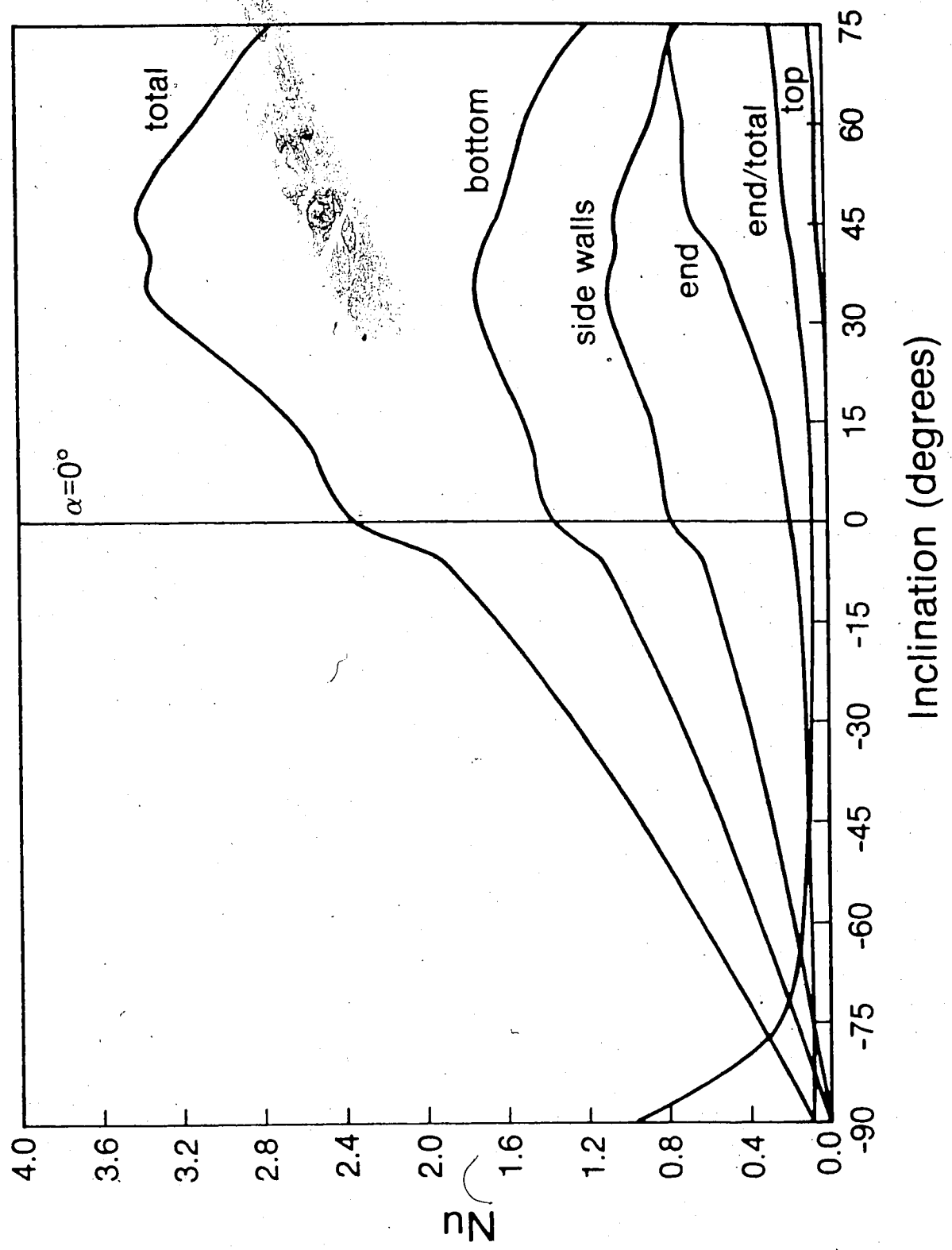


Figure IV.10 Nusselt number for different tilt angle

for  $\alpha=5^\circ$  to  $40^\circ$ , Nu again increases monotonically but in a slightly different way. For  $\alpha \geq 45^\circ$ , Nu decreases. Corresponding roughly to these regimes of Nu, three different flow patterns take over sequentially.

#### Horizontal Pattern

For  $\alpha=-90^\circ$  to  $15^\circ$ , detailed examination of the flow pattern reveals that for all these configurations there is no substantial change in flow pattern. The flow pattern is the same as that at A -- the horizontal pattern. However, quantitative changes in the strength of the flow do occur.

At  $\alpha=-90^\circ$ , the GTG has the same direction as GA. The fluid is stably stratified and there is no fluid motion. The LGT is the same as the GTG and conduction is the heat transfer mechanism. As  $\alpha$  increases from  $-90^\circ$ , The GTG forms an increasing angle with GA - resulting in stronger and stronger primary circulation. The resultant LTG from the primary circulation in turn produces two pairs of vortices in the lateral xz plane. This horizontal flow pattern persists until  $\alpha \approx 20^\circ$  where the buoyancy near the end wall becomes strong enough to create a region of reverse flow.

#### Modified Horizontal Pattern

As  $\alpha$  goes beyond  $20^\circ$ , two small regions of reverse flow appear at the lower corner of the heated wall and the upper corner of the cooled wall. This may be detected in fig.IV-11 which shows the xy plane velocity at the mid-z plane for



$\alpha=30^\circ$ . These regions of reverse flow result from the buoyancy near the end walls. Take the heated wall as an example. Near the heated wall, there is always a region where the temperature  $\phi$  is greater than zero. As soon as  $\alpha>0^\circ$ , this positive temperature would result in a positive buoyancy in the y-direction which tends to drive the flow in the positive y-direction (cf. eq 'II.14)). On the other hand, the flow near the lower corner of the heated wall tends to move in the negative y-direction to accommodate the over-all primary circulation. If  $\alpha$  is not too large ( $<20^\circ$ ), the pressure gradient of the primary circulation can overcome the buoyancy so that no reverse flow happens. If  $\alpha$  is large enough ( $>20^\circ$ ), the resultant buoyancy near the heated wall is so strong that part of the fluid near the lower corner is driven to move in the positive y-direction. This back-flowing fluid will act like a wedge inserted in between the primary circulation and the bottom wall and force the circulation to be separated from the bottom wall. This separated flow will, as demonstrated in fig.IV-12, create a stagnation point on the end wall. The fluid in the "wedge" will circulate in the opposite direction to the primary circulation due the shear action at the interface of the "wedge". Thus a region of reverse flow is established.

The reverse flow described above will remain a local phenomenon as long as  $\alpha<45^\circ$ . The primary circulation is still the dominating pattern for most of the cavity; near the end wall region, it is forced by the reverse flow to be

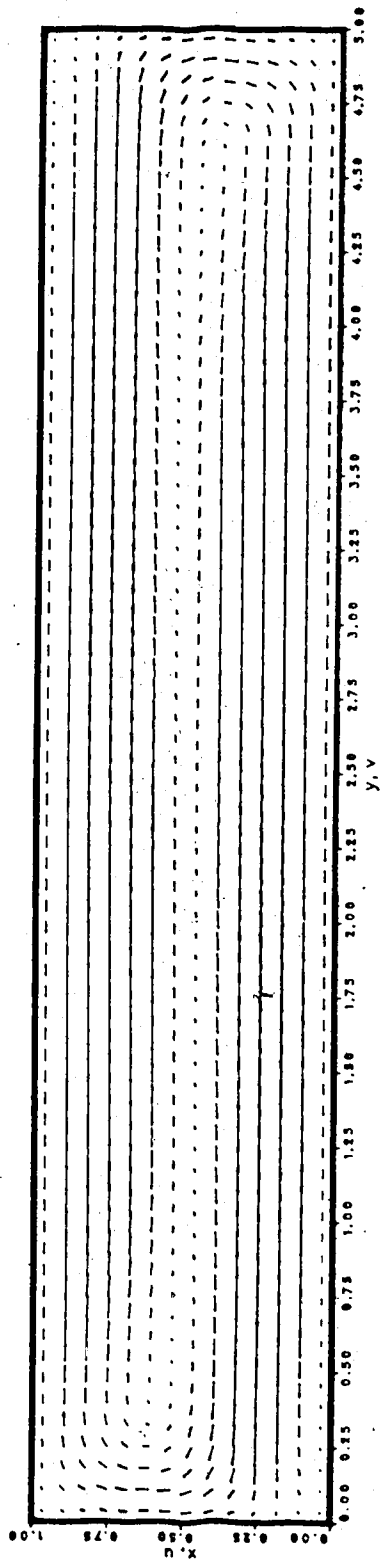


Figure IV.11 xy plane velocity,  $z=0.5$ ,  $\alpha=30^\circ$

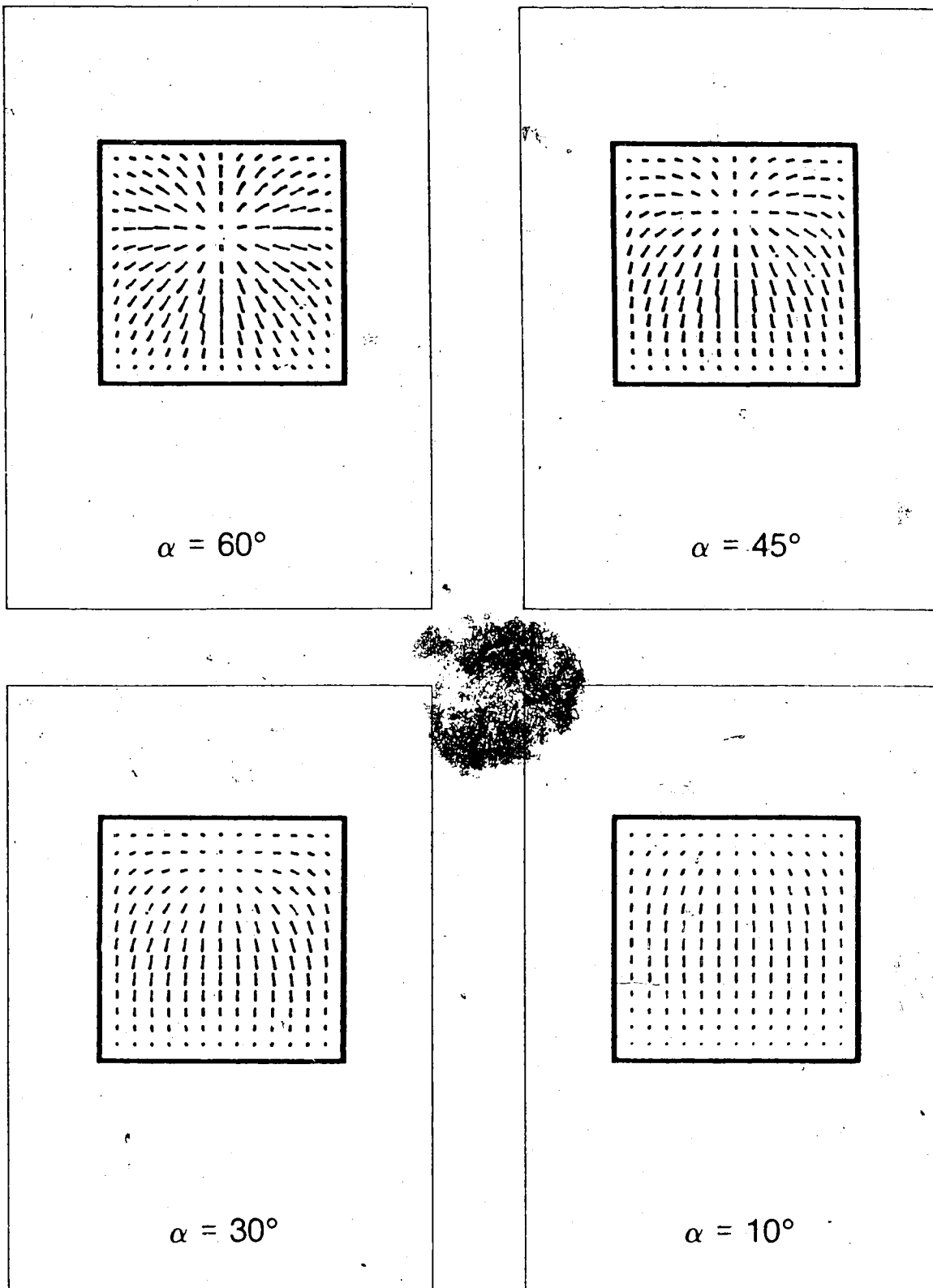


Figure IV.12 xz plane velocity,  $y=0.714$ , several  $\alpha$

separated from the bottom wall. The resultant LTG is still distributed in the fluid in such a way that two pairs of vortices appear in the  $xz$  plane. The Nusselt number keeps increasing as  $\alpha$  increases because of the ever stronger primary circulation. This horizontal pattern, together with the reverse regions produces the modified horizontal pattern which persists until  $\alpha=45^\circ$ .

#### Filament Pattern

We know that the buoyancy in the  $y$ -direction is dependent on  $\sin\alpha$ . As  $\alpha$  increases, so does the buoyancy. With ever stronger buoyancy, the reverse flow region near the end wall is expanding. This expansion can be clearly seen on fig.IV-12. which shows how the stagnation point on the end wall moves towards the center. At the extreme case of  $\alpha=90^\circ$ , the stagnation point is expected to be situated right on the center corresponding to a complete take over of the filament pattern as shown in fig.IV-13. Actually, far below  $90^\circ$ , at  $\alpha=45^\circ$ , the reverse flow has already grown so large that one cannot regard the reverse flow as a local phenomenon. This is believed to be the boundary between the modified horizontal pattern and the filament pattern in which a central core is surrounded by an annulus of fluid flowing in the opposite direction.

The reasons for setting the boundary at  $\alpha=45^\circ$  are several. First of all, at  $\alpha=45^\circ$  the  $Nu$  versus  $\alpha$  curve finally reaches a turning point to start a decreasing trend.

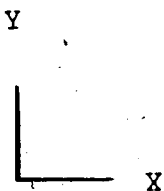
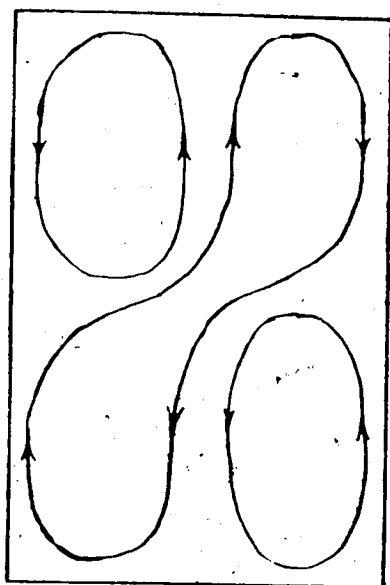


Figure IV.13 Sketch of filament model

This critical point would be expected to make a pattern transition. In the modified horizontal pattern, there is still a strong primary circulation which brings the hot fluid from the heated end wall to the cooled end wall and thus the flow has an effective energy transport ability. For the filament pattern, the previously strong primary circulation has been shrinking with the reverse flow growing comparably strong, as suggested in fig.IV-13. Hot fluid now can travel to the cold wall only through a restricted path in between the two reverse flows; thus the heat transfer ability of the convection is impaired. This overall picture is confirmed by fig.IV-14. The second reason for treating  $\alpha=45^\circ$  as the critical point is that the extension of the reverse flow itself is too big to be considered as a mere modification. Fig.IV-15, as an example, shows the  $v$  velocity along the  $y$ -direction for  $\alpha=60^\circ$ . One can see that at  $y=1$  (40% of the half length of the cavity) there is still reverse flow. With this extension of reverse flow, it is reasonable to take the reverse flow as a major feature of the flow pattern. The last, but the most decisive reason is the observation that when  $\alpha \geq 45^\circ$ , the two pairs of vortices in the  $xz$  plane previously found for  $\alpha < 45^\circ$  disappear and are replaced by sections of four filaments (fig.IV-16). This is why the name filament pattern has been used.

Once the filament pattern prevails, for reasons given above, the Nusselt number drops off sharply as  $\alpha$  increases further. This explains the behavior evident in fig.IV-12.

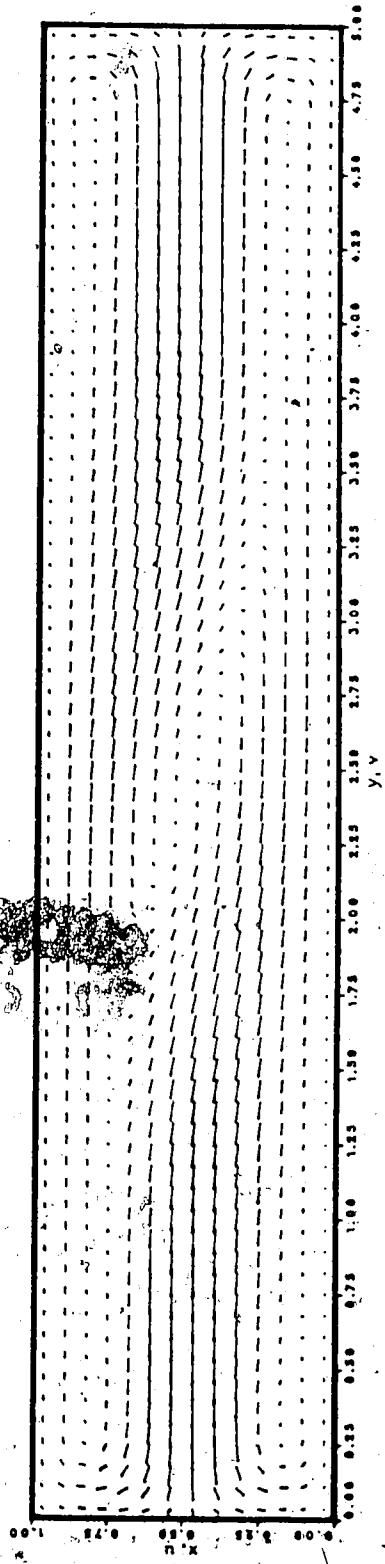
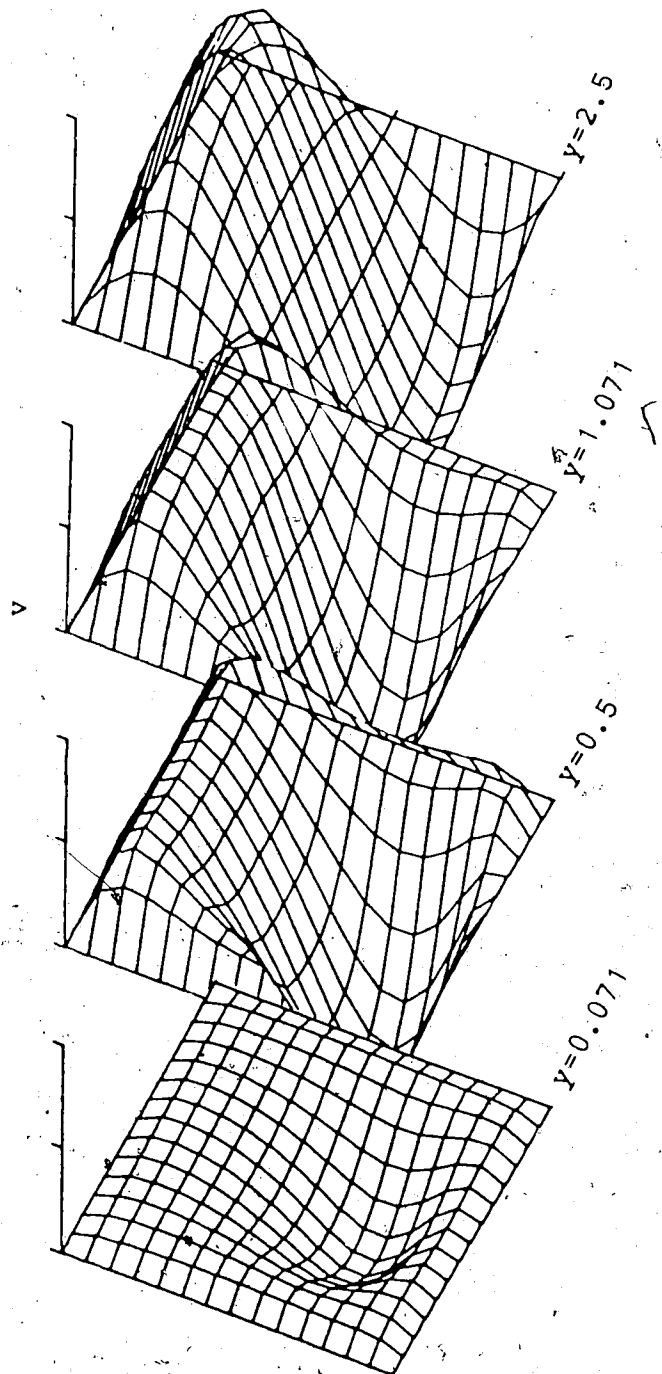


Figure IV.14 xy plane velocity,  $z=0.5$ ,  $\alpha=85^\circ$



$Ra = 2.5 \times 10^4$

Figure IV.15  $v$  velocity along  $y$ ,  $\alpha=60^\circ$



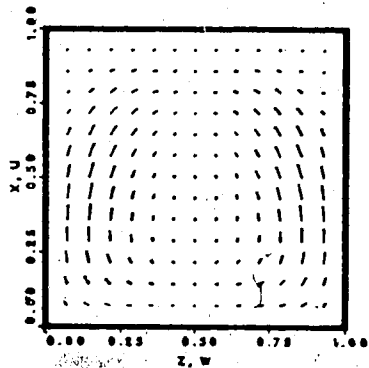
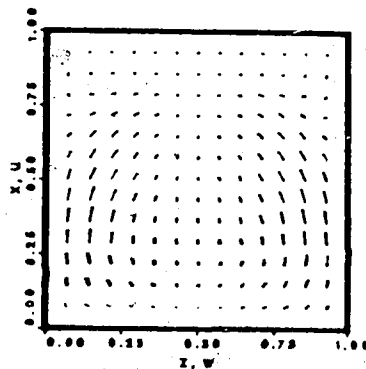
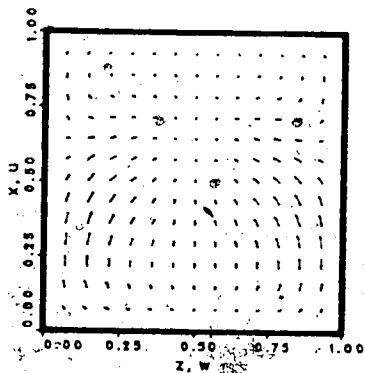
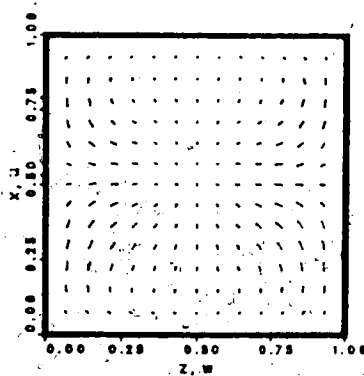
 $y=1.643$  $y=1.929$  $y=2.214$  $y=2.5$ 

Figure IV.16 xz plane velocity along  $y$ ,  $\alpha=45^\circ$

### C. THE EFFECT OF SKEW

When the box is skewed from  $A$  at an angle  $\theta$ , the GTG is unchanged but the primary plane will form an angle  $\theta$  with the  $xy$  plane. Since the GTG is the same as that when the box is at  $A$ , the flow pattern discussed in section A is not expected to undergo fundamental change. We may expect that the primary circulation previously found in the  $xy$  plane at  $A$  would now take place in the primary plane. However, since the nodal points for calculation are generally not located on a primary plane, the primary circulation is hard to present. However, if the flow pattern is the same as that at  $A$ , the secondary plane velocity, which is easy to check, must have the same pattern as before. Fig. IV-17, showing the  $xz$  plane velocity at  $y=2.5$ , confirms that the flow pattern is essentially the same as that obtained with  $\theta=0^\circ$ . For  $\theta=0^\circ$  to  $45^\circ$  (because of symmetry, this is the whole  $\theta$  domain), two pairs of counter-rotating vortices are the pattern in the  $xz$  plane. Thus skewing has no fundamental effect on the flow pattern. Changes are due to the adjustment to best fit the geometry.

### D. CONCLUSIONS

In this chapter, the three-dimensional structure of the flow pattern and heat transfer properties of natural convection of air in a  $A_x=A_z=0.2$  cavity under various conditions were studied. The following conclusions can be drawn from the study.

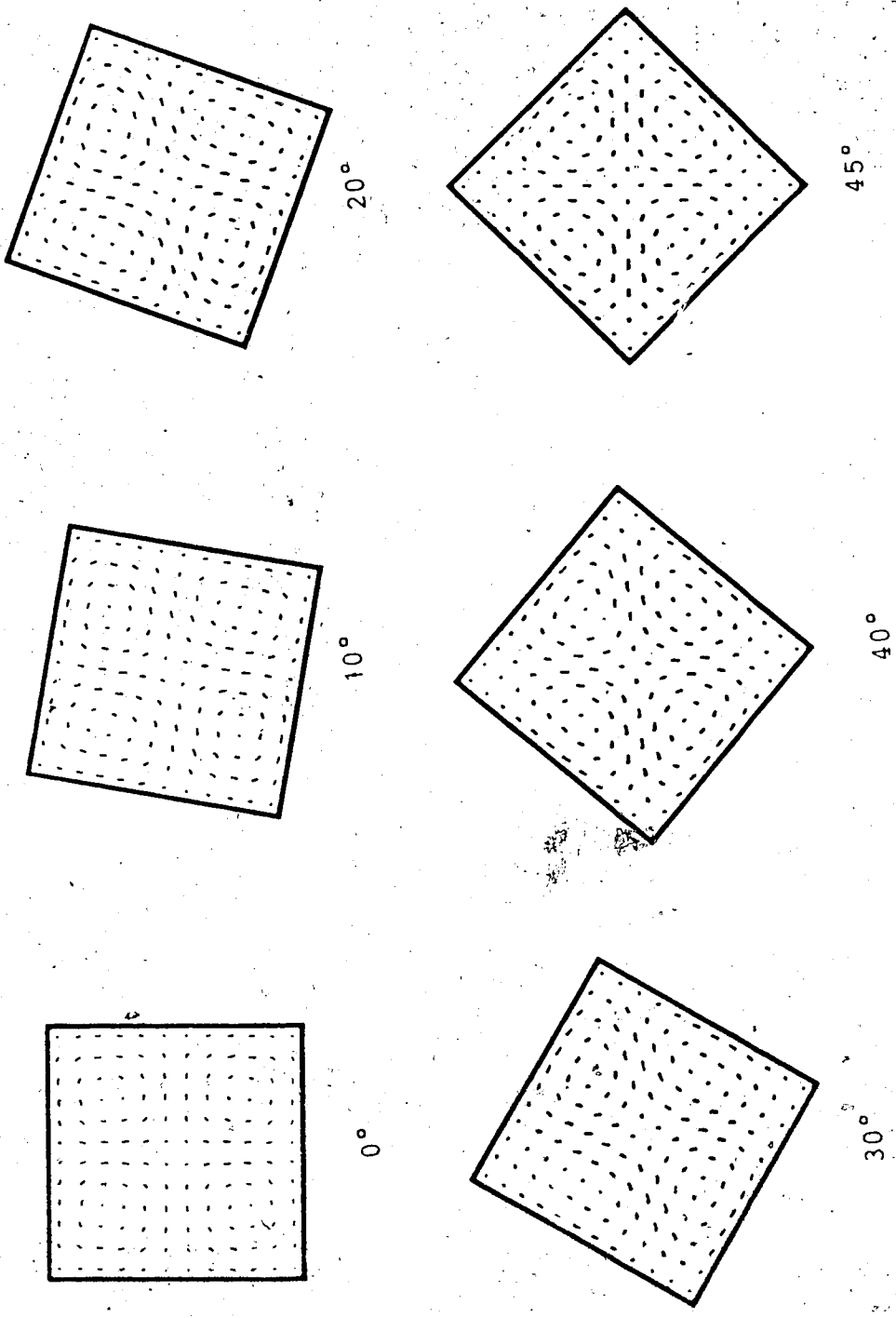


Figure IV.17 xz plane velocity,  $y=2.5$ , several  $\theta$

Because of the driving force, the pressure gradient, for the major velocity component,  $v$ , in this  $Ax=0.2$  cavity is different from the driving force, the buoyancy, for the major velocity component,  $u$ , in the  $Ax \geq 1$  cavity; the flow regimes division in the  $Ax \geq 1$  cavity is not appropriate for the  $Ax=0.2$  cavity. There is a lack of evidence for transitions of regimes for  $Ra=50$  to  $10^4$ . For this range of  $Ra$ , the primary flow always has an S-shaped velocity profile. As the result of the primary circulation, the LTG becomes nonuniform and this creates two pairs of counter-rotating vortices in the lateral planes. These vortices increase the heat transfer rate significantly.

The way by which the GTG is imposed is relatively unimportant in determining the behavior of the system as demonstrated by substituting BC3 for BC1.

As the cavity is tilted from  $\alpha=-90^\circ$  to  $85^\circ$ , three different flow patterns take over sequentially. For  $\alpha=-90^\circ$  to  $20^\circ$ , the flow pattern is essentially the same as that for  $\alpha=0^\circ$  and is thus referred to as the horizontal flow pattern. For this flow pattern, the heat transfer rate increases monotonically as the result of ever stronger circulation due to the ever stronger buoyancy when  $\alpha$  goes from  $-90^\circ$  to  $20^\circ$ .

For  $\alpha=20^\circ$  to  $40^\circ$ , the buoyancies near the end walls will be strong enough to offset the primary circulation pressure gradient to create regions of reverse flow near the end walls. These end reverse flow regions will force the primary circulation to become separated from the bottom and

top walls to create two stagnation points on the end walls. Yet for this range of  $\alpha$ , the reverse flow regions remain a local phenomena and will not change the basic features of the horizontal flow pattern. This flow pattern is called the modified horizontal flow pattern.

As  $\alpha \geq 45^\circ$ , the reverse flow regions become comparable with the dimensions of the cavity and the previous 'modification' becomes a major feature of the flow. The original primary circulation, under competition with the reverse flow, shrinks to a size that it is no longer 'primary' but two filaments of four comparably strong ones. The secondary vortices in the lateral plane are replaced by filament sections. The original flow pattern is completely destroyed and the filament pattern prevails. The heat transfer rate drops sharply as a result of the impedance to the advective mechanism of this pattern.

When the cavity is skewed, the GTG is left unchanged, and therefore there is no fundamental change of flow pattern from the unskewed case.

## V. TRANSVERSE TEMPERATURE GRADIENT $Ax=5$ , $Az=1$ CAVITY

In this chapter we will study the buoyant flow in a cavity with  $Ax=5$  and  $Az=1$  while the Rayleigh number is kept constant at  $10^4$ . By following several paths, transitions between different flow patterns and associated heat transfer rates are observed. New features of flow near configuration  $B$  are investigated.

In section A, the system will be rotated following path  $AD$ . At  $A$ , being the familiar vertical cavity, a single transverse cell with three-dimensional modification is the flow pattern. Then the box will be skewed up to  $90^\circ$  to get the configuration  $D$ . At  $D$ , a single longitudinal roll (LR) is the prevailing flow pattern. Between  $A$  and  $D$ , a gradual transition from the transverse cell to the longitudinal roll is observed.

In section B, paths  $DB$  and  $BD$  will be followed. It is known that  $B$  is the configuration of Benard-Rayleigh convection. Linear theory predicts that a number of transverse rolls (TR) with roughly square cross-section is the motion mode. However, it is found that the flow pattern is heavily dependent on the initial condition. If nominally zero-value field variables are used as the starting point of numerical iterations, six rolls appear in contrast to five rolls for a  $-0.5$  input. The situation is further complicated by the fact that by following  $DB$ , a longitudinal roll would be obtained at  $B$ , in sharp contrast to the linear theory prediction. The latter feature of bifurcation has not been

reported before to the author's knowledge.

In section C, the path  $AB$  and paths  $BA$  with two different initial flow pattern at  $B$  will be investigated. Once again, bifurcation at configurations near  $B$  was observed. For example, at  $\alpha=75^\circ$  from  $A$ , the flow pattern can either be a single transverse cell, five rolls or six rolls depending upon the path that has been followed.

In the first three sections, BC1 is used throughout. The computational domain is covered by a  $51 \times 13 \times 13$  mesh network and no symmetric property of solution is presumed. In section D, cases for other mesh systems, various box sizes and different boundary conditions are tested to see the effect of these factors.

The previous sections are mainly for phenomenological descriptions of the flow patterns and the associated heat transfer rates. Since the situation is rather complicated by bifurcations near  $B$ , it deserves more discussion. These are the subjects of section E. In this section, we will try to understand the behavior of the the system near configuration  $B$  using the working principle devised in II-C-2 (WP II-C-2).

#### A. THE EFFECT OF SKEW

##### Configuration A

This is the classical vertical cavity in which, for  $Ra=10^4$ , the flow does not possess a boundary layer. The primary flow pattern as shown in Fig.V-1 is clearly in

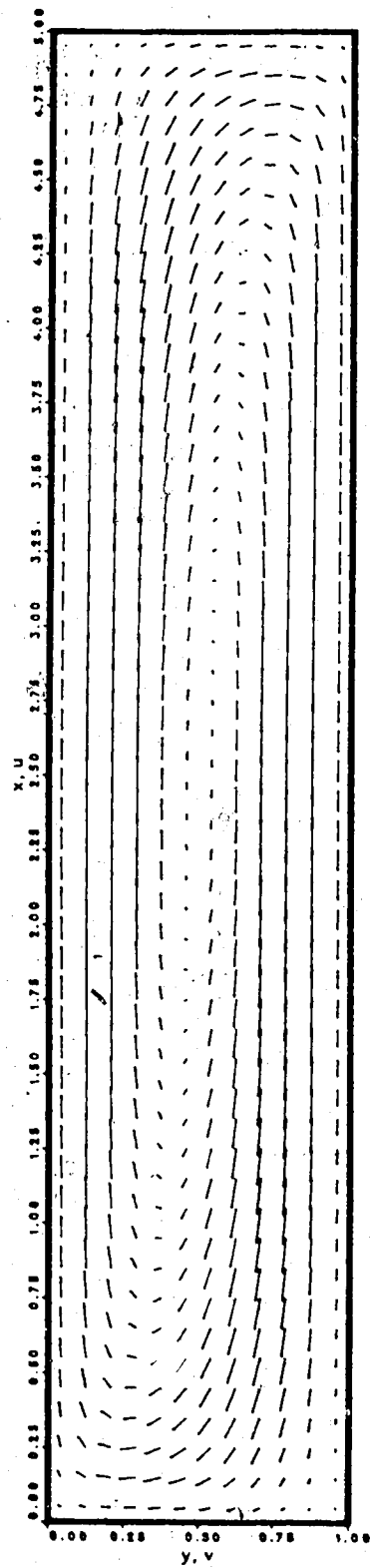


Figure V:1 xy plane velocity, z=0.5, at A



accord with the previous two-dimensional result, as expected. However, because of the presence of the walls in the z-direction, the flow is no longer two-dimensional. This can best be seen from Fig.V-2 which is a top view of the plane flow near the top wall. Fig.V-3 illustrates the u velocity profile. Combining all the figures, the flow may be pictured as follows. The rising flow near the bottom wall is bi-maximal under the influence of the perfectly conducting z-walls (fig.V-3a). As the flow rises, the strength increases and the two local maxima converge (fig.V-3b). At the mid-x plane, the maxima merge to form a single maximum and the flow reaches the highest velocity (fig.V-3c). Further up in the x-direction, the flow slows down with the single maximum established. When approaching close to the top wall, the flow diverges and a bi-maximal returning flow is formed (fig.V-2). The flow pattern is symmetric about the x-z plane and anti-symmetric about the mid-y plane.

At A, the primary plane is the xy plane and a transverse cell is the primary flow pattern. At D, the primary plane is the yz plane, and a longitudinal roll would be expected to be the flow pattern. For a configuration between A and D, the buoyancy force has components in both the xy-plane and the yz-plane. Thus the whole flow pattern can be considered as the superposition of the transverse cell and the longitudinal roll. However, since the motions

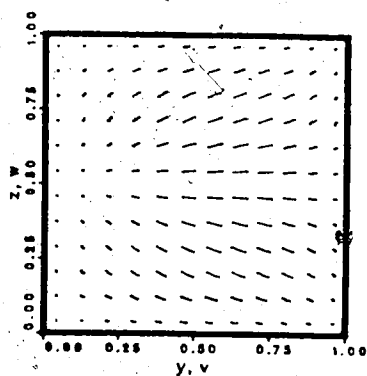


Figure V.2 yz plane velocity,  $x=4.95$ , at A

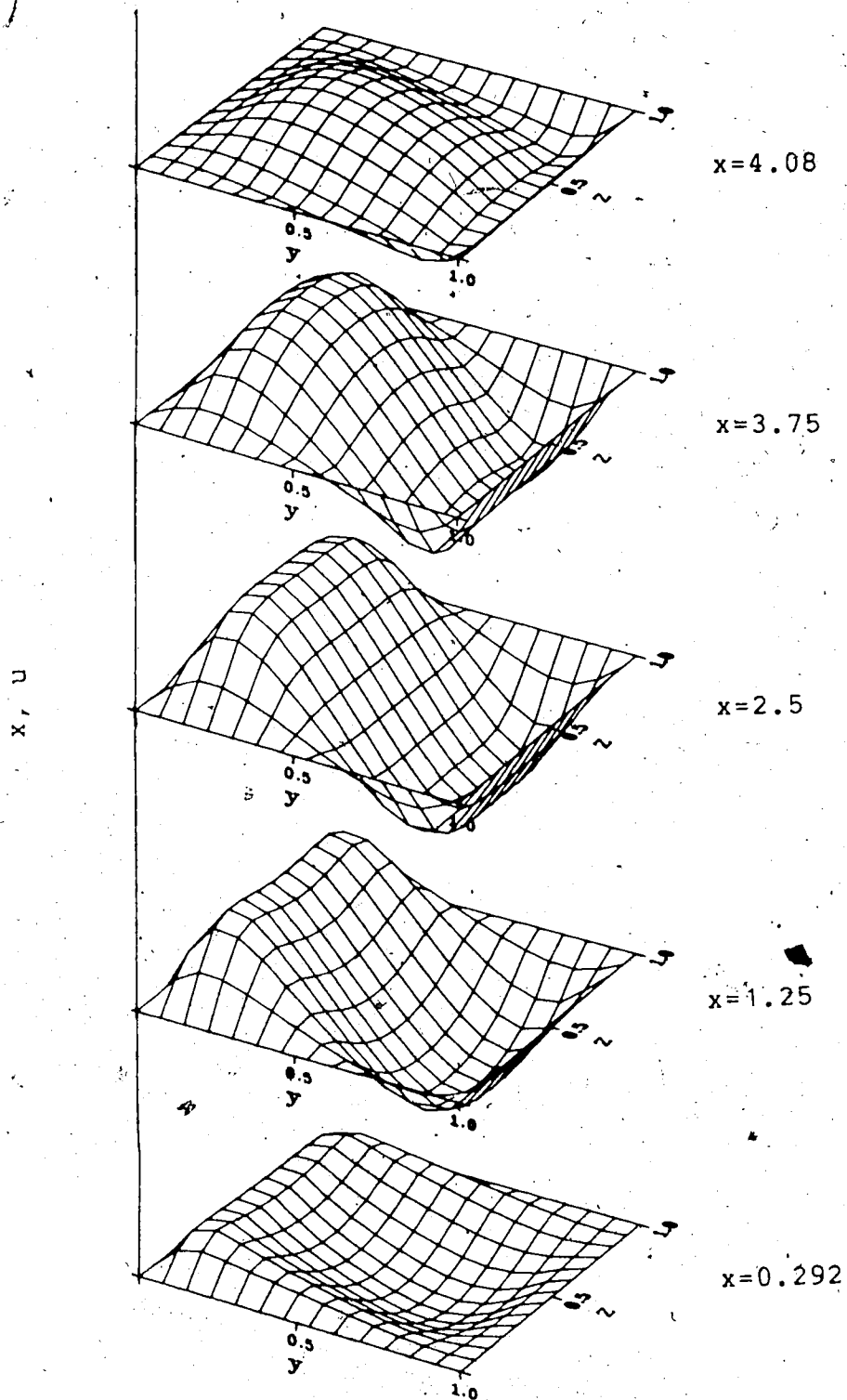
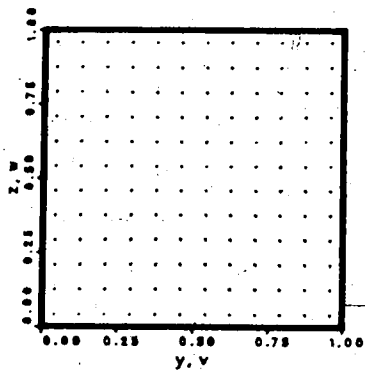


Figure V.3 u velocity along x, at A

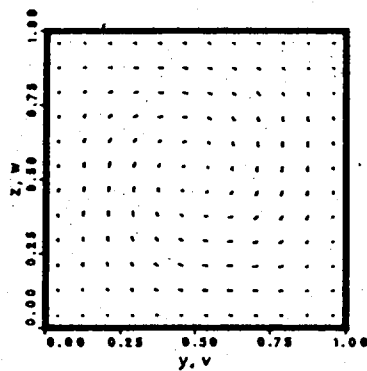
of both the transverse cell and the longitudinal are not rigid body rotations (or constant vorticity) adding the two rotating vectors to form a single roll with a new axis has little meaning.

The relative magnitudes of the components, which change with  $\theta$ , will determine which flow mode plays the dominating role in forming the flow pattern. In configuration A, in the absence of a buoyancy component in yz-plane, the flow is a single transverse cell, while at the other end of the spectrum, configuration D, the flow pattern is a longitudinal roll as the result of the buoyancy completely lying in the yz-plane. The process A→D, through a skew angle of  $90^\circ$ , is the process in which the longitudinal roll grows to full dominance and the transverse cell decays to nothing. This process is well revealed by the yz-plane velocity plots.

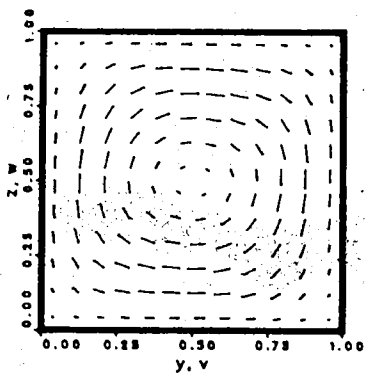
As soon as there is a non-zero skew angle, however small, the buoyancy has a component in the yz-plane. This component will establish a longitudinal roll. Fig.V-4, showing the yz-plane velocity at  $x=2.45$  for  $\theta=0^\circ, 5^\circ, 45^\circ$  and  $90^\circ$ , gives us an idea of how the longitudinal roll develops in the central region of the cavity. Fig.V-4b shows that for  $\theta=5^\circ$  there is a weak circulation in yz-plane; fig.V-4c shows that this circulation is well developed for  $\theta=45^\circ$  in the central region. Away from the central region the longitudinal roll is evident until  $\theta=60^\circ$ , as revealed by fig.V-5 which plots the yz-plane velocity near the bottom



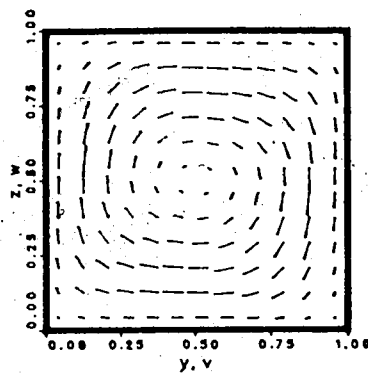
0°



5°



45°



90°

Figure V.4 yz plane velocity, x=2.45, several  $\theta$

end wall for several skew angles.

Fig.V-6 shows the  $xz$  plane velocity at  $y=0.9583$ , while Fig.V-7 provides corresponding details at  $z=0.9583$ . These figures tell the same story about how the transverse cell at  $A$  gradually transforms to a longitudinal roll as  $\theta$  changes from  $0^\circ$  to  $90^\circ$ .

Fig.V-8 shows the heat transfer rates for different skew angles. An immediate observation is that the longitudinal roll creates higher heat transfer than the transverse cell ( $Nu$  at  $D$  is 19% higher than that at  $A$ ). Having this in mind, it is easy to explain the monotonically increasing trend of  $Nu$  when  $\theta$  exceeds  $30^\circ$  because the flow becomes more and more dominated by the longitudinal roll. In the range of  $0^\circ \leq \theta \leq 30^\circ$ , however, there is a competition between the two modes. More specifically, for  $0^\circ \leq \theta \leq 15^\circ$ , the flow is transverse-cell dominated. The geometry of the flow pattern and the cavity is not well matched thereby causing a decrease in  $Nu$ . For  $15^\circ \leq \theta \leq 30^\circ$ , the longitudinal roll becomes more and more important bringing a reversal in  $Nu$ . The longitudinal roll dominates at  $\theta=30^\circ$ , based on the fact that the Nusselt number is higher than that at  $A$ .

Throughout the process  $A \rightarrow D$  (or  $D \rightarrow A$ ), the GTG keeps perpendicular to  $GA$ . So for all the configurations, there is no bifurcation of any kind and the solution is path-independent. For situations where the GTG, or a substantial component of it, has the same direction as the  $GA$ , bifurcation is likely to occur.

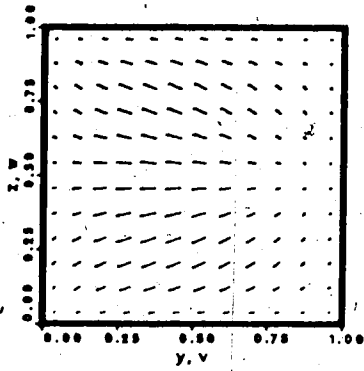
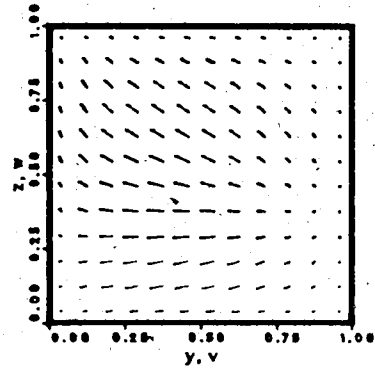
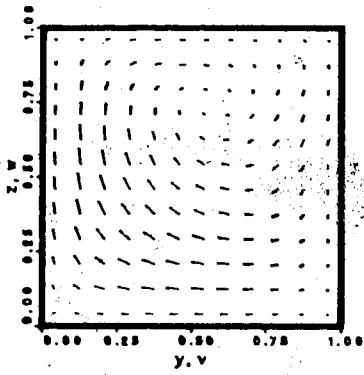
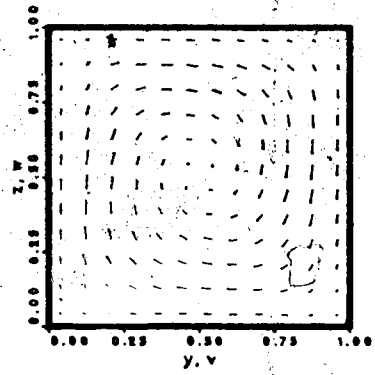
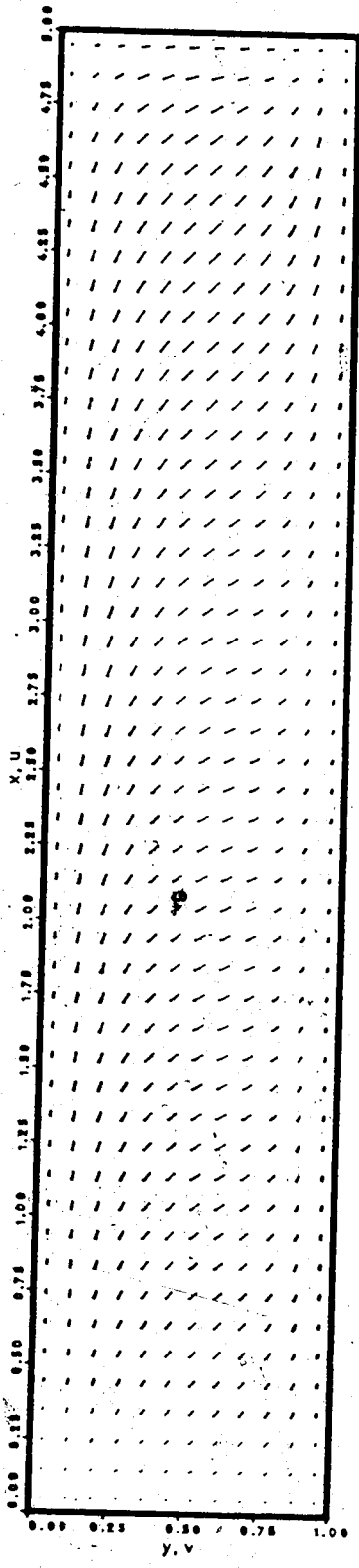
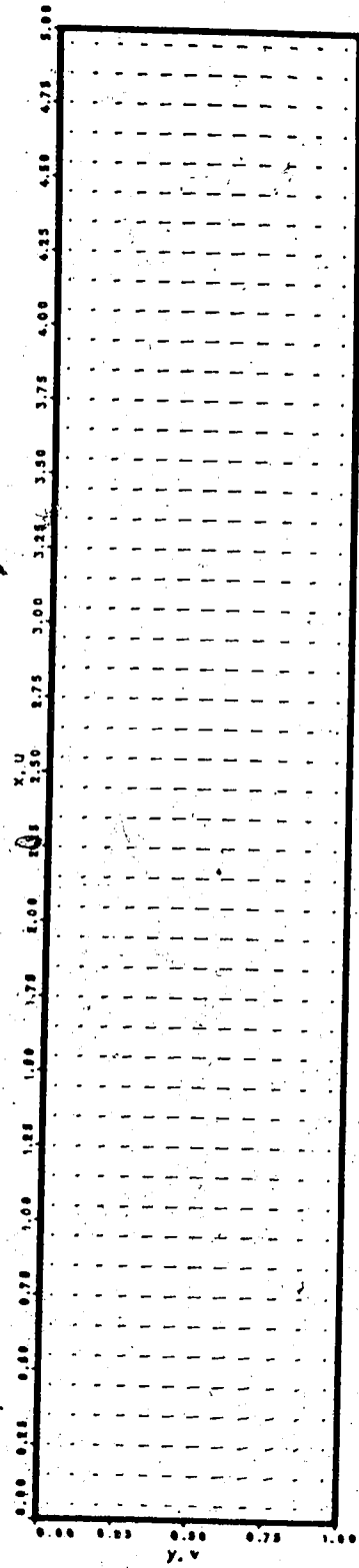
 $0^\circ$  $15^\circ$  $60^\circ$  $90^\circ$ 

Figure V.5 yz plane velocity,  $x=0.05$ , several  $\theta$



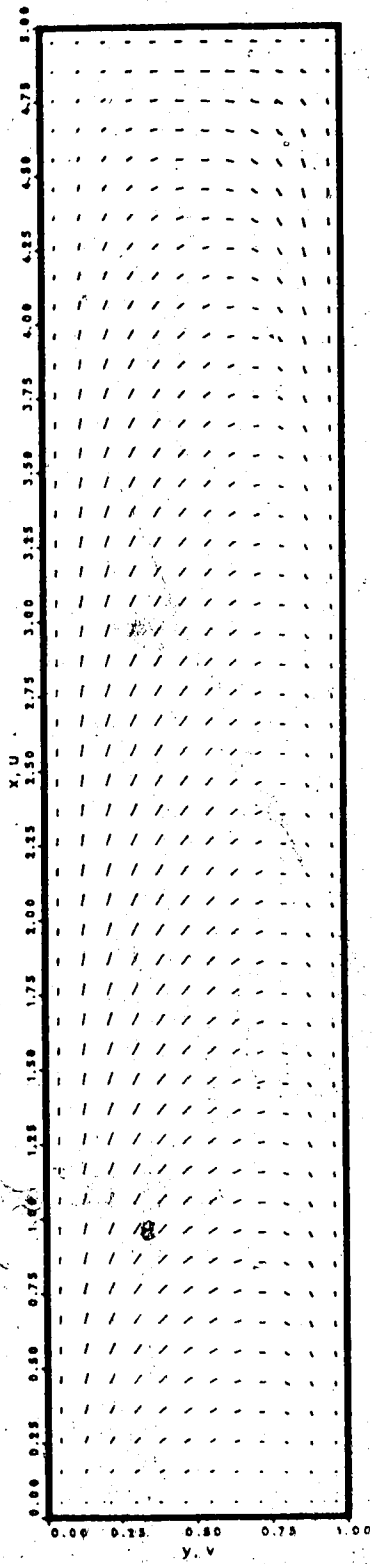
45°



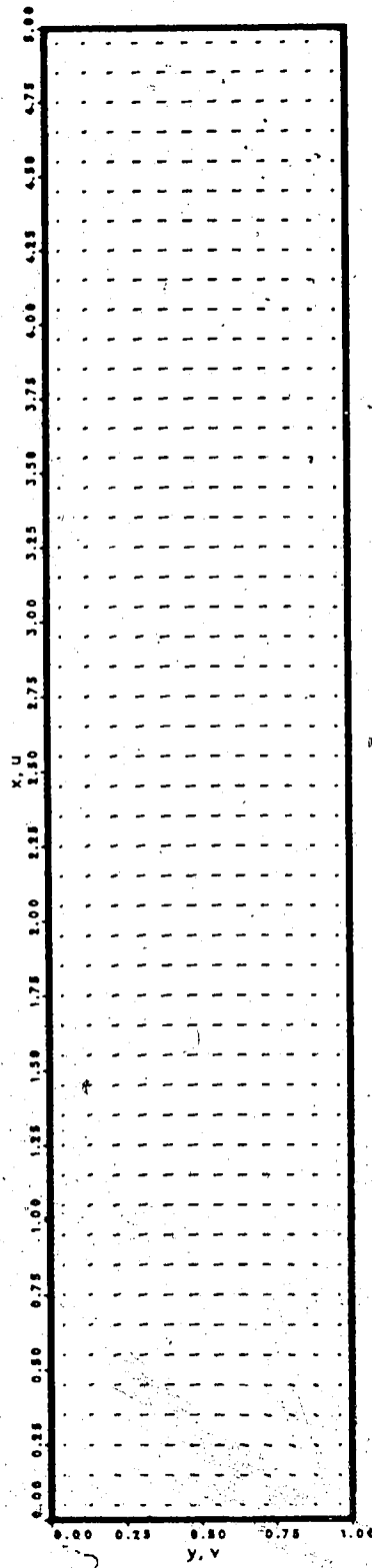
90°

Figure V.6 xz plane velocity,  $y=0.958$ , several  $\theta$





45°



90°

Figure V.7 xy plane velocity, z=0.958, several  $\theta$

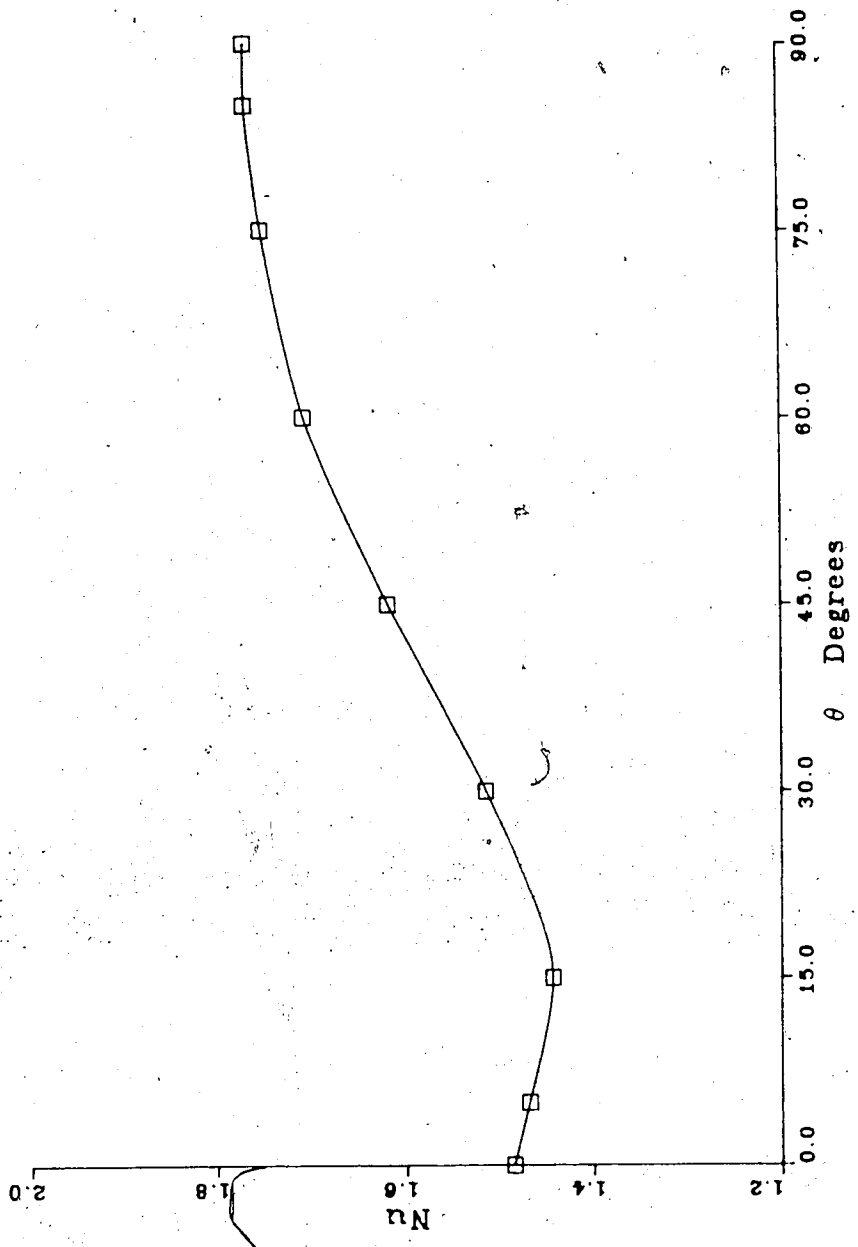


Figure V.8 Nusselt number for different skew angles

## B. THE EFFECT OF ROLL

It has been shown that at configuration  $D$  the flow is a longitudinal roll. On the other hand, previous studies ([23, 24]) have shown that five transverse rolls would be the preferred mode in configuration  $B$ . In the last section, it was noted that the flow experienced a gradual transition from a transverse cell to a longitudinal roll (and vice versa) by rotating the cavity gradually from  $A$  to  $D$  (or  $D$  to  $A$ ). It was also found that between  $A$  and  $D$  the flow pattern is unique regardless of the path by which this configuration was reached, i.e., for all the configurations between  $A$  and  $D$  the flow pattern is independent of the initial input of the numerical solution. In examining the behavior of the system in configurations between  $D$  and  $B$ , the following questions naturally come to mind. First, Starting at  $D$  with a longitudinal roll, will five transverse rolls be produced by rotating the box  $90^\circ$  about the  $x$ -axis to configuration  $B$ ; and is the behavior reversible? Second, are the flow patterns at configurations between  $D$  and  $B$  path-independent?

Let us start with configuration  $D$  and then rotate the box up to  $90^\circ$  to get configuration  $B$ . Then path  $BD$  will be followed by starting with a flow pattern at  $B$  obtained from a zero initial input. In this section the roll angle is always measured from configuration  $D$ .

### Path DB

The curve connecting the squares in fig.V-9 shows the Nusselt number plotted against the roll angle  $\gamma$  for path DB. The monotonically decreasing behavior of the curve for  $\gamma \geq 30^\circ$  suggests that there is no abrupt transition in the flow pattern since a higher Nu would be expected for the mode with transverse rolls. Turning to the details of the flow field, it is confirmed that there is no transition from the longitudinal roll to transverse rolls.

Fig.V-10 shows the yz-plane velocity at  $x=2.45$  for  $\gamma=0^\circ$ ,  $30^\circ$ ,  $75^\circ$  and  $90^\circ$ . According to this figure, the flow change is only quantitative as  $\gamma$  sweeps through  $90^\circ$ . For  $\gamma=0^\circ \rightarrow 30^\circ$  the circulation increases slightly because of an increase of buoyancy in the y-direction, resulting in an increase in Nu. For  $\gamma=30^\circ \rightarrow 90^\circ$  the buoyancy in the z-direction continuously decreases causing a decrease in Nu. As  $\gamma$  increases, a crosssectional view of the roll changes from a "circle" at  $\gamma=0^\circ$  to an "ellipse" with the primary axis of the "ellipse" continuously rotating with the skew angle, as can be seen by comparing a, b, c and d of fig.V-10. However, all the changes are quantitative. In configuration B the flow pattern is still a longitudinal roll. This conclusion is also supported by figs.V-11 and 12 which are xy-plane and xz-plane velocity representations at B.

One notable thing about configuration B is that, while the governing equations and boundary conditions admit

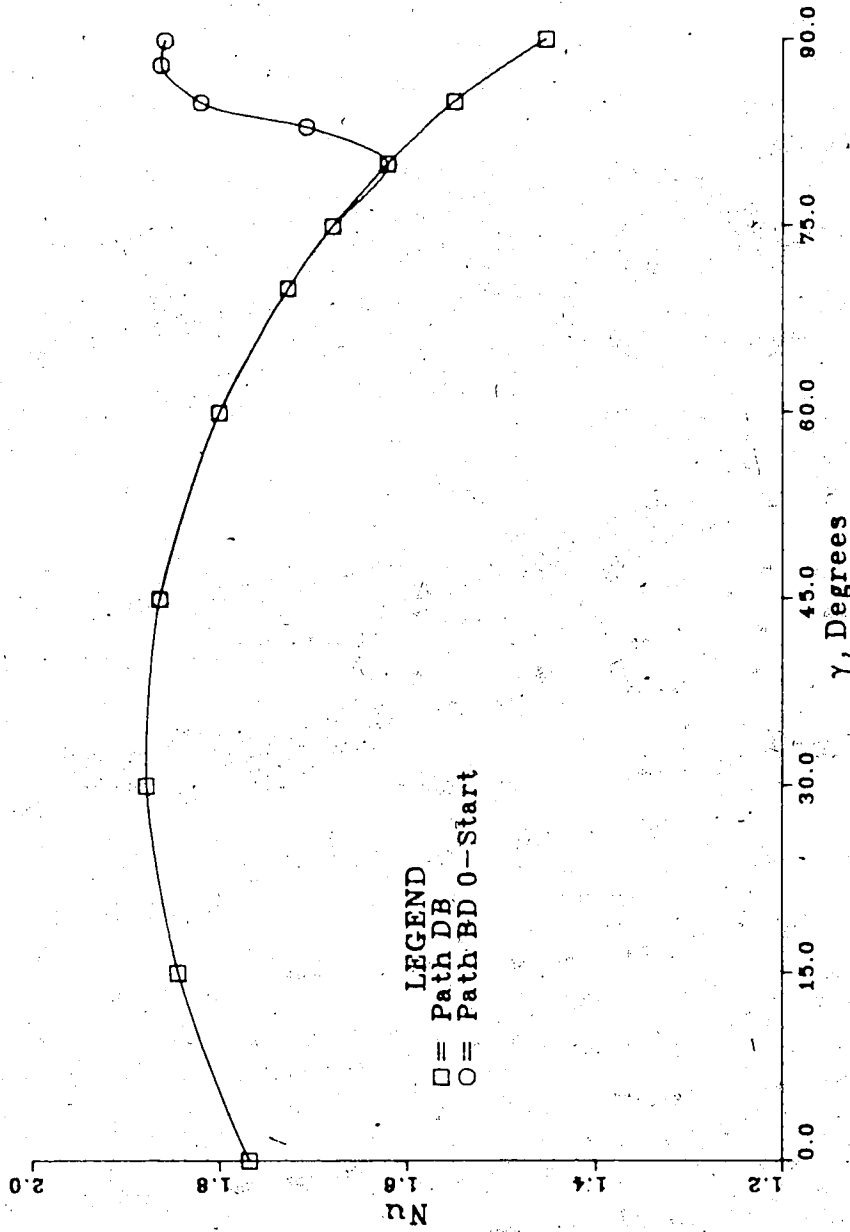
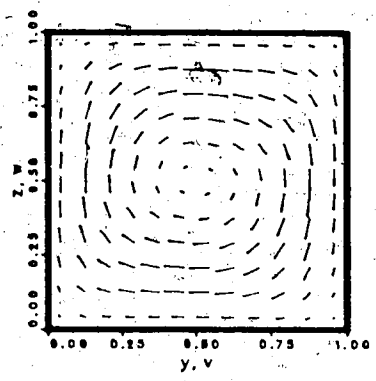
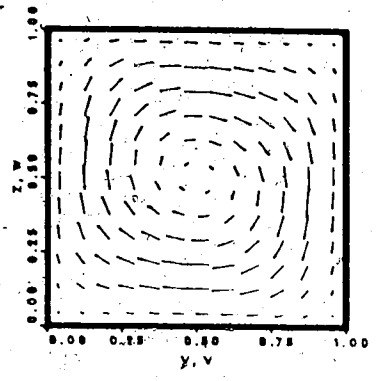


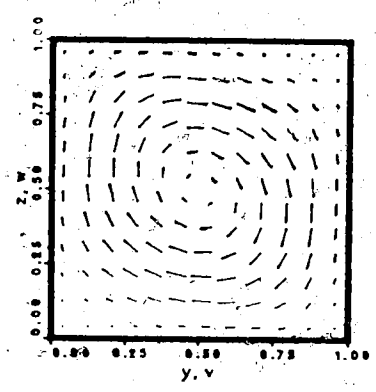
Figure V.9 Nusselt number for different roll angles



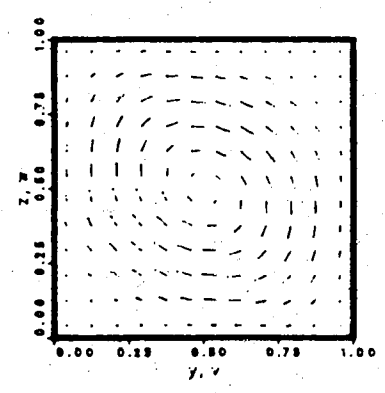
0°  
(a)



45°  
(b)



75°  
(c)



90°  
(d)

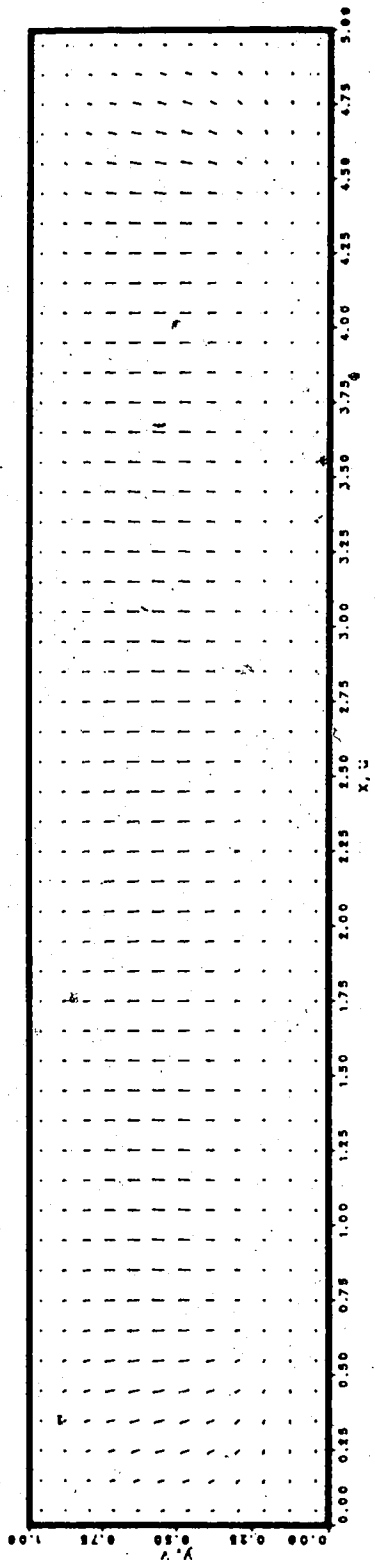


Figure V.11 xy plane velocity,  $z=0.208$ , at B

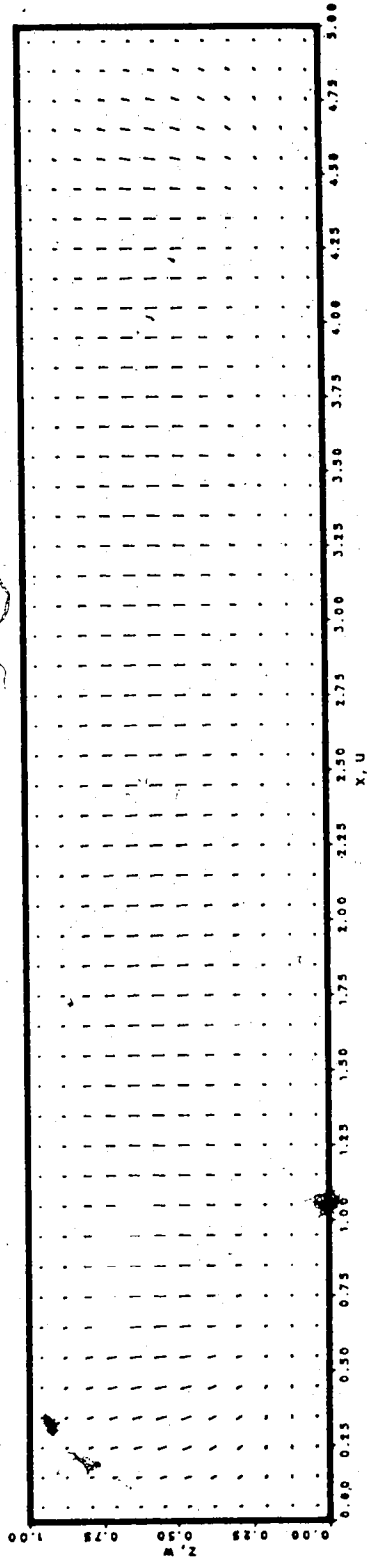


Figure V.12 xz plane velocity,  $y=0.208$ , at B



solutions being symmetric about the mid-z plane, the solution obtained by rotating the box from *D* to *B* does not possess this symmetric property. This indicates, as we mentioned before, that a symmetric solution is only one possible solution of the governing equations. Caution should therefore be exercised when dealing with configurations near *B* using the symmetric property of the solution because non-symmetric solutions also appear to be possible.

#### *B* Obtained by Uniform Input

It was shown in the last section that if a longitudinal roll was taken as the initial condition the flow pattern remained a longitudinal roll at *B*. However, it is doubtful that this longitudinal roll is the unique solution at *B* for all kinds of initial inputs. In this section two different uniform field inputs are tried so that other possible flow patterns at *B* may be studied.

First, a nominally zero, ( $10^{-5}$ ) field is used as input. (We cannot input zero identically because the Error Check Subroutine does not then work.) For this input, the solution does converge to a series of transverse rolls; but six instead of five. This can be seen most clearly at the mid-z xy-plane as plotted in fig.V-13. Near both end walls, the flow goes downward as a result of applying the same physical boundary conditions for both walls and an isotropic initial condition in the end wall regions. This symmetry with respect to the two walls, necessitating an even number of

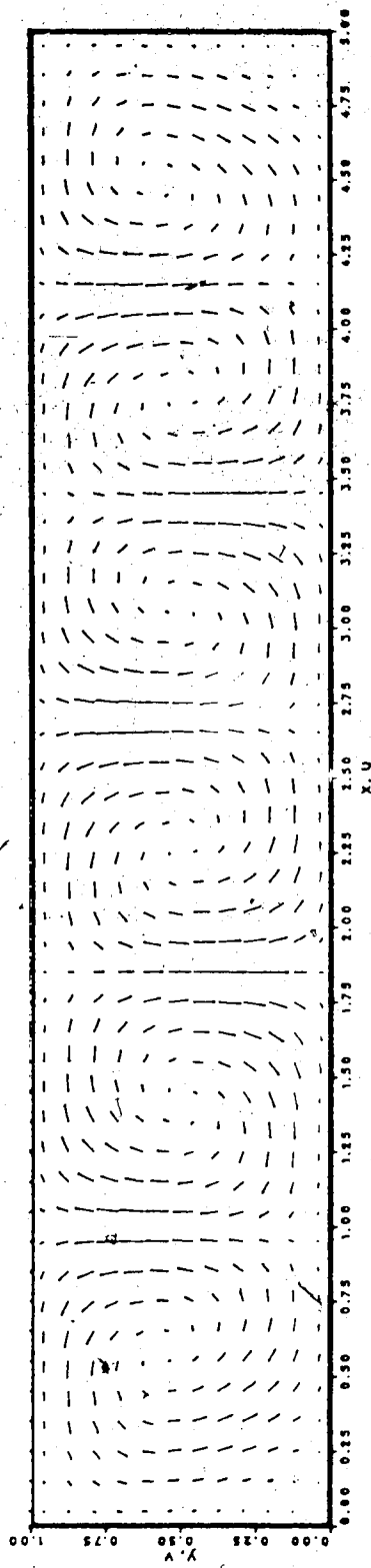


Figure V.13 xy plane velocity,  $z=0.5$ , at  $B, 0$  input

rolls, produced six rolls for  $Ax=5$ . However, it is not surprising that the flow is not strictly symmetric about  $z=2.5$  plane for reasons explained before. For later convenience this flow pattern will be referred to as  $B(6TR)$

Beginning with a  $-0.5$  uniform field input, a five transverse roll flow pattern is generated as shown in fig.V-14. The anisotropic initial input induced a non-symmetric flow pattern with the fluid moving in opposite directions in the end regions. This in turn induced (odd number) five transverse rolls.

In terms of heat transfer, transverse rolls are a much more efficient energy transport system than a single longitudinal roll near the configuration  $B$ . Also the 5-roll is better than the 6-roll mode. Respective Nusselt number for the 1LR, 6TR and 5TR modes are 1.45, 1.86 and 1.92, respectively.

It has been shown that at least three flow patterns are possible, each resulting from a different initial input. One might well ask, how many more are possible and is there one preferred (most stable) mode? We will try to answer these questions in section E. Meanwhile, the structure of a typical transverse roll will be examined in detail.

The longitudinal roll is almost two-dimensional because of the 5:1 aspect ratio in the roll axis direction. However, for transverse rolls, since the  $z$ -direction has one of the smallest dimensions, a strong three-dimensional effect is anticipated. Actually, one can hardly call the flow pattern

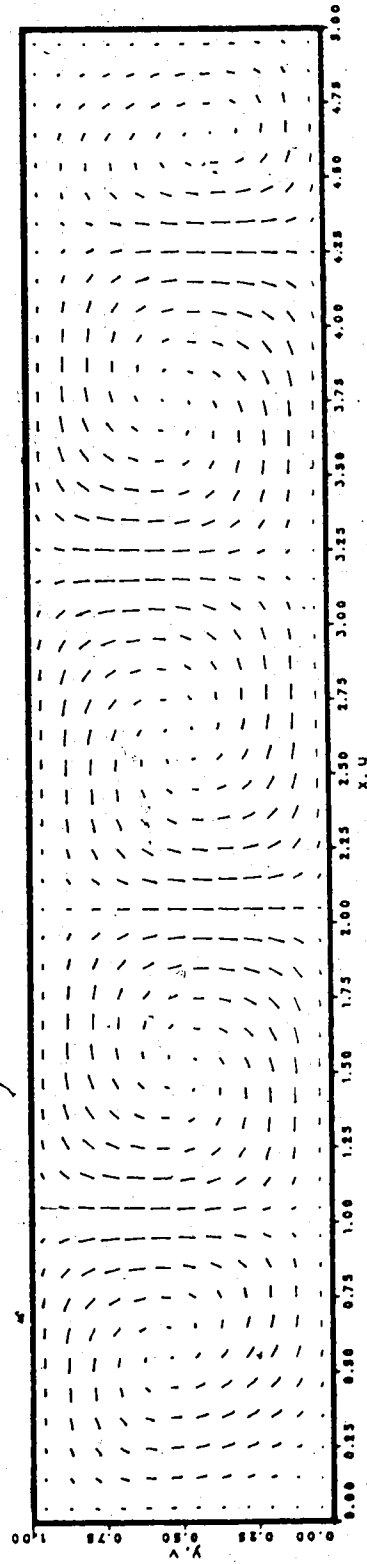


Figure V.14 xy plane velocity,  $z=0.5$ , at  $B$ ,  $-0.5$  input

a series of two-dimensional rolls as may be seen by looking at fig.V-15 which portrays the top view of the plane flow near the top (cold) wall for B(6TR). It looks more like three jets impinging on the wall and spreading the fluid radially.

By cutting slices in the yz-plane along a typical roll, a vivid picture of the three-dimensional nature of the flow can be obtained. Fig.V-16 shows several sections of the number 3 roll in B(6TR). The roll is roughly anti-symmetric about its rolling axis. In the region where the fluid rises, the flow first converges in the z-direction; it then approaches the top wall and diverges to create an embryonic pair of vortices at the upper corners (fig.V-16a,b). These upper vortices form and grow, causing another pair of vortices to form beneath in order to make the flow compatible (fig.V-16c). At the central plane of the roll, two pairs of counter-rotating vortices are established (fig.V-16d). It is found that every transverse roll basically repeats this flow structure regardless of the numbers of rolls the pattern has.

#### Path *BD*

It appears that either longitudinal or transverse rolls are possible forms of flow pattern in configuration *B*. At *D*, however, only the longitudinal roll is observed. It is, therefore, interesting to trace the path *BD* by starting at *B* with, say, six transverse rolls. Rolling the box back to *D*,

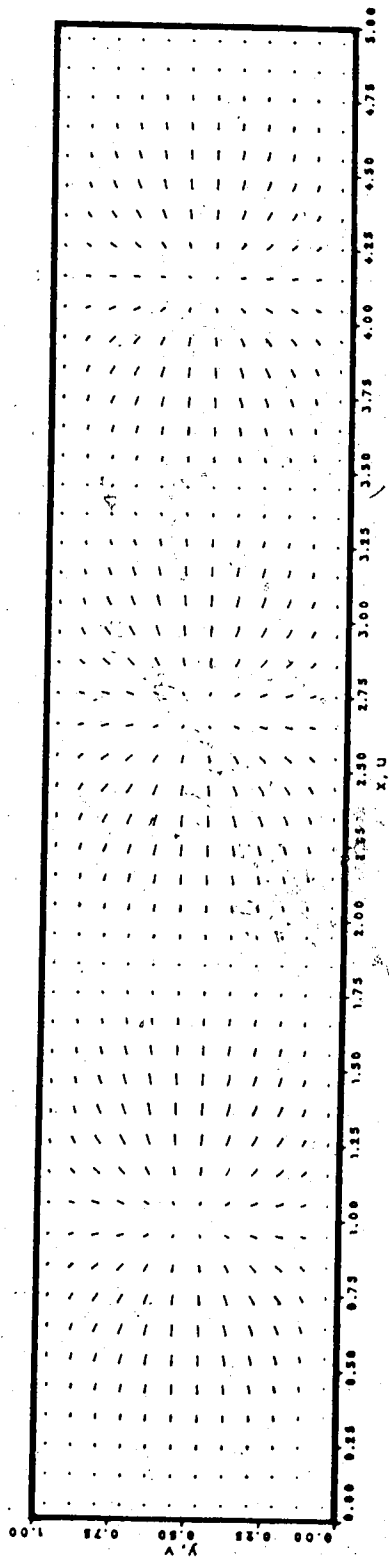
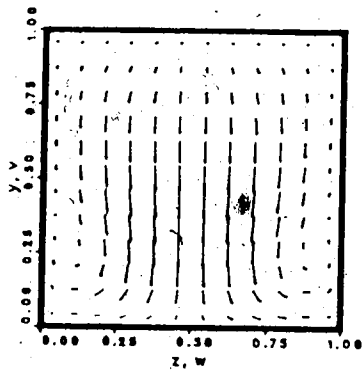
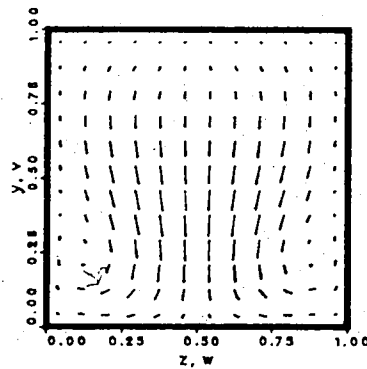


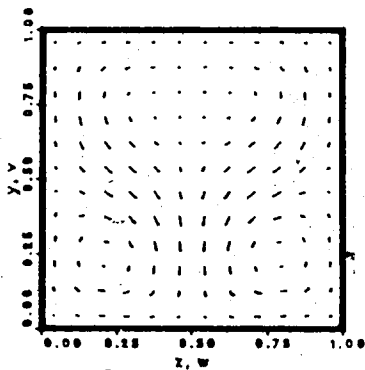
Figure V.15 xz plane velocity,  $y=0.917$ , at B(6TR)



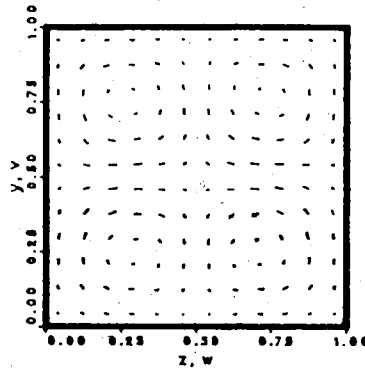
x=1.85



x=1.95



x=2.15



x=2.25

Figure V.16  $v_z$  plane velocity along  $x$ . at B(6TR)

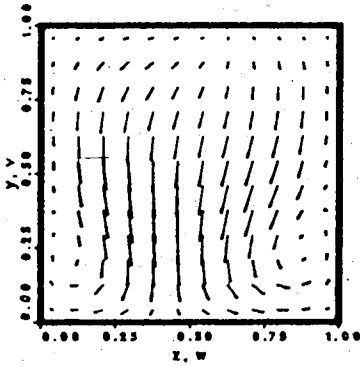
various stages of transition of the flow pattern from transverse rolls to a longitudinal roll can be observed.

Let us first go back to fig.V-9 and re-examine the curve connecting the circles representing path  $BD$ . At  $B$  the 6-roll mode is used. It can be seen that  $Nu$  drops sharply as  $\gamma$  goes from  $90^\circ \rightarrow 80^\circ$ . For  $\gamma \leq 80^\circ$ , the circles coincide with the squares indicating that it makes no difference whether we follow path  $BD$  or  $DB$  in calculating the flow field for these configurations. So the transition from 6TR to 1LR takes place between  $\gamma=90^\circ$  and  $80^\circ$ .

Fig.V-17, being a representative  $yz$ -plane view, shows the process of transition very clearly. At  $\gamma=88^\circ$  (fig.V-17a), the flow is still described by a transverse roll. At  $\gamma=85^\circ$ , the longitudinal roll has grown noticeably and at  $\gamma=83^\circ$  it dominates, thus resulting in a sharp decrease in Nusselt number. At  $\gamma \leq 80^\circ$  there is no trace of any kind of transverse roll, only a complete longitudinal roll, exactly the same as obtained by following path  $DB$ .

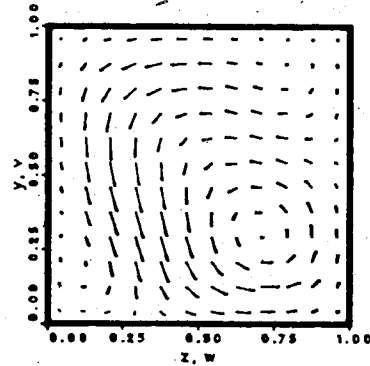
In concluding this section, we answer the questions raised at the beginning of the section by saying that for configurations of  $\gamma \leq 80^\circ$ , the flow pattern is definitely a longitudinal roll independent of path; while for  $\gamma > 80^\circ$ , the flow pattern is branched, thus permitting both longitudinal and transverse rolls of different numbers depending upon the initial input.





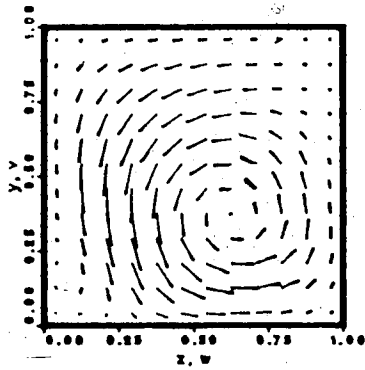
$\gamma=88^\circ$

(a)



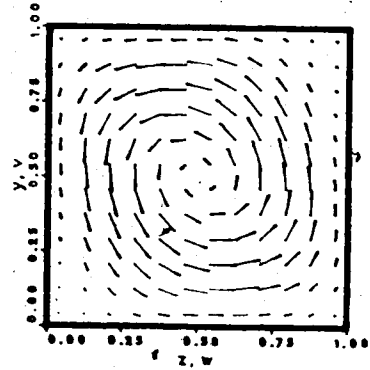
$\gamma=85^\circ$

(b)



$\gamma=83^\circ$

(c)



$\gamma=80^\circ$

(d)

### C. THE EFFECT OF TILT

In previous sections, several paths were followed by rotating the box in two ways: skewing and rolling. In the process of skewing the global temperature gradient is always perpendicular to gravity, while in the process of rolling the temperature gradient rotates from perpendicular to parallel (or opposite) to gravity, the longest dimension of the box remaining horizontal. Besides skewing and rolling, there is another way of rotating the box: tilting, in which process the temperature gradient rotates between horizontal and vertical along with the longest dimension of the box. Starting from *A*, we can either tilt the box by  $90^\circ$  to get *B* or by  $-90^\circ$  to get *C*, thus having travelled along paths *AB* and *AC*. Paths *BA* and *CA* are also possible. All these alternatives will now be discussed.

In this section, the tilt angle  $\alpha$  is measured from configuration *A*.

#### Path *AB*

The flow pattern established at *A* prevails as long as  $\alpha \leq 30^\circ$ . Buoyancy in the *y*-direction appears to increase the heat transfer as  $\alpha$  increases from  $0^\circ$  to  $30^\circ$ . This is shown in fig.V-18. For  $\alpha$  between  $30^\circ$  and  $75^\circ$ , no major change of flow pattern is observed. However, there is a minor change consisting of a three-dimensional modification propagated from the end wall regions to the interior. For  $\alpha > 30^\circ$  the structure of the cell resembles that of a transverse roll,

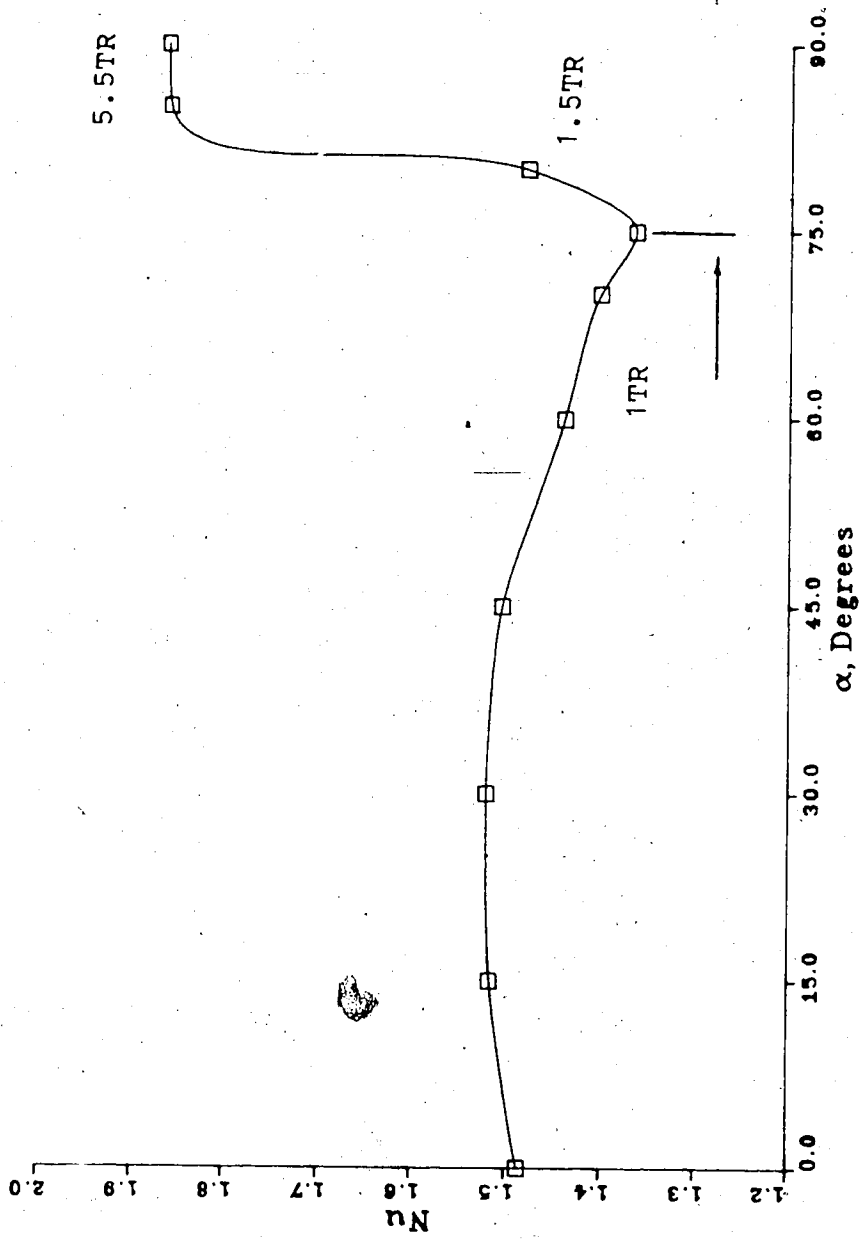


Figure V.18 Nusselt number along path AB

as discussed in Section C. At  $\alpha=80^\circ$  the single transverse roll pattern is disturbed as two regions of reverse flow caused by local temperature gradient appear (fig.V-19). At  $\alpha=85^\circ$ , the flow abruptly breaks into five and a half rolls thereby increasing the Nusselt number by 25.8%. This "5.5TR" pattern remains up to  $\alpha=90^\circ$ . It can be seen from fig.V-20 that the left-most roll is not very well developed and would not be seen in the z wall regions. That is why it is only counted as a half roll.

#### Path B(6TR) $\rightarrow$ A

Starting with B(6TR), the box is tilted back to A. Between  $\alpha=90^\circ$  and  $80^\circ$  the flow pattern remains unchanged. At  $\alpha=75^\circ$  the flow switches to a 4.5TR structure accompanied by a small decrease in Nusselt number. At  $\alpha=70^\circ$ , the flow changes to 3TR with a greater decrease in Nu. However, between  $\alpha=70^\circ$  and  $60^\circ$  the flow pattern, being relatively stable, changes from 3TR to 2.5TR leaving the Nu almost unchanged. For  $\alpha=60^\circ\rightarrow 45^\circ$ , another big jump occurs in both flow pattern and heat transfer rate. For  $\alpha\leq 45^\circ$ , the flow assumes the original single transverse cell pattern, exactly the same as that obtained from following path AB. The Nusselt number is plotted versus  $\alpha$  in fig.V-21 with the flow pattern labeled for each point. Fig.V-22 is a representative flow pattern which shows the 3TR pattern at  $\alpha=70^\circ$ .

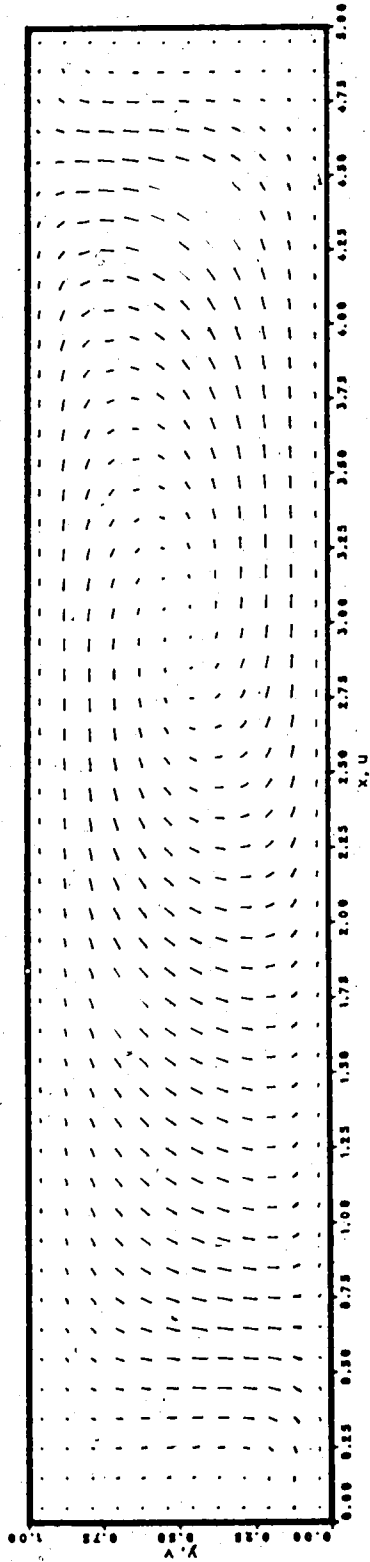


Figure V.19 xy plane velocity,  $z=0.5$ ,  $\alpha=80^\circ$ , path AB

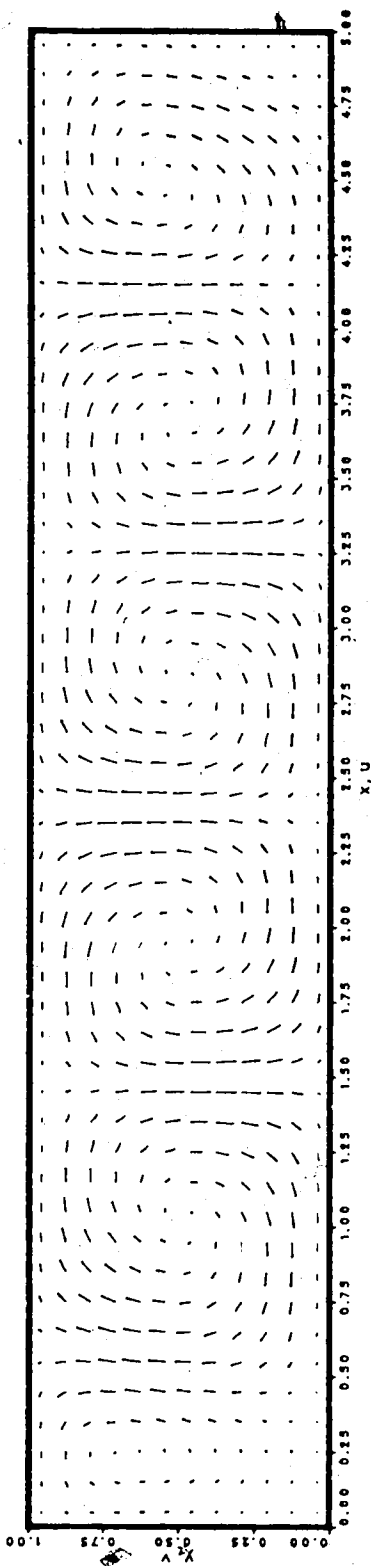


Figure V.20 xy plane velocity,  $z=0.5$ ,  $\alpha=90^\circ$ , path AB

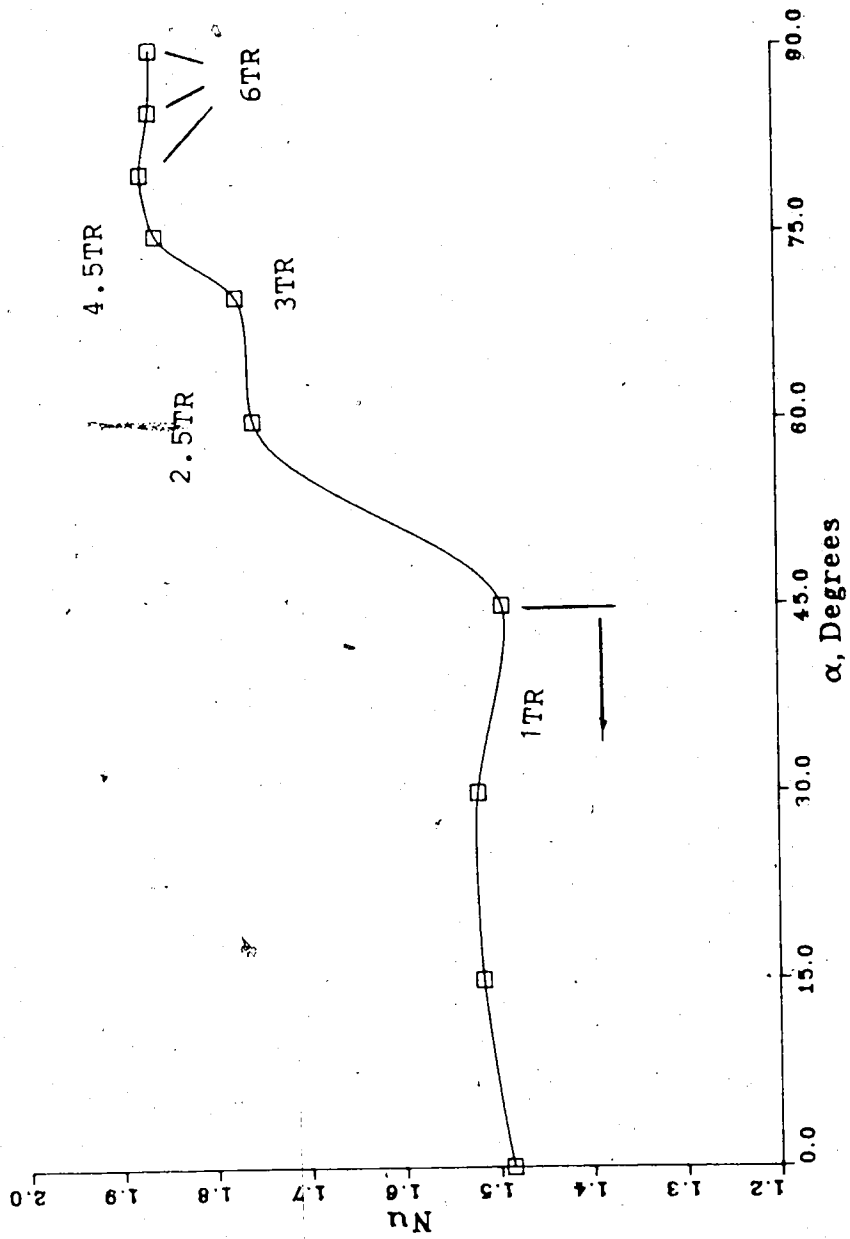


Figure V.21 Nusselt number along path B(6TR)A

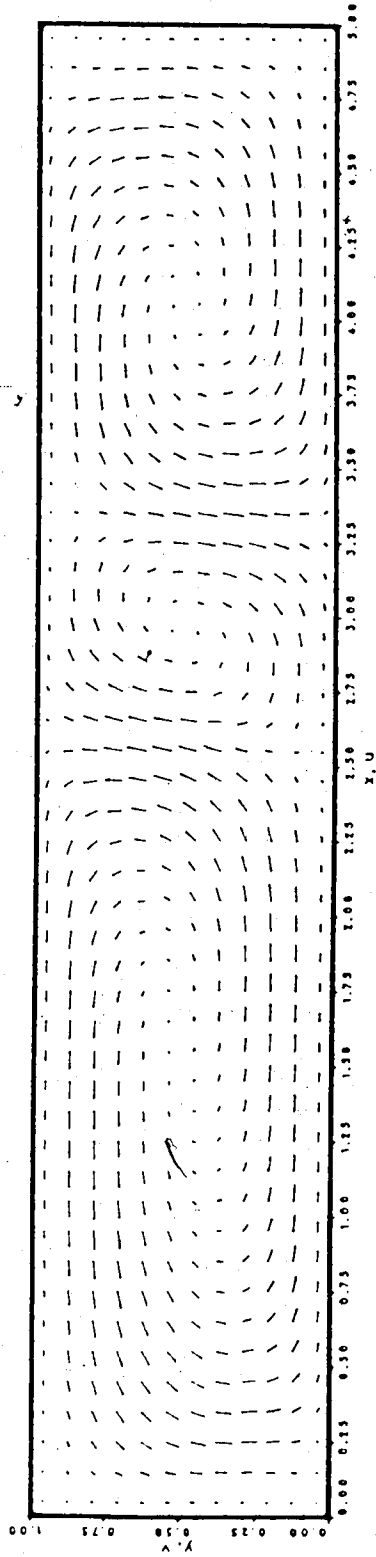


Figure V.22 xy plane velocity,  $z=0.5$ ,  $\alpha=70$ , path B(6TR)A

82



## Path B(LR)→A

Using the B(LR) as the starting point, the above process is repeated. The heat transfer rate and the flow pattern at different angles is shown in fig.V-23. It is interesting to see that the flow immediately changes to a 5TR mode as  $\alpha$  decreases to  $85^\circ$  thus leading to a huge jump in Nu. At  $\alpha=80^\circ$  the the 5TR pattern, established at  $85^\circ$ , is further developed. Transition from 5TR to 3TR, associated with a large decrease in Nu, takes place when  $\alpha$  goes from  $80^\circ$  to  $75^\circ$ . Between  $\alpha=75^\circ$  and  $70^\circ$  the flow changes little. Before the flow goes back to the single transverse cell at  $\alpha \leq 45^\circ$ , however, the pattern undergoes transitions from 3TR to 2TR for  $\alpha=70^\circ \rightarrow 60^\circ$ , and 2TR to 1TR for  $\alpha=60^\circ \rightarrow 45^\circ$ . Once again, for configurations of  $\alpha \leq 45^\circ$ , no bifurcation is observed. Finally, fig.V-24, taken as an example, shows the flow pattern at  $\alpha=80^\circ$ .

The evidence presented above suggests that there are two roughly equal regions of  $\alpha$  each with different solution properties. For  $0^\circ \leq \alpha \leq 45^\circ$  the flow pattern is a unique single transverse cell independent of the initial input; the heat transfer rate is smooth and definite. For  $45^\circ < \alpha \leq 90^\circ$  the flow pattern is branched and complicated. The final pattern for any given configuration in this region is dependent on the initial input and/or the path by which this configuration was reached. There is a certain amount of unpredictability

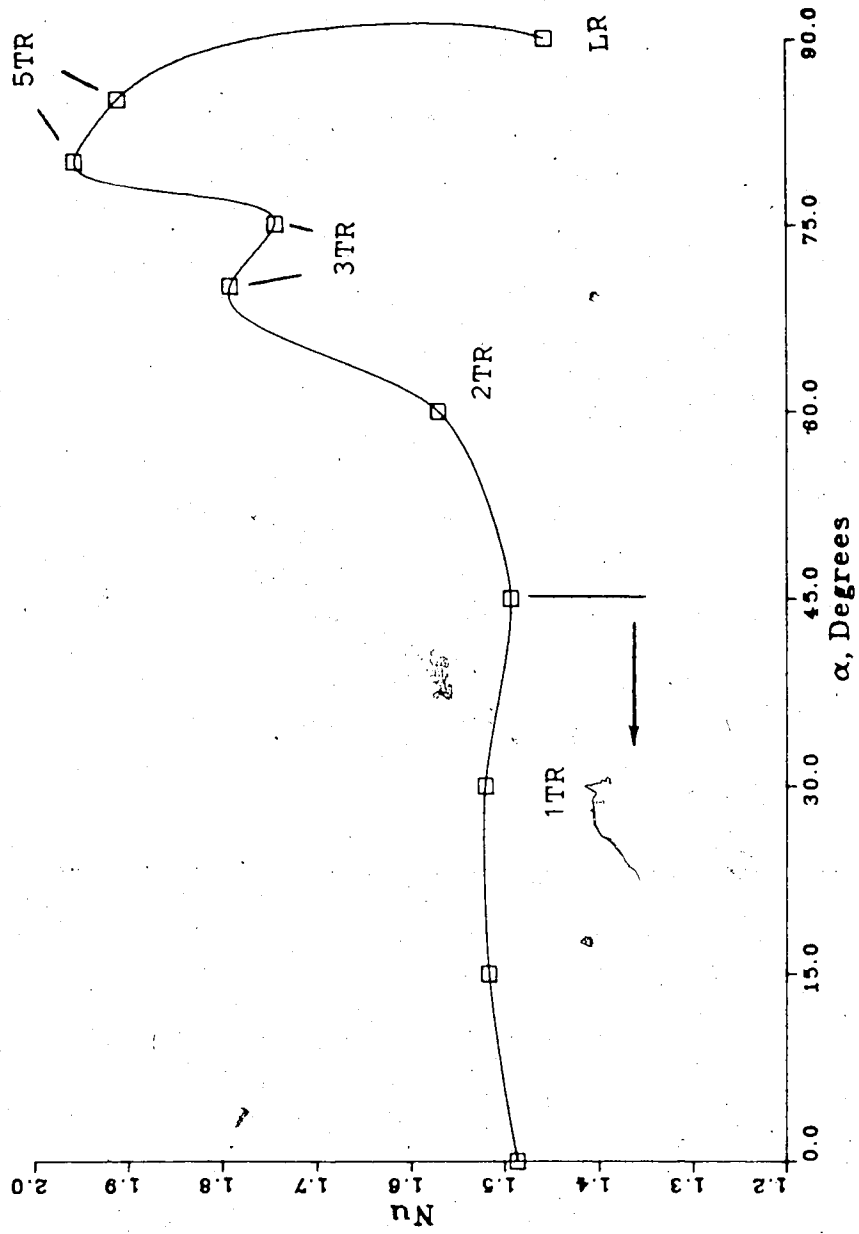


Figure V.23 Nusselt number along path B(LR)A

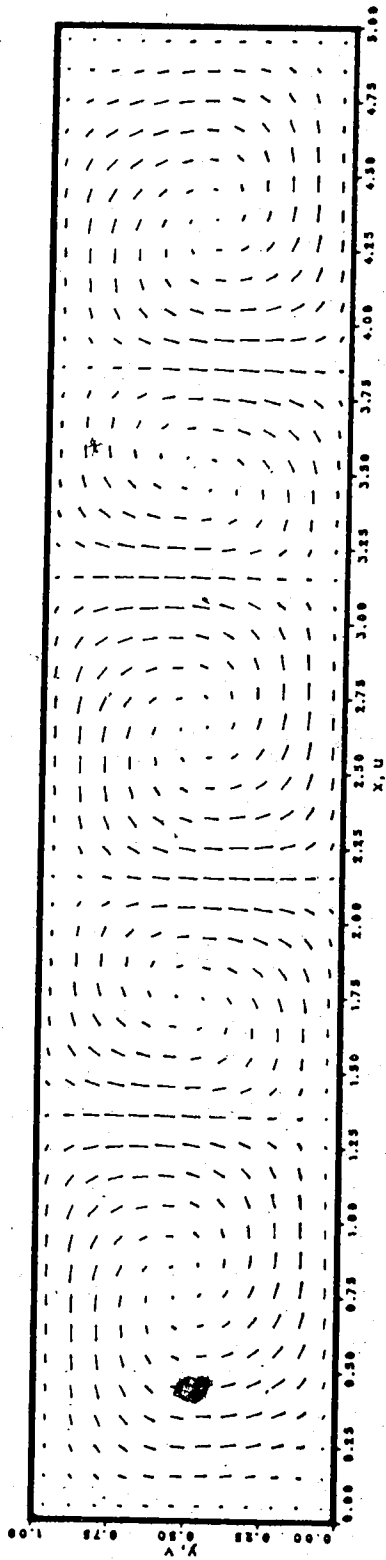


Figure V.24 xy plane velocity,  $z=0.5$ ,  $\alpha=80$ , path B(LR)A

this region. As  $\alpha$  goes from  $45^\circ$  to  $90^\circ$  the unpredictability increases. For example, at  $\alpha=60^\circ$  three possible flow patterns are 1TR, 2TR and 2.5TR with Nu varying between 1.40 and 1.75, a variation of 25%. At  $\alpha=80^\circ$  three possible flow patterns are 1TR, 6TR and 5TR with Nu varying between 1.47 and 1.91, a variation of 30%. At  $\alpha=90^\circ$  bifurcation between transverse rolls and longitudinal roll is even observed. This increasing trend of uncertainty is believed to be caused by the increasingly important role which the vertical component of global temperature gradient plays as  $\alpha$  goes to  $90^\circ$ .

Finally, it is instructive to present the Nu histogram in terms of the number of transverse rolls. Fig.V-25 shows this with 0 representing the longitudinal roll. It can be seen that, a) 5TR is the most effective heat transfer mode probably due to the geometry fitness; b) Nu generally increases with an increasing TR number; c) the 4TR mode does not appear to exist!

#### D. OTHER SITUATIONS

Paths AB and AC have also been calculated using the mid-z plane symmetric 71x15x8 grid system for  $A_x=5$  and  $A_z=1$ . For path AB, the results are qualitatively the same as those reported in the last section. The single transverse cell breaks up to 5.5TR at  $\alpha=85^\circ$ . For path AC, the single transverse cell becomes weaker and weaker and finally

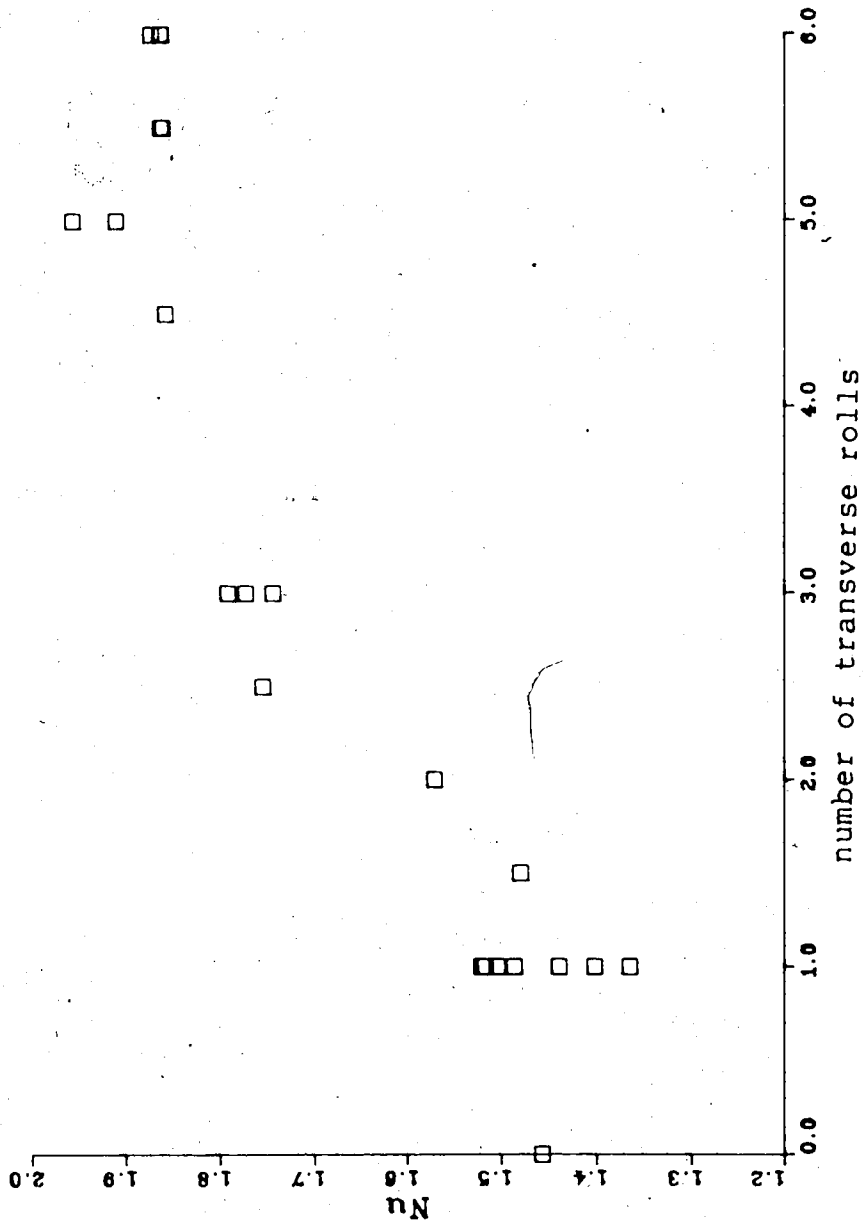


Figure V.25 Nusselt numbers for various cell structures

2

conduction. In this particular geometry, a different mesh system makes no qualitative difference in the solution even for configurations near  $B$ .

The  $A_x=1$  and  $A_z=2$  cavity with BC2 has also been tested. This is the same cavity geometry and boundary condition as that reported in [35]. It was reported in [35] that, for  $Ra=2060$  to  $4460$ , at  $B$ , LR, 1TR, 2TR and the mixture of them were possible flow patterns; each would show up for a different Rayleigh number. One Rayleigh number corresponded to a unique flow pattern. However, it is found in this study that, for  $Ra=10^4$ , LR, 2TR and 3TR are possible flow patterns. The final flow pattern is determined by initial input. It appears that changes in geometry of the box and boundary conditions do not alter the bifurcation situations near  $B$  for sufficiently large  $Ra$  ( $O(10^4)$ ).

## E. SOME THOUGHTS ON BENARD CONVECTION

### Uniqueness Versus Bifurcation

Most of the previous studies of supercritical Benard convection had a particular objective in mind: to predict the planform and the wave number of the convection. This objective is based on the assumption that the planform and wave number (flow pattern) under certain prescribed conditions are unique and completely predictable, at least

solution which is independent of the initial conditions. The frequently mentioned alternative flow patterns in experimental reports are usually dismissed as exceptions caused by uncertain factors, and thus taken to be meaningless. It was believed that the difference between theory and experiment could be attributed to: a) the lack of control over the experimental conditions and, b) the inability to solve the nonlinear governing equations accurately. To overcome these difficulties, extremum principles were introduced to help predict the flow pattern ([24,25]). According to these extremum principles, the flow pattern for any given Rayleigh number must be such that: a) the resultant viscous dissipation rate is a minimum or, b) the resultant heat transfer rate is a maximum or, c) the entropy production rate of the system is an extremum.

In the present study, solutions of the governing equation were obtained using a numerical method which is one of the best methods known today in dealing with equations of this type. Although the results for the  $Ax=5$  and  $Az=1$  cavity did show that the 5TR mode satisfied the maximum heat transfer criterion and probably the minimum viscous dissipation condition, it nonetheless was not THE solution. The evidence overwhelmingly suggests that there is no unique 1LR, 5TR, 6TR, etc. are all possible solutions. Which one is finally realized appears to be determined by the initial

pattern can not be predicted unless the initial conditions are specified.

The unpredictability of a system governed by deterministic laws is not unusual. It is only one more manifestation of the intrinsic properties of most nonlinear systems. Recent studies have shown ([33,34]) that even a one-degree-of-freedom nonlinear system may have chaotic behavior. So it is no surprise that a continuum having an infinite number of degrees of freedom governed by nonlinear laws would exhibit certain degrees of unpredictability.

#### Formation of a Flow Pattern

Mathematically, the unpredictability of solutions is an intrinsic property of the nonlinear governing equations for the system at  $B$ . But no attempt will be made here to study this property in a mathematically strict manner. However, by applying the working principle for predicting the flow pattern for a given temperature gradient (WP II-C-2), we can get some insight into the physical processes involved.

When the TG is not parallel to the GA, it will lead to a circulation in the direction predicted by WP II-C-2. Once convection occurs, the temperature distribution, thus the TG distribution, will be modified accordingly. If the circulation alters the temperature distribution in such a



circulation and temperature field are not mutually reinforcing, then the flow pattern is not likely to be stable and will be changed until a reinforcing interaction is formed.

When the TG is parallel to GA, the circulation direction is indeterminate. For configuration B, the TG provided by the GTG is parallel to GA. So the pattern of motion (if any) is not determined by the GTG but by local horizontal temperature gradients (LHTG) provided by means other than the GTG. The LHTG can be furnished by: a) fluctuations in the fluid or, b) initial conditions. If the LHTG's are such that a positive feedback loop of temperature-circulation is formed, a certain flow pattern is likely to emerge. In the whole process, the GTG is only acting as a source of energy for motion of any permissible flow pattern. The pattern itself appears to be determined by the LHTG's. If the initial condition and/or fluctuations are to some degree arbitrary, so is the flow pattern.

We can take the B(LR) situation as an example. We know that at D, the temperature is stratified in the z-direction as a result of the LR convection. There is a temperature gradient in the positive z-direction. When this LR pattern is used as input at B, this z-TG is a LHTG. According to WP II-C-2, the circulation direction under this LHTG is

### Validity of Numerical Methods

It has been shown that the solution at  $B$  is not unique but branched, and it is not stable to certain disturbances. Since a numerical method is necessarily an approximation procedure, it will introduce inherent disturbances to the solution. Different solutions may be generated simply by applying, say, different grid systems.

The question of how reliable a numerical solution is is hard to answer. It deserves full investigation. Different numerical methods, different grid systems for the same method, or even, the application of different sweeping sequences when solving the algebraic equations, might make substantial differences. But, hopefully, the consistency of using exactly the same numerical procedure might to some degree reduce, if not remove, the ambiguity.

### F. CONCLUSIONS

In this chapter, natural convection of air in a  $Ax=5$  and  $Az=1$  cavity rotating along several paths has been studied. The Rayleigh number was fixed at  $10^4$ . Transitions between different flow patterns have been identified and the associated heat transfer rates presented. Path-dependent behavior of the system has been found for configurations around  $B$ .

roll dominates. Along path  $AD$ , the longitudinal roll is a more effective heat transfer mode. No solution bifurcation was found along  $AD$  because the GTG is always perpendicular to  $GA$ .

The flow pattern for configurations between  $D$  and  $B$  obtained by following path  $AD$  is a longitudinal roll. The temperature stratification in the  $z$ -direction caused by LR convection results in a TG in the  $z$ -direction. This TG, which is horizontal at  $B$ , is responsible for the formation of the LR pattern at  $B$ . As for heat transfer,  $Nu$  increases slightly between  $\gamma=0^\circ$  and  $30^\circ$  but decreases monotonically from  $30^\circ$  to  $90^\circ$ .

There is a region of  $\gamma$  spanning about  $10^\circ$  near  $B$  where the solution is path-dependent. In this region, flow patterns of several transverse rolls (TR) have been found if the initial condition is a series of transverse rolls. The transverse roll mode is a much more effective heat transfer mode than the LR mode in this region.

When tilting the box from  $A$  to  $B$ , the path-dependent region is much larger. For  $\alpha \leq 45^\circ$ , the flow pattern is a single transverse cell. For  $\alpha = 45^\circ$  to  $90^\circ$ , the flow pattern can be 1TR, 2TR, 3TR, 5TR or 6TR, the resulting variations in  $Nu$  being as high as 30%. Following the path  $AB$ , the 1TR persisted until  $\alpha = 85^\circ$  at which point 5.5TR's were suddenly formed. Following the path  $B(6TR)A$ , the flow pattern exhibited a series of transitions with decreasing numbers of TR's before finally settling down to 1TR at  $\alpha = 45^\circ$ . For the

path  $B(LR)A$ , the system first jumped to 5TR at  $\alpha=85^\circ$  and then repeated the same behavior as the  $B(6TR)A$  path. The most effective heat transfer mode is 5TR and the least is LR in configuration  $B$ .

Limited studies of other situations suggest that the path-dependent behavior of the system has not been changed by the size of the box, boundary conditions and the computing grid network.

When the GTG of the system is parallel to the GA, the flow pattern is not determined by the GTG but by combined effects of local horizontal temperature gradients (LHTG). The LHTG's are usually furnished by fluctuations in the fluid or the initial conditions. The randomness of the mechanism in providing the LHTG's determines that the bifurcation of solution in this situation is a rule rather than an exception. Previous attempts to work out a unique solution for a given set of principle parameters have thus put the problem in a misleading perspective.

## REFERENCES

1. Bejan, A., Convection Heat Transfer, John-Wiley & Sons, 1984.
2. Kakac, S., Aung, W. and Viskanta, R. ed., Natural Convection: Fundamentals and Applications, Hemisphere Publishing Corp., Washington, 1985.
3. Batchelor, G. K., Heat transfer by free convection across a closed cavity between vertical boundaries at different temperatures, *Quart. Appl. Math.*, 12, 209, 1954.
4. Poots, G., Heat transfer by laminar free convection in enclosed plane gas layers, *Quart. J. Mech. Appl. Math.*, 11, 257, 1958.
5. Eckert, E. R. G. and Carlson, W. O., Natural convection in an air layer enclosed between two vertical plates with different temperatures, *Int. J. Heat Mass Transfer*, 2, 106, 1961.
6. Elder, J. W., Laminar convection in a vertical slot, *J. Fluid Mech.*, 23, 77, 1965.
7. Elder, J. W., Numerical experiments with free convection in a vertical slot. *J. Fluid Mech.*, 24, 823, 1966.
8. Vest, C. M. and Arpaci, V. S., Stability of natural convection in a vertical slot, *J. Fluid Mech.*, 36, 1, 1969.
9. Gill, A. E. and Kirkham, C. C., A note on the stability of convection in a vertical slot, *J. Fluid Mech.*, 42, 125, 1970.
10. de Vahl Davis, G. and Mallinson, G. D., A note on natural convection in a vertical slot. *J. Fluid Mech.*, 72, 87, 1975.
11. Seki, N., Fukusako, S. and Inaba, H., Visual observation of natural convection flow in a narrow vertical cavity, *J. Fluid Mech.*, 84, 695, 1978.
12. Lee, Y. and Korpela, S. A., Multicellular natural convection in a vertical slot. *J. Fluid Mech.*, 126, 91, 1983.
13. Catton, I., Natural convection in enclosures, *6th International Heat Transfer Conferences, Toronto, 1978*,

- 6, 13, Hemisphere Publishing Corp., 1979.
14. Ozoe, H., Yamamoto, K., Churchill, S. W., and Sayama, H., Three-dimensional, numerical analysis of laminar natural convection in a confined fluid heated from below, *J. Heat Transfer*, 98, Pt. 2, 202, 1976.
  15. Mallinson, G. D. and de Vahl Davis, G., Three-dimensional natural convection in a box: a numerical study. *J. Fluid Mech.*, 83, 1, 1977.
  16. Bontoux, P., Smutek, C., Roux, B. and Lacroix, J. M., Three-dimensional buoyancy-driven flows in cylindrical cavities with differentially heated endwalls: Part 1. Horizontal cylinders, *J. Fluid Mech.*, 169, 211, 1986.
  17. Yang, H. Q., Yang, K. T. and Lloyd, J. R., Laminar natural convection flow transitions in tilted three-dimensional longitudinal rectangular enclosures, *Int. J. Heat Mass Transfer*, 30, No.8, 1637, 1987.
  18. Benard, H., *Rev. Gen. Sci. Pure Appl.*, 11, 1261, 1900.
  19. Lord Rayleigh, On convection currents in a horizontal layer of fluid when the higher temperature is on the underside, *Philos. Mag.*, 6, No.32, 529, 1916.
  20. Chandrasekhar, S., Hydrodynamic and Hydromagnetic Stability, Clarendon Press, Oxford, 1961.
  21. Davis, S. H., Convection in a box: linear theory. *J. Fluid Mech.*, 30, 465, 1967.
  22. Catton, I., Convection in a rectangular region: onset of motion, *J. Heat Transfer*, 92, 186, 1970.
  23. Stork, K. and Muller, U., Convection in boxes: experiments, *J. Fluid Mech.*, 54, 599, 1972.
  24. Busse, F., Transition to turbulence in the Rayleigh-Benard convection, In Hydrodynamic Instabilities and the Transition to Turbulence (ed. Swinney, H. L. and Gollub, J. P.), 97, Springer, 1981.
  25. Koschmieder, E. L., Experimental aspects of hydrodynamic instability, In Order and Fluctuations in Equilibrium and Non-equilibrium Statistical Mechanics (ed. Nicolis, E., Dewel, G. and Turner, J. W.), John Wiley and Sons. 1981.
  26. Boussinesq, J. Theorie Analytique de la Chaleur, 2, Gauthier-Villars, Paris, 1903.
  27. Chenoweth, D. R., and Paolucci, S., Natural convection

- in an vertical air layer with large horizontal temperature differences, *J. Fluid Mech.*, 169, 173, 1986.
28. Gershuni, G. Z., Zhukhovitskii, E. M., Convective Stability of Incompressible Fluids, Keter Publishing House Jerusalem Ltd., 1976.
  29. Finlayson, B. A., The Method of Weighted Residuals and Variational Principles, With Its Application in Fluid Mechanics, Heat and Mass Transfer, Academic Press, New York, 1972.
  30. Shih, T. M., Numerical Heat Transfer, Hemisphere Publishing Corporation, Washington D. C., 1984.
  31. Patankar, S. V., Numerical Heat Transfer and Fluid Flow, Hemisphere Publishing Corporation, 1980.
  32. Van Doormaal, J. P. and Raithby, G. D., Enhancements of the SIMPLE method for predicting incompressible fluid flows, *Numerical Heat Transfer*, 7, 147, 1984.
  33. Tatsumi, T. ed., Turbulence and Chaotic Phenomena in Fluids, North-Holland, 1984.
  34. Thompson, J. M. T. and Stewart, H. B., Nonlinear Dynamics and Chaos: geometrical methods for engineers and scientists, Chichester Wiley, New York, 1986.
  35. Winters, K. H. and Brown, T. W., Benard convection in a three-dimensional cavity: the effects of aspect ratio and tilt, Harwell Report AERE HL85/1177, April 1985.

## APPENDIX

### LISTING OF PROGRAM

THIS IS A PROGRAM SOLVING NATURAL CONVECTION PROBLEMS

```

PARAMETER(N=51,M=13,L=13,NN=N+1,MM=M+1,LL=L+1)
PARAMETER(NP=N-1,MP=M-1,LP=L-1)
DIMENSION UP(N,MM,LL),VP(NN,M,LL),WP(NN,MM,L)
DIMENSION T(NN,MM,LL),PP(NN,MM,LL),P(NN,MM,LL)
DIMENSION U(N,MM,LL),V(NN,M,LL),W(NN,MM,L),GRADT(MM)
DIMENSION DX(NN),DY(MM),DZ(LL),AP3(2:N,2:M,2:L)
DIMENSION PX(NN),QX(NN),PY(MM),QY(MM),PZ(LL),QZ(LL)
DIMENSION AP1(2:N,2:M,2:L),AP2(2:N,2:M,2:L),S(2:N,2:M,2:L)
DIMENSION AE(2:N,2:M,2:L),AW(2:N,2:M,2:L),AN(2:N,2:M,2:L)
DIMENSION AS(2:N,2:M,2:L),AT(2:N,2:M,2:L),AB(2:N,2:M,2:L)
DIMENSION
PSB(2:N,2:L),QSB(2:N,2:L),ANB(2:N,2:L),CNB(2:N,2:L)
DIMENSION
PWB(2:M,2:L),QWB(2:M,2:L),AEB(2:M,2:L),CEB(2:M,2:L)
DIMENSION
PBB(2:N,2:M),QBB(2:N,2:M),ATB(2:N,2:M),CTB(2:N,2:M)
DIMENSION SEB(2:M,2:L),SNB(2:N,2:L),STB(2:N,2:M)
CALL SYS$DISEXC(0,0,0,4)
OPEN(5,FILE='D1')
READ(5,*)AX,AZ,ANGL
READ(5,*)RY,PRD
READ(5,*)ALFV
READ(5,*)TOLV1,TOLV2,TOLT1,TOLT2,TOLP
READ(5,*)(DX(I),I=1,NN)
READ(5,*)(DY(J),J=1,MM)
READ(5,*)(DZ(K),K=1,LL)
READ(5,*)NCR,NCCR,AMP
AA1=1.0/(1.0-ALFV)
SN=SIN(ANGL)
CN=COS(ANGL)
AX2=AX*AX
AZ2=AZ*AZ
RX=RY*AX2
RZ=RY*AZ2
AXI=1.0/AX
AXI2=AXI*AXI
AZI=1.0/AZ
AZI2=AZI*AZI
RA=2.0*RY*RY*PRD
GX=1.0/RX
GY=1.0/RY
GZ=1.0/RZ
GTZ=GZ/PRD
GTX=GX/PRD
GTY=GY/PRD

```



```

NCC=0
INPUT INITIAL GUESSED VALUES FOR U, V AND T
OPEN(4,FILE='INPUT')
READ(4,11)((UP(I,J,K),I=1,N),J=1,MM),K=1,LL)
READ(4,11)((VP(I,J,K),I=1,NN),J=1,M),K=1,LL)
READ(4,11)((WP(I,J,K),I=1,NN),J=1,MM),K=1,L)
READ(4,11)((T(I,J,K),I=1,NN),J=1,MM),K=1,LL)
READ(4,11)((PP(I,J,K),I=2,N),J=2,M),K=2,L)
DO 22 K=1,LL
DO 22 J=1,MM
DO 22 I=1,N
22 U(I,J,K)=UP(I,J,K)
DO 24 K=1,LL
DO 24 J=1,M
DO 24 I=1,NN
24 V(I,J,K)=VP(I,J,K)
DO 26 K=1,L
DO 26 J=1,MM
DO 26 I=1,NN
26 W(I,J,K)=WP(I,J,K)
APPLY BOUNDARY CONDITIONS
GRADT(1)=1.0
DO 33 J=1,M
33 GRADT(J+1)=GRADT(J)-DY(J)-DY(J+1)
DO 45 K=2,L
DO 45 I=2,N
PSB(I,K)=0.0
ANB(I,K)=1.0
45 CNB(I,K)=0.0
DO 50 K=2,L
DO 50 J=2,M
PWB(J,K)=0.0
AEB(J,K)=1.0
50 CEB(J,K)=0.0
DO 55 J=2,M
DO 55 I=2,N
PBB(I,J)=0.0
ATB(I,J)=1.0
55 CTB(I,J)=0.0
SOLVING U, V AND W FOR GIVEN P AND T
1000 DO 75 K=2,L
DO 75 I=2,N
QSB(I,K)=0.0
75 SNB(I,K)=0.0
DO 80 K=2,L
DO 80 J=2,M
QWB(J,K)=0.0
80 SEB(J,K)=0.0
DO 85 J=2,M
DO 85 I=2,N
QBB(I,J)=0.0
85 STB(I,J)=0.0
DO 120 K=2 L

```

```

DO 120 I=2,NP
CALL FLUX(DX(I+1),DX(I),T(I+1,J,K),T(I,J,K),ST)
120 S(I,J,K)=0.5*(DX(I)+DX(I+1))*DY(J)*DZ(K)*AXI*ST*CN+
+AXI2*DY(J)*DZ(K)*(PP(I,J,K)-PP(I+1,J,K))
DO 130 K=2,L
DO 130 J=2,M
DO 130 I=2,NP
AE(I,J,K)=0.5*(UP(I,J,K)+UP(I+1,J,K))
AW(I,J,K)=0.5*(UP(I-1,J,K)+UP(I,J,K))
CALL FLUX(DX(I+1),DX(I),VP(I+1,J,K),VP(I,J,K),AN(I,J,K))
CALL FLUX(DX(I+1),DX(I),VP(I+1,J-1,K),VP(I,J-1,K),AS(I,J,K))
CALL FLUX(DX(I+1),DX(I),WP(I+1,J,K),WP(I,J,K),AT(I,J,K))
CALL FLUX(DX(I+1),DX(I),WP(I+1,J,K-1),WP(I,J,K-1),AB(I,J,K))
130 CONTINUE
CALL COEF(DX,DY,DZ,AP1,AE,AW,AN,AS,AT,AB,GX,GY,GZ,
+NN,MM,LL,N,M,L,NP,M,L,0,1,1,ALFV)
CALL SOLVER(AP1,AE,AW,AN,AS,AT,AB,S,U,PX,QX,PY,QY,PZ,QZ,
+PSB,QSB,ANB,CNB,SNB,PWB,QWB,AEB,CEB,SEB,PBB,QBB,ATB,CTB,STB,
+N,M,L,NN,MM,LL,N,MM,LL,ALFV,TOLV1)
DO 220 K=2,L
DO 220 J=2,MP
DO 220 I=2,N
CALL FLUX(DY(J+1),DY(J),T(I,J+1,K),T(I,J,K),ST)
220 S(I,J,K)=0.5*DX(I)*(DY(J)+DY(J+1))*DZ(K)*ST*SN+
+DX(I)*DZ(K)*(PP(I,J,K)-PP(I,J+1,K))
DO 230 K=2,L
DO 230 J=2,MP
DO 230 I=2,N
CALL FLUX(DY(J+1),DY(J),UP(I,J+1,K),UP(I,J,K),AE(I,J,K))
CALL FLUX(DY(J+1),DY(J),UP(I-1,J+1,K),UP(I-1,J,K),AW(I,J,K))
AN(I,J,K)=0.5*(VP(I,J,K)+VP(I,J+1,K))
AS(I,J,K)=0.5*(VP(I,J-1,K)+VP(I,J,K))
CALL FLUX(DY(J+1),DY(J),WP(I,J+1,K),WP(I,J,K),AT(I,J,K))
CALL FLUX(DY(J+1),DY(J),WP(I,J+1,K-1),WP(I,J,K-1),AB(I,J,K))
230 CONTINUE
CALL COEF(DX,DY,DZ,AP2,AE,AW,AN,AS,AT,AB,GX,GY,GZ,
+NN,MM,LL,N,M,L,N,MP,L,1,0,1,ALFV)
CALL SOLVER(AP2,AE,AW,AN,AS,AT,AB,S,V,PX,QX,PY,QY,PZ,QZ,
+PSB,QSB,ANB,CNB,SNB,PWB,QWB,AEB,CEB,SEB,PBB,QBB,ATB,CTB,STB,
+N,M,L,NN,MM,LL,NN,M,LL,ALFV,TOLV1)
DO 720 K=2,LP
DO 720 J=2,M
DO 720 I=2,N
CALL FLUX(DZ(K+1),DZ(K),T(I,J,K+1),T(I,J,K),ST)
720 S(I,J,K)=AZI2*DX(I)*DY(J)*(PP(I,J,K)-PP(I,J,K+1))
DO 730 K=2,LP
DO 730 J=2,M
DO 730 I=2,N
CALL FLUX(DZ(K+1),DZ(K),UP(I,J,K+1),UP(I,J,K),AE(I,J,K))
CALL FLUX(DZ(K+1),DZ(K),UP(I-1,J,K+1),UP(I-1,J,K),AW(I,J,K))
CALL FLUX(DZ(K+1),DZ(K),VP(I,J,K+1),VP(I,J,K),AN(I,J,K))
CALL FLUX(DZ(K+1),DZ(K),VP(I,J-1,K+1),VP(I,J-1,K),AS(I,J,K))

```

```

730 CONTINUE
CALL COEF(DX,DY,DZ,AP3,AE,AW,AN,AS,AT,AB,GX,GY,GZ,
+NN,MM,LL,N,M,L,N,M,LP,1,1,0,ALFV)
CALL SOLVER(AP3,AE,AW,AN,AS,AT,AB,S,W,PX,QX,PY,QY,PZ,QZ,
+PSB,QSB,ANB,CNB,SNB,PWB,QWB,AEB,CEB,SEB,PBB,QBB,ATB,CTB,STB,
+N,M,L,NN,MM,LL,NN,MM,L,ALFV,TOLV1)
PRESSURE CORRECTIONS
DO 310 K=2,L
DO 310 J=2,M
DO 310 I=2,N
310 S(I,J,K)=DY(J)*DZ(K)*(U(I-1,J,K)-U(I,J,K))+
+DZ(K)*DX(I)*(V(I,J-1,K)-V(I,J,K))+
+DX(I)*DY(J)*(W(I,J,K-1)-W(I,J,K))
DO 320 K=2,L
DO 320 J=2,M
AW(2,J,K)=0.0
320 AE(N,J,K)=0.0
DO 330 K=2,L
DO 330 J=2,M
DO 330 I=2,NP
AE(I,J,K)=AA1*AXI2*DY(J)*DZ(K)*DY(J)*DZ(K)/AP1(I,J,K)
330 AW(I+1,J,K)=AE(I,J,K)
DO 340 K=2,L
DO 340 J=2,N
AS(I,2,K)=0.0
340 AN(I,M,K)=0.0
DO 350 K=2,L
DO 350 J=2,MP
DO 350 I=2,N
AN(I,J,K)=AA1*DZ(K)*DX(I)*DZ(K)*DX(I)/AP2(I,J,K)
350 AS(I,J+1,K)=AN(I,J,K)
DO 353 J=2,M
DO 353 I=2,N
AB(I,J,2)=0.0
353 AT(I,J,L)=0.0
DO 357 K=2,LP
DO 357 J=2,M
DO 357 I=2,N
AT(I,J,K)=AA1*AZI2*DX(I)*DY(J)*DX(I)*DY(J)/AP3(I,J,K)
357 AB(I,J,K+1)=AT(I,J,K)
DO 360 K=2,L
DO 360 J=2,M
DO 360 I=2,N
360 AP1(I,J,K)=AE(I,J,K)+AW(I,J,K)+AN(I,J,K)+AS(I,J,K)
++AT(I,J,K)+AB(I,J,K)
CALL SOLVER(AP1,AE,AW,AN,AS,AT,AB,S,P,PX,QX,PY,QY,PZ,QZ,
+PSB,QSB,ANB,CNB,SNB,PWB,QWB,AEB,CEB,SEB,PBB,QBB,ATB,CTB,STB,
+N,M,L,NN,MM,LL,NN,MM,LL,1.0,TOLP)
DO 365 K=2,L
DO 365 J=2,M
DO 365 I=2,N

```

```

DO 370 I=2,NP
370
U(I,J,K)=U(I,J,K)+AE(I,J,K)/DY(J)/DZ(K)*(P(I,J,K)-P(I+1,J,K))
DO 380 K=2,L
DO 380 J=2,MP
DO 380 I=2,N
380
V(I,J,K)=V(I,J,K)+AN(I,J,K)/DZ(K)/DX(I)*(P(I,J,K)-P(I,J+1,K))
DO 385 K=2,LP
DO 385 J=2,M
DO 385 I=2,N
385
W(I,J,K)=W(I,J,K)+AT(I,J,K)/DX(I)/DY(J)*(P(I,J,K)-P(I,J,K+1))
DO 390 K=2,L
DO 390 I=2,N
DO 390 J=2,M
390 PP(I,J,K)=PP(I,J,K)+P(I,J,K)
SOLVING T
RNU0=RNU
DO 450 K=2,L
DO 450 I=2,N
QSB(I,K)=1.0
450 SNB(I,K)=-1.0
DO 453 K=2,L
DO 453 J=2,M
QWB(J,K)=GRADT(J)
453 SEB(J,K)=GRADT(J)
DO 455 J=2,M
DO 455 I=2,N
QBB(I,J)=GRADT(J)
455 STB(I,J)=GRADT(J)
DO 420 K=2,L
DO 420 J=2,M
DO 420 I=2,N
420 S(I,J,K)=0.0
DO 430 K=2,L
DO 430 J=2,M
DO 430 I=2,N
AE(I,J,K)=U(I,J,K)
AW(I,J,K)=U(I-1,J,K)
AN(I,J,K)=V(I,J,K)
AS(I,J,K)=V(I,J-1,K)
AT(I,J,K)=W(I,J,K)
AB(I,J,K)=W(I,J,K-1)
430 CONTINUE
CALL COEF(DX,DY,DZ,AP1,AE,AW,AN,AS,AT,AB,GTX,GTY,GTZ,
+NN,MM,LL,N,M,L,N,M,L,1,1,1,1.0)
CALL SOLVER(AP1,AE,AW,AN,AS,AT,AB,S,T,PX,QX,PY,QY,PZ,QZ,
+PSB,QSB,ANB,CNB,SNB,PWB,QWB,AEB,CEB,SEB,PBB,QBB,ATB,CTB,STB,
+N,M,L,NN,MM,LL,NN,MM,LL,1.0,TOLT1)
NCC=NCC+1

```

```

END IF
NCOUNT=NCOUNT+1
IF(NCOUNT.GE.NCR) THEN
GO TO 4000.
END IF
RNU=0.0
DO 500 K=2,L
DO 500 I=2,N
500 RNU=RNU+DX(I)*DZ(K)*(T(I,1,K)-T(I,2,K))
ERT=RNU-RNUO
ERT=ABS(ERT)
ERT=ERT/RNU
IF(ERT.GT.TOLT2) THEN
DO 503 K=2,L
DO 503 J=2,M
DO 503 I=2,NP
503 UP(I,J,K)=U(I,J,K)
DO 505 K=2,L
DO 505 J=2,MP
DO 505 I=2,N
505 VP(I,J,K)=V(I,J,K)
DO 507 K=2,LP
DO 507 J=2,M
DO 507 I=2,N
507 WP(I,J,K)=W(I,J,K)
GO TO 1000
END IF
CALL ERR(UP,U,N,MM,LL,EU)
CALL ERR(VP,V,NN,M,LL,EV)
CALL ERR(WP,W,NN,MM,L,EW)
IF (EU.GT.TOLV2.OR.EV.GT.TOLV2.OR.EW.GT.TOLV2) THEN
DO 520 K=2,L
DO 520 J=2,M
DO 520 I=2,NP
520 UP(I,J,K)=U(I,J,K)
DO 530 K=2,L
DO 530 J=2,MP
DO 530 I=2,N
530 VP(I,J,K)=V(I,J,K)
DO 540 K=2,LP
DO 540 J=2,M
DO 540 I=2,N
540 WP(I,J,K)=W(I,J,K)
GO TO 1000
END IF
4000 X=2.0*RY*RY*PRD
X=ALOG10(X)
RNU=RNU/DY(2)
Y=ALOG10(RNU)
OPEN(7,FILE='OUTPUT')

```

```

WRITE(7,11)((PP(I,J,K),I=2,N),J=2,M),K=2,L)
WRITE(7,111)AX,AZ,ANGL
WRITE(7,222)RA,X
WRITE(7,333)PRD
WRITE(7,444)RNU,Y
WRITE(7,555)N,M,L
WRITE(7,666)NCOUNT,TOLP
WRITE(7,777)EU,EV,EW,ERT
11 FORMAT(13E15.5)
111 FORMAT('Ax:',F5.2,'Az:',F5.2,'Angl:',F5.2)
222 FORMAT('Ra:',E11.3,'Log(Ra/A):',E13.5)
333 FORMAT('Pr:',E11.3)
444 FORMAT('Nu:',E14.5,'LogNu:',E14.5)
555 FORMAT('Mesh:',I3,'X',I2,'X',I2)
666 FORMAT('NCOUNT:',I5,'TOLP',E15.5)
777 FORMAT('Eu:',E10.3,'Ev:',E10.3,'Ew:',E10.3,
Et:',E10.3)
STOP
END
SUBROUTINE FLUX(DF,DB,VF,VB,OPT)
R=1.0/(DF+DB)
OPT=R*(DB*VF+DF*VB)
RETURN
END
SUBROUTINE PWRLW(GXY,WW,DDS,DS,JUU)
F=DDS*WW
DDI=GXY*DDS/DS
P=F/DDI
X=1.0-0.1*ABS(P)
X=X*X*X*X*X
X=AMAX1(0.0,X)
IF (JUU.EQ.1) THEN
WW=DDI*X+AMAX1(-F,0.0)
ELSE
WW=DDI*X+AMAX1(F,0.0)
END IF
RETURN
END
SUBROUTINE COEF(DX,DY,DZ,AP,AE,AW,AN,AS,AT,AB,GX,GY,GZ,
+NN,MM,LL,N,M,L,NX,NY,NZ,JX,JY,JZ,AL)
DIMENSION DX(NN),DY(MM),DZ(LL),AP(2:N,2:M,2:L)
DIMENSION AE(2:N,2:M,2:L),AW(2:N,2:M,2:L),AN(2:N,2:M,2:L)
DIMENSION AS(2:N,2:M,2:L),AT(2:N,2:M,2:L),AB(2:N,2:M,2:L)
ALI=1.0/AL
DO 25 K=2,NZ
DO 25 J=2,NY
DO 25 I=2,NX
IF (JX.EQ.1) THEN
DXE=0.5*(DX(I+1)+DX(I))
DXW=0.5*(DX(I)+DX(I-1))

```

```

DDX=0.5*(DX(I)+DX(I+1))
END IF
IF (JY.EQ.1) THEN
DYN=0.5*(DY(J+1)+DY(J))
DYS=0.5*(DY(J)+DY(J-1))
DDY=DY(J)
ELSE
DYN=DY(J+1)
DYS=DY(J)
DDY=0.5*(DY(J)+DY(J+1))
END IF
IF (JZ.EQ.1) THEN
DZT=0.5*(DZ(K+1)+DZ(K))
DZB=0.5*(DZ(K)+DZ(K-1))
DDZ=DZ(K)
ELSE
DZT=DZ(K+1)
DZB=DZ(K)
DDZ=0.5*(DZ(K+1)+DZ(K))
END IF
AEW=DDY*DDZ
ANS=DDZ*DDX
ATB=DDX*DDY
CALL PWRLW(GX,AE(I,J,K),AEW,DXE,1)
CALL PWRLW(GX,AW(I,J,K),AEW,DXW,0)
CALL PWRLW(GY,AN(I,J,K),ANS,DYN,1)
CALL PWRLW(GY,AS(I,J,K),ANS,DYS,0)
CALL PWRLW(GZ,AT(I,J,K),ATB,DZT,1)
CALL PWRLW(GZ,AB(I,J,K),ATB,DZB,0)
AP(I,J,K)=ALI*(AE(I,J,K)+AW(I,J,K)+AN(I,J,K)+
+AS(I,J,K)+AT(I,J,K)+AB(I,J,K))
25 CONTINUE
RETURN
END
SUBROUTINE SOLVER(AP,AE,AW,AN,AS,AT,AB,S,QQ,PX,QX,PY,QY,
+PZ,QZ,PSB,QSB,ANB,CNB,SNB,PWB,QWB,AEB,CEB,SEB,PBB,QBB,
+ATB,CTB,STB,N,M,L,NN,MM,LL,NX,NY,NZ,ALF,TOL)
DIMENSION AE(2:N,2:M,2:L),AW(2:N,2:M,2:L),AN(2:N,2:M,2:L)
DIMENSION AS(2:N,2:M,2:L),AT(2:N,2:M,2:L),AB(2:N,2:M,2:L)
DIMENSION AP(2:N,2:M,2:L),S(2:N,2:M,2:L),QQ(NX,NY,NZ)
DIMENSION
PSB(2:N,2:L),QSB(2:N,2:L),SNB(2:N,2:L),CNB(2:N,2:L)
DIMENSION
PWB(2:M,2:L),QWB(2:M,2:L),SEB(2:M,2:L),CEB(2:M,2:L)
DIMENSION
PBB(2:N,2:M),QBB(2:N,2:M),STB(2:N,2:M),CTB(2:N,2:M)
DIMENSION ANB(2:N,2:L),AEB(2:M,2:L),ATB(2:N,2:M)
DIMENSION PX(NN),QX(NN),PY(MM),QY(MM),PZ(LL),QZ(LL)
NXP=NX-1

```

```

DO 10 I=2,NXP
  10 S(I,J,K)=S(I,J,K)+A1*AP(I,J,K)*QQ(I,J,K)
  100 DO 30 K=2,NZP
    DO 30 I=2,NXP
      PY(1)=PSB(I,K)
      QY(1)=QSB(I,K)
    DO 35 J=2,NYP
      ST=S(I,J,K)+AE(I,J,K)*QQ(I+1,J,K)+AW(I,J,K)*QQ(I-1,J,K)
      ++AT(I,J,K)*QQ(I,J,K+1)+AB(I,J,K)*QQ(I,J,K-1)
      PY(J)=AN(I,J,K)/(AP(I,J,K)-AS(I,J,K)*PY(J-1))
    35
      QY(J)=(ST+AS(I,J,K)*(J-1))/(AP(I,J,K)-AS(I,J,K)*PY(J-1))
      QY(NY)=(SNB(I,K)+CNB(I,K)*QY(NYP))/(ANB(I,K)-CNB(I,K)*PY(NYP))
      QQ(I,NY,K)=QY(NY)
    DO 40 J=1,NYP
      40 QQ(I,NY-J,K)=PY(NY-J)*QQ(I,NY-J+1,K)+QY(NY-J)
    30 CONTINUE
    DO 50 K=2,NZP
      DO 50 J=2,NYP
        PX(1)=PWB(J,K)
        QX(1)=QWB(J,K)
      DO 55 I=2,NXP
        ST=S(I,J,K)+AN(I,J,K)*QQ(I,J+1,K)+AS(I,J,K)*QQ(I,J-1,K)
        ++AT(I,J,K)*QQ(I,J,K+1)+AB(I,J,K)*QQ(I,J,K-1)
        PX(I)=AE(I,J,K)/(AP(I,J,K)-AW(I,J,K)*PX(I-1))
      55
        QX(I)=(ST+AW(I,J,K)*QX(I-1))/(AP(I,J,K)-AW(I,J,K)*PX(I-1))
        QX(NX)=(SEB(J,K)+CEB(J,K)*QX(NXP))/(AEB(J,K)-CEB(J,K)*PX(NXP))
        QQ(NX,J,K)=QX(NX)
      DO 50 I=1,NXP
        50 QQ(NX-I,J,K)=PX(NX-I)*QQ(NX-I+1,J,K)+QX(NX-I)
      DO 150 J=2,NYP
        DO 150 I=2,NXP
          PZ(1)=PBB(I,J)
          QZ(1)=QBB(I,J)
        DO 155 K=2,NZP
          ST=S(I,J,K)+AE(I,J,K)*QQ(I+1,J,K)+AW(I,J,K)*QQ(I-1,J,K)
          ++AN(I,J,K)*QQ(I,J+1,K)+AS(I,J,K)*QQ(I,J-1,K)
          PZ(K)=AT(I,J,K)/(AP(I,J,K)-AB(I,J,K)*PZ(K-1))
        155
          QZ(K)=(ST+AB(I,J,K)*QZ(K-1))/(AP(I,J,K)-AB(I,J,K)*PZ(K-1))
          QZ(NZ)=(STB(I,J)+CTB(I,J)*QZ(I))/(ATB(I,J)-CTB(I,J)*PZ(NZP))
          QQ(I,J,NZ)=QZ(NZ)
        DO 160 K=1,NZP
          160 QQ(I,J,NZ-K)=PZ(NZ-K)*QQ(I,J,NZ-K-1)+QZ(NZ-K)
        150 CONTINUE
      ER=0.0
      DO 60 K=2,NZP
        DO 60 J=2,NYP

```